

Modeling and Analysis of Three-Phase Grid-Tied Photovoltaic Systems

by

Anand Narayanan

A Thesis Presented in Partial Fulfillment
of the Requirements for the Degree
Master of Science

Approved November 2010 by the
Graduate Supervisory Committee:

Raja Ayyanar, Chair
Vijay Vittal
Gerald T. Heydt

ARIZONA STATE UNIVERSITY

December 2010

ABSTRACT

Market acceptability of distributed energy resource (DER) technologies and the gradual and consistent increase in their depth of penetration have generated significant interest over the past few years. In particular, in Arizona and several other states there has been a substantial increase in distributed photovoltaic (PV) generation interfaced to the power distribution systems, and is expected to continue to grow at a significant rate. This has made integration, control and optimal operation of DER units a main area of focus in the design and operation of distribution systems. Grid-connected, distributed PV covers a wide range of power levels ranging from small, single phase residential roof-top systems to large three-phase, multi-megawatt systems. The focus of this work is on analyzing large, three-phase systems, with the power distribution system of the Arizona State University (ASU) Tempe campus used as the test bed for analysis and simulation. The Tempe campus of ASU has presently 4.5 MW of installed PV capacity, with another 4.5 MW expected to be added by 2011, which will represent about 22% of PV penetration.

The PV systems are interfaced to the grid invariably by a power electronic inverter. Many of the important characteristics of the PV generation are influenced by the design and performance of the inverter, and hence suitable models of the inverter are needed to analyze PV systems. Several models of distributed generation (DG), including switching and average models, suitable for different study objectives, and different control modes of the inverter have been described in this thesis. A critical function of the inverters is to quickly detect and eliminate unintentional islands during grid failure. In this thesis, many active anti-islanding techniques with voltage and frequency positive feedback have been studied. Effectiveness of these techniques in terms of the tripping times specified in IEEE Std. 1547 for interconnecting distributed resources with electric power systems has been analyzed.

The impact of distributed PV on the voltage profile of a distribution system has been analyzed with ASU system as the test bed using power systems analysis tools namely PowerWorld and CYMDIST. The present inverters complying with IEEE 1547 do not regulate the system voltage. However, the future inverters especially at higher power levels are expected to perform sev-

eral grid support functions including voltage regulation and reactive power support. Hence, the impact of inverters with the reactive power support capabilities is also analyzed. Various test scenarios corresponding to different grid conditions are simulated and it is shown that distributed PV improves the voltage profile of the system. The improvements are more significant when the PV generators are capable of reactive power support. Detailed short circuit analyses are also performed on the system, and the impact of distributed PV on the fault current magnitude, with and without reactive power injection, have been studied.

ACKNOWLEDGMENTS

I would like to thank Arizona State University for providing me an opportunity to perform this research work. I appreciate the contributions of Dr. Xiaolin Mao at Arizona State University, towards this research. I am deeply indebted to my advisor Dr. Raja Ayyanar for advising me and for the direction he has lent to this project. His expertise and insight have been influential in performing this research work. His teaching and work ethic are an inspiration. I would also like to thank the members of my supervisory committee, Dr. Vijay Vittal and Dr. Gerald T. Heydt for their support. I thank Robert Vandling and Karl Kauffman from ASU, David Ludlow from APSES, and Randy Clawson from APS for their help in this research project, esp. for providing us with the ASU distribution system data. I also thank Dr. Devarajan Srinivasan from ViaSol Energy Solutions for providing us with the PV installation physical data. I am also obliged to the faculty of the power systems group at Arizona State University for their guidance, and the students for their companionship.

Last but never the least, I would like to thank my parents, Mrs. and Mr. Narayanan for having been there through all my hardships and helping me sail through them in the best possible frame of mind.

TABLE OF CONTENTS

	Page
LIST OF TABLES	vii
LIST OF FIGURES	viii
NOMENCLATURE	xii
CHAPTER	
1 INTRODUCTION	1
1.1 Background.....	1
1.2 Literature Review.....	1
Distributed generation.....	2
Islanding	4
System impacts of DG	7
1.3 Organization of the Thesis	7
2 THREE PHASE GRID-TIED PV INVERTERS	9
2.1 Introduction	9
2.2 Inverter Modeling	9
Switching model	10
Average model.....	10
Control modes.....	11
2.3 Utility Interface of PV Systems – IEEE Standard 929-2000 [33].....	13
2.4 MATLAB Model of Grid-Tied PV Inverter.....	15
Controller design specifications	16
Simulation results	22
2.5 Summary	23
3 ANTI-ISLANDING TECHNIQUES.....	24
3.1 Introduction	24
3.2 Anti-Islanding Schemes	24
Positive feedback.....	24

Chapter	Page
dq implementation	26
Voltage schemes	29
Frequency schemes	30
3.3 Simulink Model of Anti-Islanding Techniques	31
3.4 Anti-Islanding Results.....	33
3.5 Summary	38
4 POWER FLOW MODEL.....	39
4.1 Introduction	39
4.2 Data Acquisition for the ASU Distribution System.....	40
ASU distribution system map and one-line diagram	40
ASU PV physical data.....	43
ASU load data and solar generation data from EIS website—EIS data	44
Impedances of the APS grid	46
4.3 Development of a Model in PowerWorld for the Entire ASU Distribution System ...	46
Creation of the system model	46
Rendering the EIS load data and solar data suitable for power flow studies	53
4.4 Model Development in CYMDIST	53
5 POWER FLOW RESULTS AND FAULT ANALYSIS	60
5.1 Introduction	60
5.2 Case Study Results using the PowerWorld ASU Distribution Model.....	60
5.3 Case Study Results using the CYMDIST ASU Distribution Model	66
5.4 Time Step Simulation.....	69
5.5 Fault Current Analysis	72
Fault flow analysis	76
6 CONCLUSIONS AND FUTURE WORK.....	80
6.1 Conclusions	80
6.2 Future Work.....	82

	Page
REFERENCES.....	83
APPENDIX A PV GENERATION SITES IN TEMPE CAMPUS	86
APPENDIX B SUBROUTINES TO READ EIS DATA, CREATE LOAD PROFILE AND LOAD IT IN POWERWORLD	89

LIST OF TABLES

Table	Page
2.1 DATA FOR THE INVERTER, RLC LOAD AND GRID	16
4.1 SOLAR MODULE SPECIFICATION	44
5.1 POWER FLOW STUDY WITHOUT PV GENERATION	60
5.2 POWER FLOW STUDY WITH EXISTING PV INSTALLATION	61
5.3 POWER FLOW STUDY WITH PLANNED PV INSTALLATION	61
5.4 FEEDER GENERATION FOR CASE 0.....	68
5.5 FEEDER GENERATION FOR CASE 1.....	68
5.6 FEEDER GENERATION FOR CASE 2.....	69
5.7 FEEDER GENERATION FOR CASE 3.....	69
5.8 PERCENTAGE INCREASE IN FAULT CURRENT DUE TO PV REPRESENTING 22% PENETRATION.....	75
A.1 PV SITES IN ASU TEMPE CAMPUS	87

LIST OF FIGURES

Figure	Page
2.1. Switching model of three-phase inverter [12].....	10
2.2. Inverter average model with RLC load and grid [12].....	11
2.3. Block diagram of constant-current-controlled inverter [12].	13
2.4. Non-islanding inverter test circuit in Simulink	15
2.5. Bode plot of loop gain of the current control loop	17
2.6. Detailed inverter average model in MATLAB/Simulink.....	18
2.7. Plant model in MATLAB/Simulink	19
2.8. Inverter model with averaged three phase inverter and L filter in MATLAB/Simulink	20
2.9. Simulink block diagram representing the averaged three phase inverter.	20
2.10. Simulink block diagram representing L filter dynamics.....	21
2.11. Current controller block in MATLAB/Simulink	21
2.12. Voltage, current and power waveforms for inverter in grid connected mode.....	22
2.13. V_d , V_q voltages and frequency waveform of inverter.....	23
3.1. Worst case island load.....	25
3.2. Phasor diagrams showing a change in V_d causing both magnitude and angle change [12]	27
3.3. Voltage positive feedback for island detection in dq implementation [12]	27
3.4. Frequency positive feedback in dq implementation [12].....	28
3.5. Block diagram of the voltage based island detection scheme with V_d to I_{dref} positive feedback [12].....	29
3.6. Block diagram of the frequency based island detection scheme with ω to I_{qref} positive feedback [12].	30
3.7. Simulink model of feedback mechanism for V_d to I_{dref} and ω to I_{qref} with OV/UV and OF/UF protection	32
3.8. Blocks representing the voltage feedback scheme	32
3.9. Blocks representing the frequency feedback scheme.	32

Figure	Page
3.10. Implementation of over voltage/under voltage and over frequency/under frequency protection in Simulink	33
3.11. Voltage and frequency waveforms corresponding to the voltage based island detection scheme with V_d to I_{dref} positive feedback	34
3.12. Voltage and frequency waveforms corresponding to the frequency based island detection scheme with ω to I_{qref} positive feedback	35
3.13. Voltage and frequency waveforms corresponding to the voltage based island detection scheme with V_d to I_{qref} positive feedback	36
3.14. Voltage and frequency waveforms corresponding to the combined island detection scheme with V_d to I_{dref} and ω to I_{qref} positive feedback	36
3.15. Voltage and frequency waveforms corresponding to the voltage based island detection scheme with V_d to I_{dref} positive feedback for a LVRT event	37
4.1. Map of ASU 15 kV distribution system, with existing PV installations labeled.	41
4.2. A portion of the one-line diagram of the ASU 15 kV distribution system.	42
4.3. A simplified diagram of the PV system at ASU parking structure 1.....	43
4.4. EIS load data for ASU engineering research center on 8/20/2009.....	45
4.5. EIS solar generation data for ASU parking structure 1 on 8/20/2009.....	45
4.6. PowerWorld model of the entire ASU distribution system.....	48
4.7. PowerWorld model of the ASU West distribution system.	49
4.8. PowerWorld model of the ASU Central distribution system.	50
4.9. PowerWorld model of the ASU North distribution system.	51
4.10. PowerWorld model of the ASU South distribution system and APS pole (top right).....	52
4.11. CYMDIST model of the entire ASU distribution system.	55
4.12. CYMDIST model of the ASU West distribution system.	56
4.13. CYMDIST model of the ASU Central distribution system.	57
4.14. CYMDIST model of the ASU North distribution system.	58
4.15. CYMDIST model of the ASU South distribution system.	59

Figure	Page
5.1. Voltage profile for Case 0: All lines are well below their thermal loading limits. The system voltage profile is also normal.	62
5.2. Voltage profile for Case 1: The backup line is overloaded and the voltage profile is poor.	63
5.3. Voltage profile for Case 2: The backup line is not overloaded, though it is still in a warning condition. The voltage profile has improved.	64
5.4. Voltage profile for Case 3: The backup line is now in a normal condition. The voltage profile becomes much better.	65
5.5. Voltage profile in CYMDIST for Case 0.....	66
5.6. Voltage profile in CYMDIST for Case 1: there is a significant drop in the voltage level.....	66
5.7. Voltage profile in CYMDIST for Case 2: there is improvement in the voltage profile at a few places.	67
5.8. Voltage profile in CYMDIST for Case 3: the voltage profile becomes much better.	67
5.9. Load and generation profile for 8/20/2009	70
5.10. Hourly voltage profile at three locations when central feeder A is out of service without PV generation.....	71
5.11. Hourly voltage profile at three locations when central feeder A is out of service with PV generation and reactive power injection	71
5.12. LLL fault current versus distance from feeder	73
5.13. LLG fault current versus distance from feeder.....	74
5.14. LL fault current versus distance from feeder	74
5.15. LG fault current versus distance from feeder	75
5.16. Phasor diagram indicating decrease in fault current due to reactive power injection	76
5.17. Under-voltage and overload lines in ASU West for a LG fault in phase A at a PV generator location.....	77

Figure	Page
5.18. Under-voltage and overload lines in ASU West for a LL fault in phase AB at a PV generator location	78
5.19. Under-voltage and overload lines in ASU West for a LLG fault in phase AB at a PV generator location	78
5.20. Under-voltage and overload lines in ASU West for a LLL fault at a PV generator location	79

NOMENCLATURE

AC	Alternating Current
ANSI	American National Standard Institute
APS	Arizona Public Service
APSES	Arizona Public Service Energy Services
ASU	Arizona State University
AVR	Automatic VAR Regulation
AWG	American Wire Gauge
BPF	Band Pass Filter
C	Capacitance of the load
CAIDI	Customer Average Interruption Duration Index
CHP	Combined Heating and Cooling Plant
CP	Central Plant
ΔV	Change in voltage due to response
ΔI	Change in current due to feedback
$\Delta\theta$	Change in angle
d-	Direct
dq	Direct and Quadrature
DC	Direct Current
DER	Distributed Energy Resources
DG	Distributed Generation
EIS	Energy Information System
ENS	Energy Not Supplied
EPS	Electric Power Systems
GIS	Geographical Information System
I	Current before feedback
I'	Current after feedback

I_d	d-axis current
I_q	q-axis current
IEEE	Institute of Electrical and Electronics Engineers
L	Inductance of the load
LG	Line-to-Ground
LL	Line-to-Line
LLG	Double Line-to-Ground
LVRT	Low-Voltage-Ride Through
NDZ	Non-Detection Zone
OF	Over Frequency
OV	Over Voltage
P	Real Power
P_t	Park's matrix
PCC	Point of Common Coupling
PLL	Phase Locked Loop
PV	Photovoltaic
Q	Reactive Power
q-	Quadrature
R	Resistance of the Load
SAIDI	System Average Interruption Duration Index
SAIFI	System Average Interruption Frequency Index
UF	Under Frequency
UV	Under Voltage
V	Voltage before response
V'	Voltage after response
V_d	d-axis voltage
V_q	q-axis voltage

X

Reactance

CHAPTER 1

INTRODUCTION

1.1 Background

With the increasing concern about global environmental protection, the need to produce pollution-free natural energy such as solar energy has received great interest. As an alternative source of energy for the future, solar energy is clean, pollution-free and inexhaustible. Solar PVs are among the fastest growing energy sources in the world.

Towards the end of the last millennium, the primary market for PV was in off-grid applications, such as rural electrification, water pumping, and telecommunications. However, now majority of the global market is for grid-connected applications where the power is fed into the electrical network. Furthermore, most of the new PV capacity has been installed in the distribution grid as distributed generation. As the expansion of solar PV continues, concerns about its potential impact on the stability and operation of the grid have grown. Utilities and power system operators are considering changes which will integrate and manage more of this renewable energy source in their systems.

1.2 Literature Review

Modern power grids are extremely complex and widespread. Surges in power lines can cause massive network failures and permanent damage to multimillion-dollar equipment in power generation plants. After electricity is produced at power plants it has to get to the customers that use the electricity. The transmission and distribution system delivers electricity from the generating site (electric power plant) to residential, commercial, and industrial facilities through a network of power lines and associated components. In the United States typically the transmission portion of the system is designated as operating at 69 kV and above, while the distribution portion operates between 110 volts and 35 kV. A further distinction is often made between primary distribution (voltages between 2.4 kV and 35 kV) and secondary distribution (110 to 600 volts) sys-

tems. Industrial and commercial customers with large power demands often receive service directly from the primary distribution system. Transformers are a crucial link in the electric power distribution system [1]. Distribution transformers are one of the most widely used elements in the electric distribution system. They convert electricity from the high voltage levels in utility transmission systems to voltages that can safely be used in businesses and homes. As an add-on to the existing distribution system is the idea of distributed generation. Electric power distribution systems have traditionally been designed assuming that the primary substation is the sole source of power and short-circuit capacity. DG invalidates this assumption by placing power sources in the distribution system and making it an active system.

Distributed generation

DG, also known as on-site generation, generates electricity from many small energy sources. DG generally applies to relatively small generating units of 30MW or less sited at or near customer sites to meet specific customer needs, to support economic operation of the existing distribution system, or both. Reliability of the service and power quality are enhanced by the proximity to the customer. While central power systems remain critical to the nation's energy supply, their flexibility is limited. Large power generation facilities are capital-intensive undertakings that require an immense transmission and distribution grid to move the power. DG complements central power by providing a relatively low capital cost response to incremental jumps in power demand. The advantage of grid interconnection of DG systems is the effective utilization of the generated power [2]. There are a lot of economic and environmental incentives like peak shaving, renewable portfolios, transmission and distribution infrastructure deferral, which promote distributed generation. Although there are many types of distributed generation which include traditional as well as emerging technologies (fuel cells, micro-turbines, sterling engines, PV, wind turbines), there are basically two interfaces for grid interconnection: One is rotating machines which include synchronous machines and induction machines. The other is inverters—as part of the

overall power-conditioning system, inverters convert variable frequency, variable voltage AC sources or DC sources to regulated frequency/voltage AC sources that can be interconnected with the grid.

With so much focus on the installation of new distributed generation, it is critical that the power system impacts be assessed accurately. DG units need to be applied in a manner which avoids causing degradation of power quality, reliability, and control of the utility system. Unlike the large-scale generation of the transmission system, DG creates difficulties in evaluating reliability indices due to the complexity of the operation status [3, 4]. Power quality has become a real problem over the last few decades due to the ever increasing use of power electronics and sensitive load equipment. The ability to control real and reactive power injection from an inverter interfaced in grid-connected mode is of great importance and interest [5]. With the possibility of significant penetration of distributed generation, power flow studies and dynamic analysis of distribution systems are very necessary [6]. The connection of DG to the grid may affect the stability of the power system, i.e. angle, frequency and voltage stability. Voltage fluctuations may be caused due to the variation in power injection of some DG technologies such as wind turbines and PV which are known for its unpredictability [7]. The performance of a large system is not greatly affected by an intermediate increase or decrease in generation. But when the system is relatively small, these short term disturbance could lead to an uncontrolled state. Methods have been developed to provide robust control of voltage level at nodes when DG units are in stand-alone mode [8, 9]. DG also presents a significant impact on relay protection. Inclusion of DG causes a change in the value and direction of the system's power flow under normal operating conditions and under fault conditions [10]. These factors make it necessary to study the impacts in detail.

DG units are significantly and conceptually very different from conventional power system in terms of load characteristics, power quality constraints, market participation strategies and the control and operational strategies. The main reasons are as follows [11]:

- Steady-state and dynamic characteristics of DG units are different from those of the conventional large turbine-generator units.
- Presence of single-phase loads and DG units adds significantly to the imbalance of the micro-grid.
- Wind-based units which are non-controllable sources of energy form a noticeable portion of supply within a micro-grid.
- Control and operation of a micro-grid may be dependent on energy storage units.
- Economic considerations generally dictate connection and disconnection of DG units and loads during its operation.
- Power quality levels of certain loads might be pre-determined. The micro-grid might have to strictly abide by this.

Islanding

Among technical issues created by DG interconnection is the problem of islanding. Islanding is a condition in which a portion of the utility system containing both load and generation is isolated from the rest of the utility system and continues to operate on its own. Technical requirements need to be satisfied to ensure reliability of the utility grid and safety of the PV system installer. Although grid-connected micro-grids can be designed with the capability of isolated operation, the transition between grid-parallel and standalone operation can be challenging. In certain cases, the DG unit will be expected to shut down once the main grid is cut-off and then start back up so that it can continue to supply local loads. The power outage to the local loads could last between seconds and minutes, depending on the black-start time of the generation assets present within the micro-grids. In many cases, a disturbance or transient effect to the loads within the micro-grids is not acceptable. For such systems where negligible disturbance is required, a flawless transition control is needed. This transition process is called intentional islanding [12].

The intentional islanding control must be capable of maintaining voltage and frequency regulation while exhibiting fast transient disturbance rejection qualities. This is to prevent large voltage and frequency transients that generally follow the loss of the main grid. The DG must be able to support transient and brief currents far in excess of the connected load demand because of magnetizing inrush and motor dynamics. Intentional islanding is one of the most significant challenges for making grid-connected micro-grids an attractive solution for high-reliability customers. Standards compliance is a key for entry into the DG market. Among the technical requirements in various standards, voltage regulation and integration with area EPS grounding are to be handled by the utility operator. Some requirements can be designed at the inter-connect interface, such as harmonics, DC injection, and anti-islanding. In order to make intentional islanding feasible in situations where the island includes a part of the primary system, considerable engineering effort, control and communication systems are necessary [13, 14]. These kind of islanding conditions cause negative impacts on protection, operation and management of distribution systems. Therefore, it is necessary to study the islanding conditions and methods for disconnecting DG from the distribution system. Most aspects involving disconnection of DG from the network have been addressed previously. Certain requirements concerning the same have been established earlier by other standards and recommended practices [15]. Some requirements are relatively new and there are no well-established practices and solutions. Prevention of unintentional islanding is one among those new requirements.

Power quality issues, interference to grid-protection devices, equipment damage, and even personnel safety hazards are results of unintentional islanding. To prevent the islanding phenomenon, various anti-islanding methods have been studied, which are classified into passive and active methods [16]. When an inverter is equipped with an OV/UV relay and OF/UF relay, it is considered that the inverter has the basic passive anti-islanding methods. However, these passive schemes have relatively large NDZ because it only monitors the voltage magnitude or frequency of the

PCC at the PV inverter output. It fails to detect the islanding when the power of the PV system matches with the demand of the load. Passive methods like detection of harmonic content of voltage suffer from the problem of how to set an appropriate harmonic threshold. The phase jump detection method fails to detect the islanding when the load power factor is unity, and it is easy to detect the islanding by mistake when the load such as a motor starts to run.

Active methods for detection of the island introduce deliberate changes or disturbances to the connected circuit. The system response is monitored to determine if the utility grid is still connected with stable frequency, voltage and impedance. If the small perturbation is able to affect the parameters of the load connection within prescribed requirements, the active circuit causes the inverter to cease power conversion. In active methods, the output current or power of the inverter is designed to facilitate the islanding detection. For instance, both active frequency drift and sliding mode frequency shift change the frequency of output current of the inverter to detect the islanding. When the phase angle of a load matches the phase offset or starting phase angle these techniques become ineffective. When these techniques are applied to three-phase systems, if the large loads start up and stop frequently so that the frequency of utility voltage changes slightly, they may detect the islanding by mistake. Other active anti-islanding schemes have noticeable power quality degradation due to their injected harmonics, for example, zero-crossing chopping [17, 18] and asymmetrical waveforms [19]. When there is a close generation and load matching, the schemes may not be able to detect the islanding [20-22]. This is known as NDZs. Most remote techniques for detection of islands are based on communication between the utility and the DG's. Usually, remote techniques do not have a NDZ and are therefore very good approaches for anti-islanding. However, implementations of remote techniques for small DG systems that do not otherwise require communication with the utility are not economically feasible [23].

If an island should occur, it will normally persist for only a very brief period, unless the aggregate real and reactive output of all the DGs supporting the island is close to the load demand.

Otherwise, island voltage and frequency will change rapidly. High-speed OF and UF and OV and UV trip points specified in the interconnection standards bring about termination of the islanded operation. It is highly improbable to have a precise balance as most DGs are operated in a constant power, constant power factor control mode [24]. All this makes network or connection issues important from a technical point of view as there are significant differences in the design of distribution and transmission networks.

System impacts of DG

In transmission lines or urban distribution networks, the effect of line or cable resistance on voltage drop is small, since its specific magnitude is generally much less than the reactance. Hence, the reactance is the most important parameter in regards to voltage drop and line losses. In rural distribution systems, however, the resistance in the distribution lines is often larger than, or at least similar to, the inductance. Hence, the distribution line resistance causes a significant proportion of the voltage drop along the distribution lines as well as of the line losses. The connection of DG can therefore have a significant influence on the local voltage level. It has been seen that there is considerable improvement in the voltage profile of a system with the introduction of DG. Voltage stress on distribution lines have significantly reduced and reliability of the system has become better [25]. Another important difference mentioned by the author is that distribution systems are usually not designed for the connection of power generation devices, e.g. the connection of distributed generation leads to a change in the fault-current, and hence a redesign of local fault protection system is required. The fault level contribution of DG is contributed by a number of factors like type of DG, distance of DG from the fault, presence of a transformer between fault location and contributing DG and configuration of the network between DG and fault [26].

1.3 Organization of the Thesis

The principal content of this document has been partitioned in 6 chapters. Chapter I presents the overview of the research work and a literature summary of pertinent subjects –three-

phase PV inverter, islanding issues and techniques, impact of DG on distribution systems, power flow analysis and short circuit analysis. Chapter 2 presents the procedure for modeling the three phase PV inverter. The average modeling is done and a current controller is designed for the inverter. Chapter 3 extends the modeling done in Chapter 2 where, the idea of islanding a system and active anti-islanding techniques has been discussed. Positive feedback and dq implementation are two key aspects that have gone into the implementation of the anti-islanding technique for the inverter. Chapter 4 discusses power flow analysis of the distribution system. Creation of the one line diagram in PowerWorld and CYMDIST and rendering of the load data is shown. Chapter 5 portrays results of the power flow analysis and short circuit analysis of the system created in Chapter 4. The conclusions and possible extensions as future work have been shown in Chapter 6.

CHAPTER 2

THREE PHASE GRID-TIED PV INVERTERS

2.1 Introduction

Large photovoltaic systems in the 20kW to 1MW range are becoming more common, increasing the importance of three-phase grid connected inverters to the photovoltaic industry. The grid-tied inverter differs from the stand-alone unit in that it can function only when connected to the utility grid. In effect, it provides the interface between the photovoltaic array and the utility. The grid-tied inverter conditions the power output of the photovoltaic array. It also serves as the system's control mechanism and the means through which the site-generated electricity enters the utility lines [27]. Circuit topology, conversion efficiency, maximum power point tracking, power quality, anti-islanding and cost are the main design considerations that need to be examined.

This chapter deals with the modeling of a three phase inverter suitable for implementing the anti-islanding schemes discussed in Chapter 3. Most high power PV systems are three phase and all PV systems in ASU are interfaced to the three phase distribution network. The average model of the inverter has been simulated with constant current mode control. The requirements to connect the inverter to the utility grid as per relevant standards have been discussed and implemented.

2.2 Inverter Modeling

The technology for three-phase inverter is gaining more practical value in the recent past. Besides, the technology for three-phase inverters can be extended to single-phase inverters. Generally, the overall power-conditioning system includes front-end conversion and regulation. Examples of this are DC/DC conversion for prime movers with DC output which are given by fuel cell, PV, Battery, or AC/DC conversion for prime movers with AC output of micro-turbines and sterling engines. They may have an energy-management system, such as a battery charger, at the DC bus. The input to the inverter is a regulated DC source in both these cases. In the model created, the input to the inverter is modeled as a DC voltage source. A simplification in the model

is the inverter output filters, which could have different variations in practical applications; for example, the output filter could include L, or LCL, or LC plus a transformer, with or without harmonic filters. In the analysis done, an L only (inductor) filter is considered. dq implementation and controller concepts have been used for the modeling of the three phase PV inverter [28-31].

Switching model

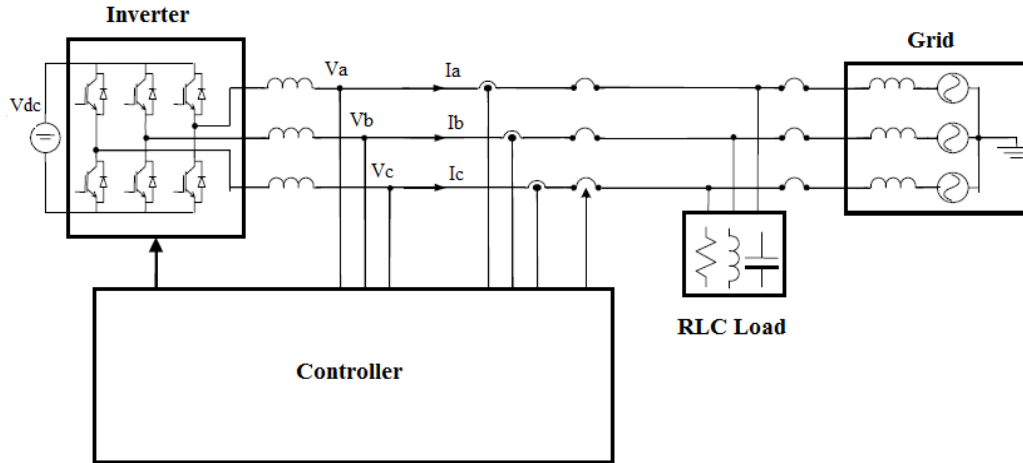


Fig. 2.1. Switching model of three-phase inverter [12].

Fig. 2.1 shows the inverter-, load- and grid-system diagram with the inverter being modeled as a switching model. The switching devices generally used for the inverter are insulated gate bipolar transistors (IGBTs). IGBTs can be modeled as ideal on/off switches that represent the inverter’s discrete switching behaviors. The switching model not only captures the voltage and current ripples, it also includes dead time and delays that are based on the IGBT device characteristics and gate-driver design in the actual hardware. This way, once the new algorithms are coded and simulated, the same code can be readily compiled and loaded to the hardware for testing.

Average model

Fig. 2.2 shows the inverter-, load- and grid-system diagram where the inverter is represented as an average model. The switching model is ideal for validating new algorithms. However, it has two limitations that motivate development of the average model:

- The switching model takes a long time to simulate.
- The process of development of new algorithms using the switching model would be inefficient. It is difficult to perform small-signal analysis directly on switching model due to its discrete behavior.

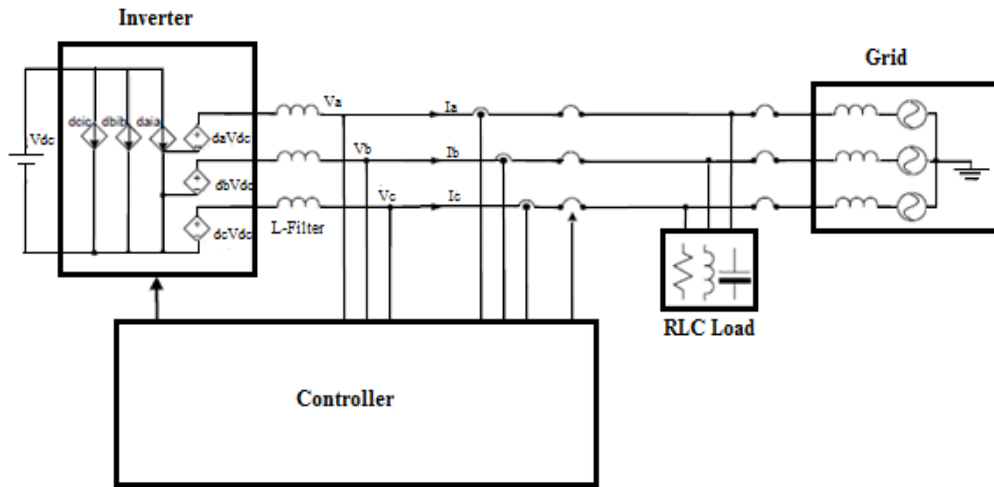


Fig. 2.2. Inverter average model with RLC load and grid [12].

The average model negates both these limitations. The averaging is a two-pronged process. One is the switching network and the other is the controller. The switching network can be represented by controlled voltage and current sources with averaged switching duty cycles. The controller, instead of using actual code with discrete behaviors, uses equivalent continuous functions, such as Proportional (P), Proportional-Integral (PI), to represent control behaviors. Because of the averaging of the switching function and simplified controls, the average model simulation speed is at least an order of magnitude faster than the switching model.

Control modes

There are two basic control modes for the grid-connected inverters. One is constant-current control; the other is constant-power control. It is still arguable whether an inverter should be permitted to regulate voltage when connected to the grid. The current IEEE 1547 standard [32] does not allow DG to actively regulate voltage, but there are suggestions that DG voltage regulation

may have some positive impact on the grid. For the detailed analysis, constant-current controlled inverters are used to exhibit the concepts, which can be easily extended to constant-power controlled inverters. In constant power control, the power loops are outside the current loops. In the case of reactive power injection, the power-factor could be the reactive power reference. The inverter output power will follow the power references. A variation of the constant power control is the constant DC bus voltage control. In this, instead of using an active power reference, DC bus voltage is regulated while the input to the inverter is a constant power source. The latter is more popular in modern digitally controlled inverters. For the purpose of this work, constant current control has been used. The control design for a three-phase inverter can be realized either in ABC (stationary) or in dq (rotating) frames.

In constant current control, the inverter output currents are regulated to the given current references which come from design specification. The controller has been created with key functional blocks like ABC/dq transformation, dq PLL, summing function, linear regulator in the form of a proportional-integral controller and dq/ABC transformation. This captures the key behaviors of the inverter and the dominant factors that may influence the AI control function. Many functions to deal with practical issues are not modeled in the average model, e.g. negative sequence regulation, dq decoupling, device protection. Park's transformation, mentioned in (1), was used to convert the ABC reference frame to dq reference frame (synchronous frame) and vice versa (zero reference frame is neglected). A controller modeled in the dq reference frame can eliminate steady state error. The decoupling control of the synchronous frame leads to fast transient responses. As part of the controller, a dq PLL was also implemented. This is illustrated in Fig. 2.3.

$$P_t = \frac{2}{3} \begin{bmatrix} \cos \theta & \cos(\theta - \frac{2\pi}{3}) & \cos(\theta + \frac{2\pi}{3}) \\ \sin \theta & \sin(\theta - \frac{2\pi}{3}) & \sin(\theta + \frac{2\pi}{3}) \\ \frac{1}{2} & \frac{1}{2} & \frac{1}{2} \end{bmatrix} \quad (1)$$

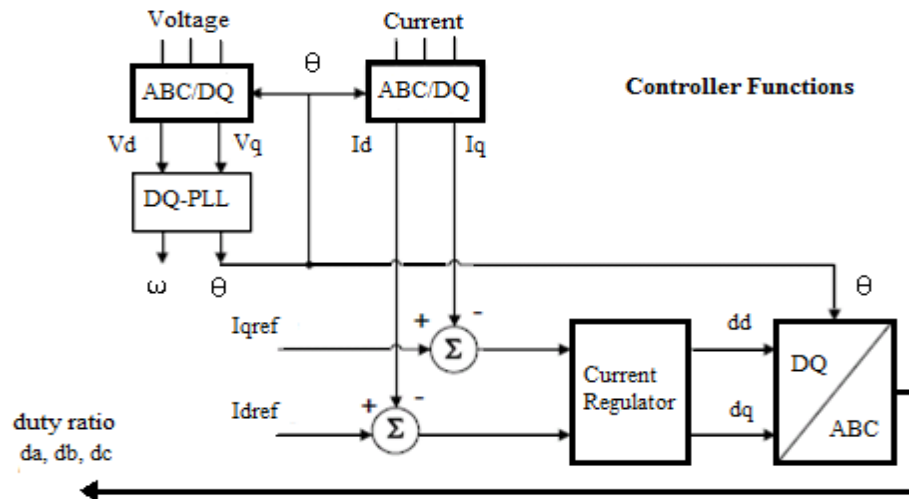


Fig. 2.3. Block diagram of constant-current-controlled inverter [12].

2.3 Utility Interface of PV systems – IEEE Standard 929-2000 [33]

This standard contains the guidance regarding equipment and function necessary to ensure compatible operation of PV systems that are connected in parallel with the electric utility. Utility-interconnected PV systems do not regulate voltage; they inject current into the utility. Therefore, the voltage operating range for PV inverters is selected not as a voltage regulation function but as a protection function that responds to abnormal utility situations. Clearly, utility voltage may be impacted due to the injection of such a large current. As long as the magnitude of current injection from PV inverters on a utility line remains less than the load on that line, the utility's voltage regulation devices will continue to operate normally. In a case where the PV current injection on a utility line exceeds the load on that line, then corrective action is required, as the voltage regulation devices do not normally have directional current sensing capability.

Small PV systems ($\leq 10\text{kW}$) should be capable of operating within the limits normally experienced on utility distribution lines. In the best interest of both the interconnected utility and the PV system owner, it is necessary that the operating window be selected in a manner that minimizes nuisance tripping. The operating window for these small and intermediate PV systems is 88% to 110% of nominal voltage. If the inverter installation is electrically close enough to the PCC to

allow negligible voltage difference between the inverter and the PCC, then the 110% of nominal voltage trip point will apply to the inverter terminals as well as the PCC. However, some systems may have installation restrictions that do not allow negligible voltage difference between the inverter and the PCC. In such cases, it is recommended that the inverter ceases to energize the utility lines whenever the voltage at the PCC deviates from the allowable voltage operating range.

PV systems have a fixed frequency operating range of 59.3 to 60.5 Hz. The test points for determining proper operation of the frequency trip function should be 59.2 Hz and 60.6 Hz. When the utility frequency is outside the range of 59.3-60.5 Hz, the inverter should cease to energize the utility line within six cycles. The purpose of the allowed time delay is to ride through short-term disturbances to avoid excessive nuisance tripping.

Non-islanding PV inverters are designed for connection as a parallel source to a utility service. In addition to fixed over-frequency, under-frequency, over-voltage, and under-voltage trips described, this type of inverter includes a way to shut down when the utility source is not present (the non-islanding feature). Once the fixed frequency and voltage limits have been verified, the inverter is tested to determine if it can maintain stable operation in the presence of a utility source. A utility source means any source capable of maintaining an island within the recommended voltage and frequency windows. Voltage should be at least 3% inside the most restrictive voltage trip limits. Frequency should be at least 0.25 Hz inside the most restrictive frequency trip limits. This test procedure is based on having the quality factor, mentioned in (2), of the islanded circuit (including load and generator) set equal to 2.5 which is the worst case loading condition.

$$\text{Quality factor} = R\sqrt{\frac{C}{L}} \quad (2)$$

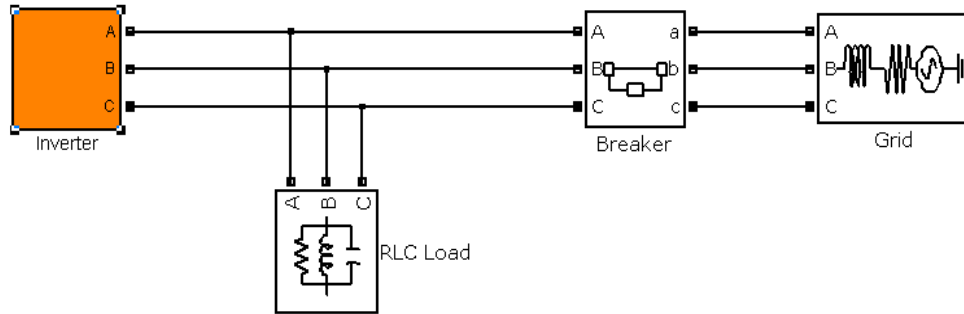


Fig. 2.4. Non-islanding inverter test circuit in Simulink.

PV systems are protected against the vast majority of potential islanding situations by voltage and frequency detection schemes. However, it is possible that circumstances may exist on a line section that has been isolated from the utility and contains a balance of load and PV generation that would allow continued operation of PV systems. Such circumstances would require a load-generation balance so that both frequency and voltage remain within the trip limits. Although such a load balance is perceived as a low-probability event, the potential impact of such an occurrence is great enough that this distributed resource islanding has been the subject of numerous studies and much research [33]. This thesis has resulted in development of active control techniques that have proven to be reliable in detecting potential distributed resource islands. After an out-of-bounds utility event that has caused the PV system to stop energizing the utility line, continuous normal voltage and frequency have to be maintained by the utility to re-energize the line. A minimum of 5 minutes is desirable, at which time the inverter can reconnect the PV generation system to the utility automatically [33].

2.4 MATLAB Model of Grid-Tied PV Inverter

The detailed average inverter model, which was created in MATLAB/Simulink, is shown in Fig. 2.5. The specifications of the three-phase inverter are listed in Table 2.1. Information on the quality factor of the load and the corresponding RLC load values connected in parallel to the inverter and the grid parameters are also mentioned. The inverter is based on a GE grid-connected inverter product.

TABLE 2.1
DATA FOR THE INVERTER, RLC LOAD AND GRID

Inverter	Value	Unit	Description
Fs	8000	Hz	Switching frequency
Vdc	900	V	Input DC bus voltage
Lf	2.1E-03	H	Output inductance
VI-l	480	V	Line-to-line voltage
VI-n	277	V	Line-to-neutral voltage
P	100000	W	Rated power
PF	1		Power factor
P	100000	W	Active power output
Q	0	Var	Reactive power output
RLC Load			
R	2.304	Ohm	Resistance
L	3.395E-03	H	Inductance
C	2.072E-03	F	Capacitance
Qf	2.5		Load quality factor
Fload	60	Hz	Load resonant frequency
Grid			
F	60	Hz	Grid frequency
VI-l	480	V	Line-to-line voltage
VI-n	277	V	Line-to-neutral voltage
Lgrid	3.056E-04	H	Grid inductance, 5% of inverter impedance
Rgrid	0.012	Ohm	Grid resistance, X/R=10

Controller design specifications

The current controller was designed for a bandwidth of 1 kHz and with a phase margin of 60°. The traditional K-factor approach is used to design the controller [34]. The advantage of using this approach is that it results in optimum pole, zero locations for a given phase margin and crossover frequency. Since the phase boost required for the given controller transfer function is less than 90°, Type II controller is used. Fig. 2.5 shows the bode plot for the current controller modeled. The controller is converted to the state space form so that it is implemented in the dq reference frame.

The plant block consists of the equations of the average inverter model and of an L filter which is shown in Fig. 2.6 through Fig. 2.9. The inputs to the block are the duty ratio for all three phases and the three phase line voltage. Inverter output current and DC link voltage are the outputs read from the block. There are blocks which do the ABC/dq conversion for the voltages and cur-

rents. Fig. 2.10 shows the AC current control block which implements the constant current control for the inverter.

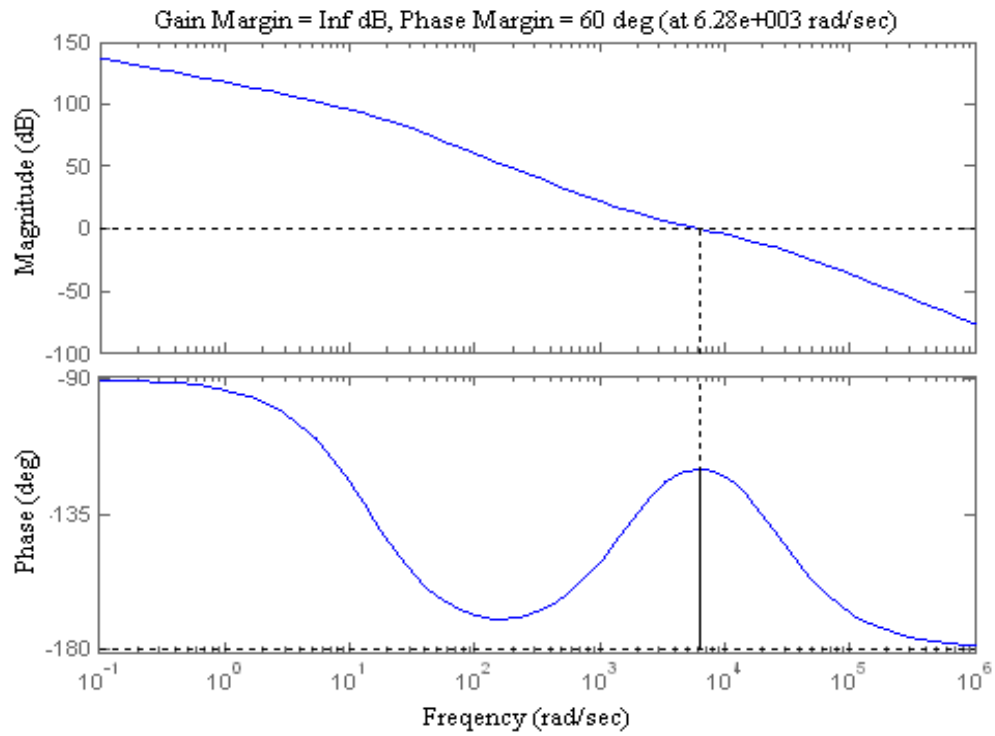


Fig. 2.5. Bode plot of loop gain of the current control loop.

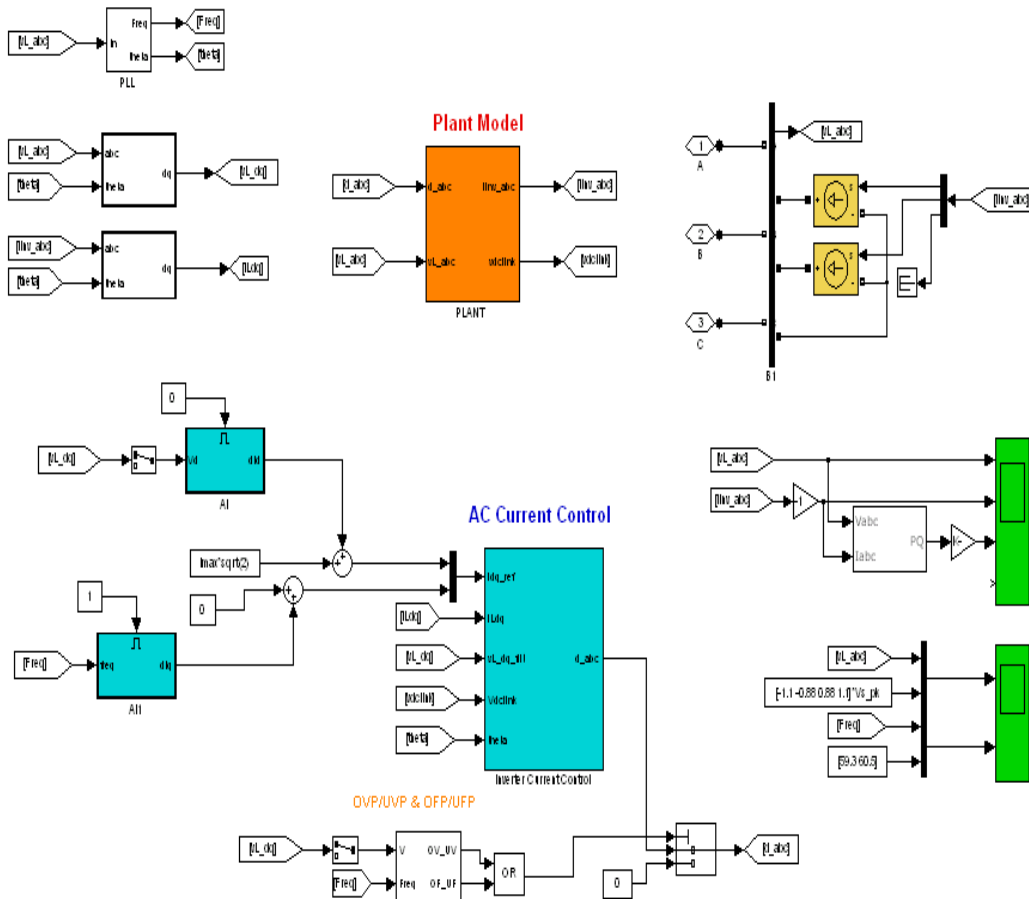
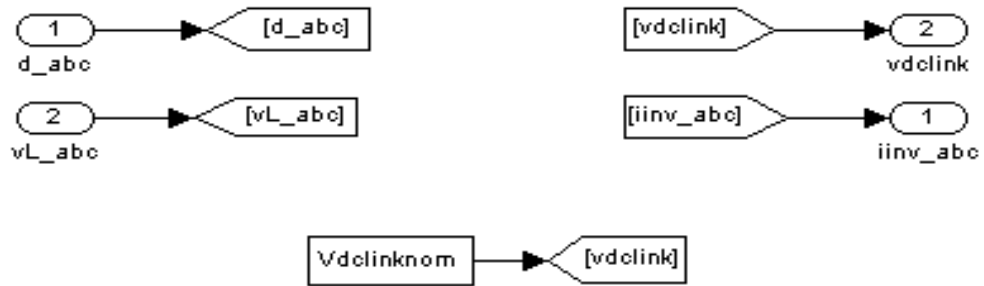


Fig. 2.6. Detailed inverter average model in MATLAB/Simulink.

PLANT



Inverter Model

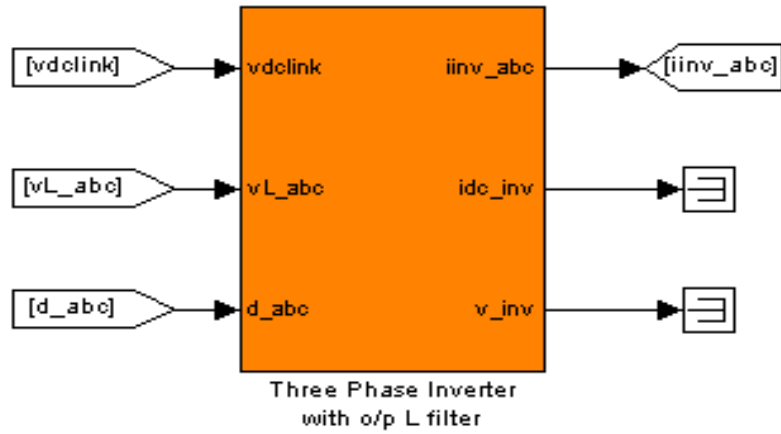


Fig. 2.7. Plant model in MATLAB/Simulink.

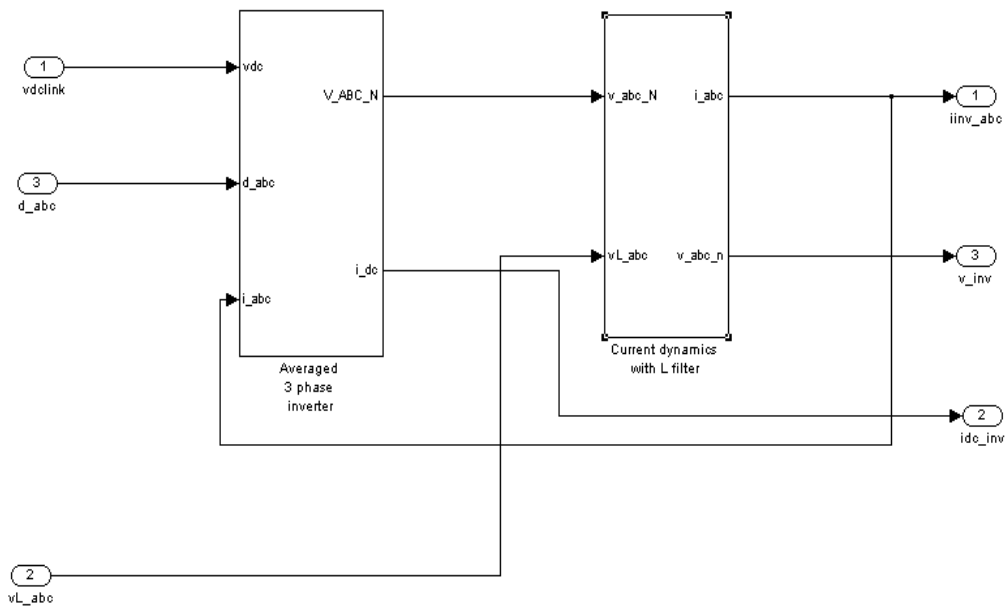


Fig. 2.8. Inverter model with averaged three phase inverter and L filter in MATLAB/Simulink.

Averaged three phase inverter

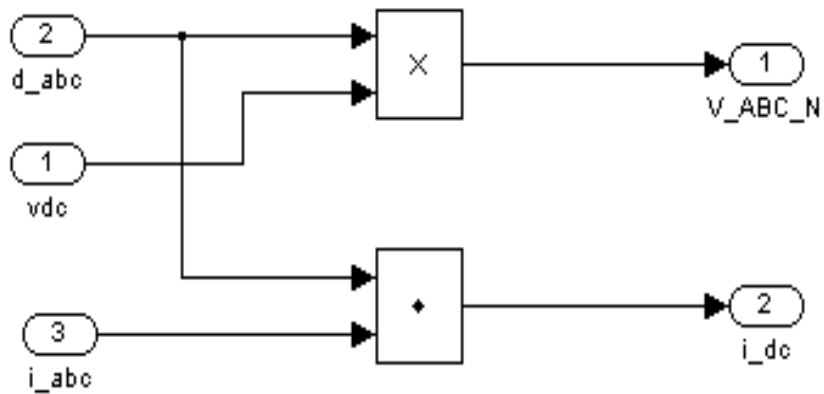


Fig. 2.9. Simulink block diagram representing the averaged three phase inverter.

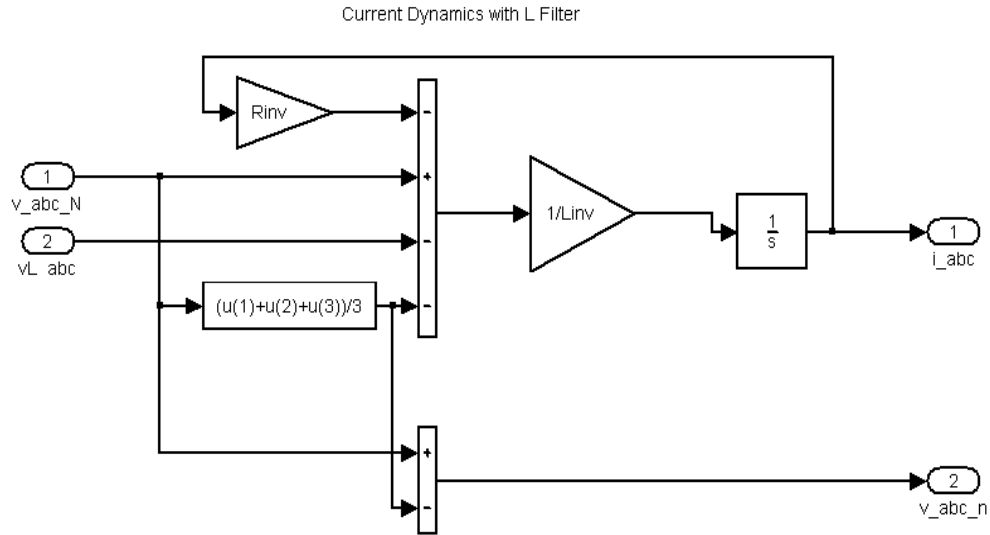


Fig. 2.10. Simulink block diagram representing L filter dynamics.

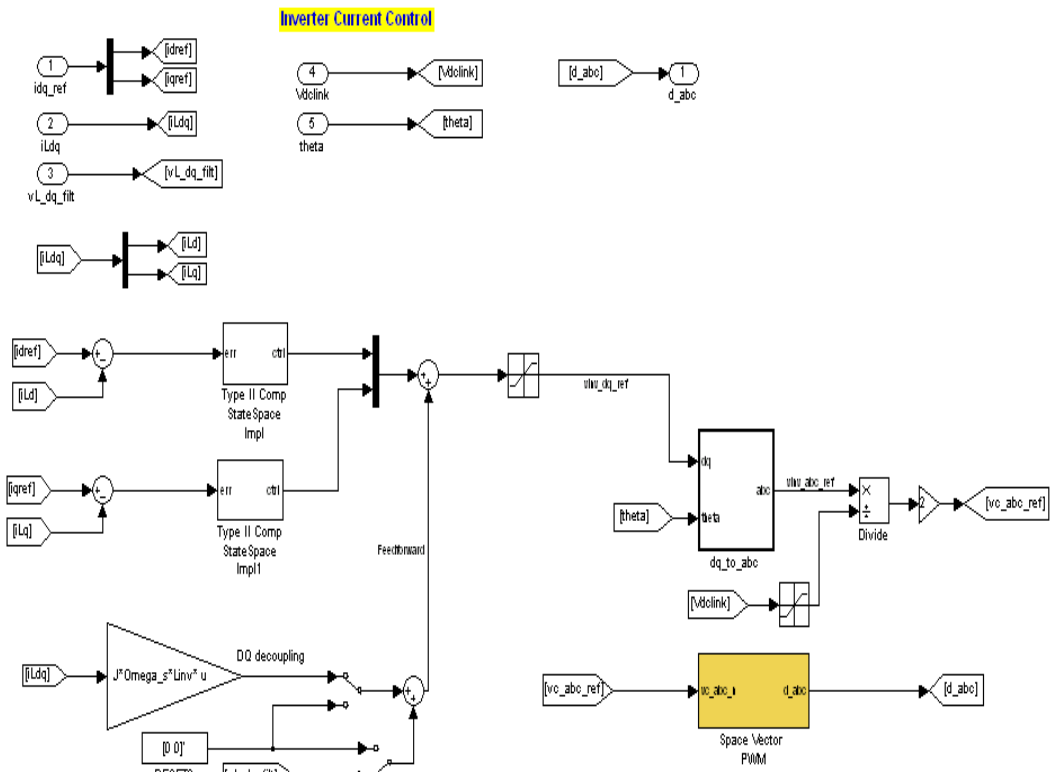


Fig. 2.11. Current controller block in MATLAB/Simulink.

Simulation results

Fig. 2.12 shows the three phase voltages, currents and real and reactive power waveforms in the grid connected mode. The inverter is supplying 100kW of real power and no reactive power. As mentioned earlier, dq based implementation is carried out which makes the controller implementation easy to use. Fig. 2.13 shows the d- and q-axis voltages along with the frequency of operation.

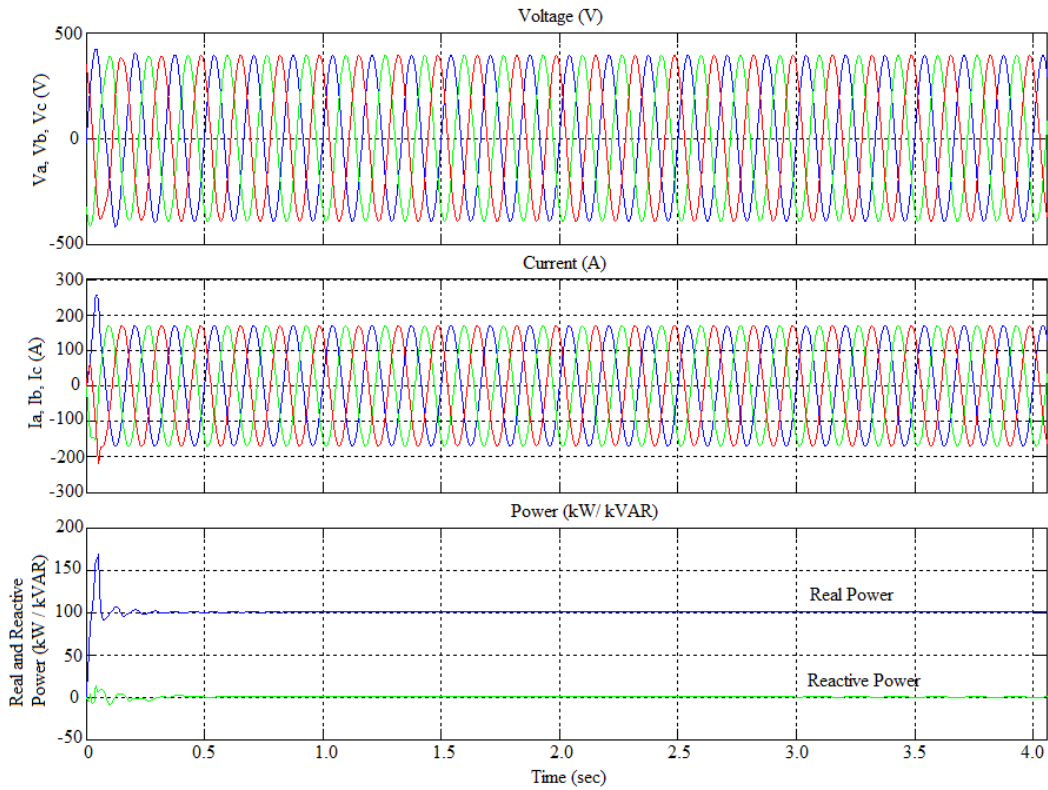


Fig. 2.12. Voltage, current and power waveforms for inverter in grid connected mode.

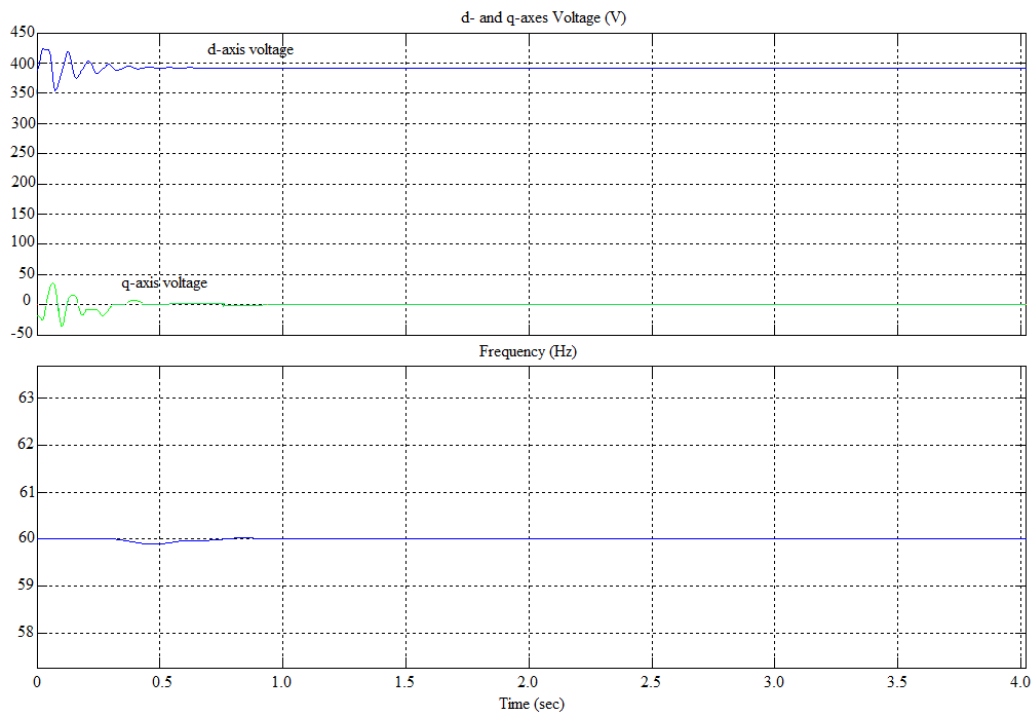


Fig. 2.13. V_d , V_q voltages and frequency waveform of inverter.

2.5 Summary

An average grid-tied three phase inverter was modeled in Simulink for the design specifications mentioned in Table 2.1. The inverter is based on a GE grid-connected inverter product. A constant DC voltage source was used as the DC link voltage in this model. A type II constant current controller was modeled based on K-factor approach. An L-only filter was included in the analysis. The ABC phase system was converted to the dq frame which reduces the three AC quantities to two DC quantities. This simplifies the calculations for control of the inverter and helps in the implementation of continuous feedback signal required for positive feedback anti-islanding techniques discussed in the next chapter. The inverter modeled helps in implementing these techniques.

CHAPTER 3

ANTI-ISLANDING TECHNIQUES

3.1 Introduction

The DG injects current into the system during a fault and needs to be isolated. It is necessary that the inverter identifies the islanding condition and ceases to energize within a specified time limit, for the purposes of personnel safety and equipment protection [12]. Islanding occurs when a portion of the distribution system becomes electrically isolated from the rest of the power system and remains energized. In present standards for DG, it is recommended that the inverter be shut down and then switched on after assessing the condition of the distribution system. In certain advanced architectures such as micro-grids or in the case of critical loads, the DG continues to energize the islanded subsystem to provide backup power and power quality. Most anti-islanding work has been targeted at single-phase inverters. Little work has been done for three-phase inverters. The objective of this chapter is to study and implement anti-islanding control for three-phase inverters. The techniques have been discussed in detail. The concept can be extended to single-phase inverters.

3.2 Anti-Islanding Schemes

The anti-islanding schemes are based on two concepts: Positive feedback and dq implementation, i.e., Park's transformation from ABC stationary coordinates to dq coordinates. Individually, these concepts are old but their combination leads to schemes which are effective and perform better than existing ones.

Positive feedback

All passive anti-islanding schemes have NDZs. Given the 100% power-matching test condition, any passive scheme will fail. Besides, passive schemes are normally subject to nuisance trips, if the settings are too aggressive in order to reduce NDZs. Some active schemes still have NDZ, if no positive feedback is used. Active controls, such as using positive feedback, should be used to guarantee no NDZs. The basic idea behind the positive feedback control is to drive away

the voltage and/or the frequency, once islanded. This positive feedback mechanism can be easily implemented in a three phase inverter with control in the dq frame.

The most difficult condition to detect absence of the electric utility is when the distributed energy system's output power is matched to the island load. In reference to Fig. 3.1, the worst-case condition is when $\Delta P=0$ and $j\Delta Q=0$. That is, at the moment of disconnect the utility is neither supplying nor absorbing real or reactive power. For this to be true, the parallel resonant circuit must be resonant at the line frequency. Higher the load quality factor, the more difficult is it to detect an island condition. Further discussions will consider this worst-case condition in which the load is a parallel RLC circuit is resonant at or near the line frequency. The quality factor equation of the parallel resonant RLC circuit was shown in (2).

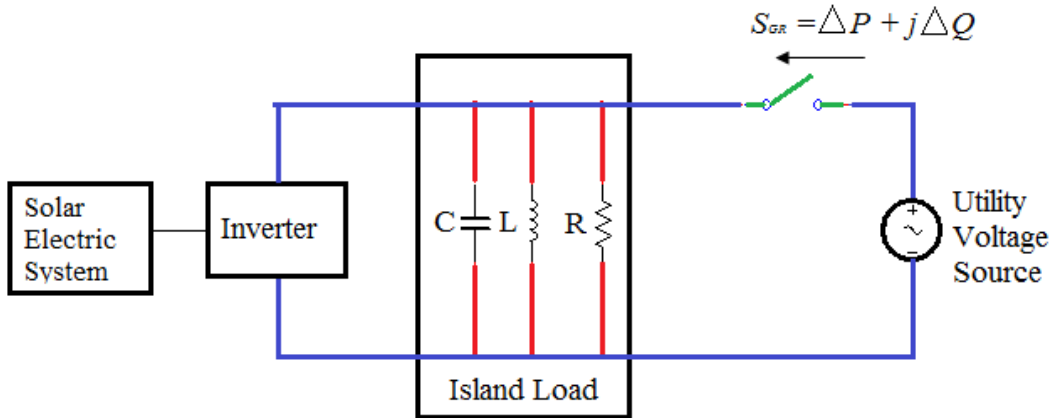


Fig. 3.1. Worst case island load

The relationships between the RLC load's active and reactive power and the voltage and frequency are:

$$P = V^2 / R \quad (3)$$

$$Q = V^2 (\omega C - 1 / \omega L) \quad (4)$$

Based on (3) and (4), two positive feedback mechanisms can be established. One is voltage (magnitude) feedback; the other is frequency (of the voltage) feedback.

In voltage feedback, when the inverter-sensed output voltage is increasing, the anti-islanding feedback will command the inverter active-power output to be increased. Due to the load characteristic in (3), the voltage will keep increasing in order to balance the active power. The increased voltage will further drive the inverter active power up due to the anti-islanding feedback. As a result, the voltage will be eventually out of the nominal ranges so that the islanding can be detected. Similar but opposite destabilization occurs when the sensed voltage is decreasing initially.

In frequency feedback, as the inverter-sensed frequency is increasing, the anti-islanding feedback will command the inverter reactive-power output to be increased. Due to the load characteristic in (4), the frequency will keep increasing in order to balance the reactive power. The increased frequency will further cause the inverter reactive power to increase due to the feedback. As a result, the frequency will be eventually out of the nominal ranges so that the islanding can be detected. A mirror image response, with similar destabilization, occurs when the sensed frequency is decreasing initially. This can apply to any DG system, including the multiple inverter based configuration and multiple machine based configuration.

dq implementation

There are two key concepts in the dq implementation. First, the active power is proportional to the d-axis components, and the reactive power is proportional to the q-axis components. Therefore, the active and reactive-power commands should feed into the d-axis and q-axis, respectively. Second, since the overall vector (voltage or current) is the synthesis of the d- and q- axes, changing one axis not only changes the magnitude of the vector, but also changes the angle between the d- and q- axes. This is shown in Fig. 3.2 where there is a change in angle due to increase in the d-axis voltage caused by a change in the current. The angle change will result in frequency change, because frequency is the derivative of the angle.

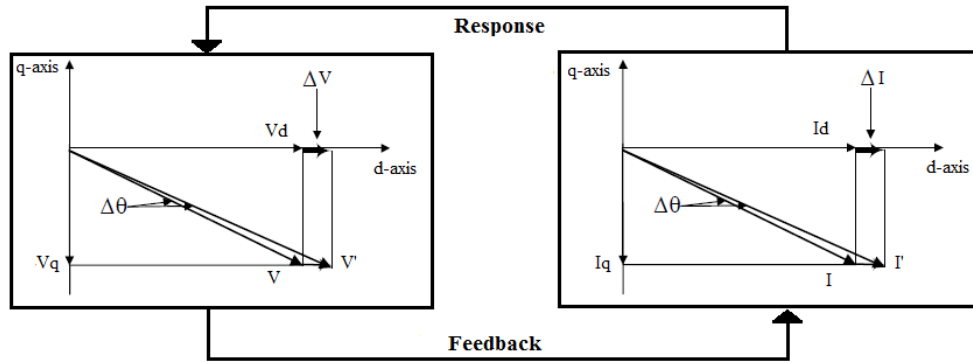


Fig. 3.2. Phasor diagrams showing a change in V_d causing both magnitude and angle change [12].

When the inverter-sensed and computed d-axis voltage is increasing, the anti-islanding feedback will command the inverter d-axis current reference to be increased. This will result in increased real power output. Due to the load characteristic in (3), the voltage will keep increasing in order to balance the active power. The increased voltage, and thus d-axis voltage, will further drive the inverter active power up due to the anti-islanding feedback. As a result, the voltage will be eventually out of the nominal range so that the islanding can be detected. This is the d-axis voltage feedback scheme. Similar but opposite destabilization occurs when the sensed voltage is decreasing initially. Fig. 3.3 shows the block diagram d-axis voltage feedback scheme.

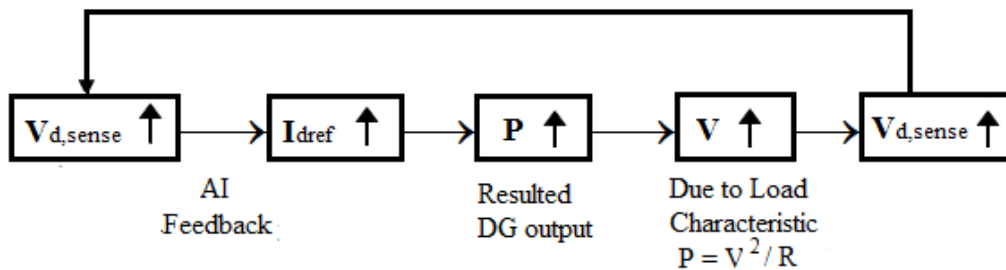


Fig. 3.3. Voltage positive feedback for island detection in dq implementation [12].

The anti-islanding feedback will command the q-axis current reference of the inverter to increase when the inverter-sensed frequency is increasing. This will result in increased reactive-power output. Due to the load characteristic in (4), the frequency will keep increasing in order to balance the reactive power. The increased frequency will further drive the inverter q-axis current,

and thus the reactive power up due to the anti-islanding feedback. As a result, the frequency will be eventually out of the nominal range so that the islanding can be detected. This is the frequency-feedback scheme. Again, destabilization also occurs when the sensed frequency is decreasing initially. This scheme is shown in Fig. 3.4.

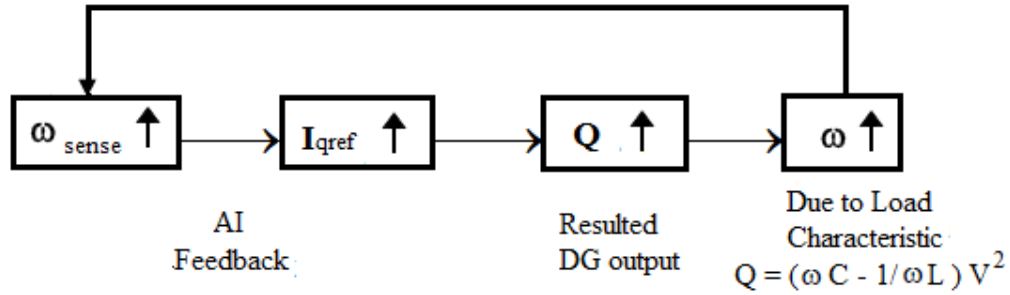


Fig. 3.4. Frequency positive feedback in dq implementation [12]

The difference between voltage and frequency feedback implementation is that, due to dq implementation in voltage feedback, both voltage and frequency is driven. As shown in Fig. 3.2, driving d-axis will impact both the vector length and angle. The angle change will result in frequency change. When the inverter is operating at unity power factor, the angle will not change as the voltage has only a d-axis component. Besides the feedback described above, the dq implementation can generate a family of schemes by using different feedback paths, for example, from V_d to $I_{d\text{ref}}$, from V_d to $I_{q\text{ref}}$, from V_q to $I_{d\text{ref}}$, from V_q to $I_{q\text{ref}}$, from ω to $I_{d\text{ref}}$, and from ω to $I_{q\text{ref}}$. As long as the feedback paths can establish the basic mechanisms of voltage and frequency feedback, the positive feedback will work as AI control. The multiple-path feedback in dq frame is the second basic concept of the GE AI schemes. Based on these concepts, a new family of anti-islanding schemes has been implemented.

Two typical schemes are defined: the voltage scheme and the frequency scheme. Because of positive feedback in dq implementation, the inverter, once islanded, will drive voltage or frequency out of nominal ranges so OV/UV relay or OF/UF relay protection can be tripped. Combined with time-delay settings of OV/UV and OF/UF, the anti-islanding schemes can successfully

ride through temporary low voltage without false trip yet detect islanding once the grid is actually lost. There is a requirement that the DG must stay on the grid when there is a large abnormal grid event. The event may cause the voltage to be lower than the normal ranges for an extended period of time. Traditional under/over voltage/frequency protection cannot reliably achieve both LVRT and anti-islanding protection. With these schemes, the problem of LVRT is solved. It is seen that even if there is a grid disturbance, the anti-islanding schemes continue to work efficiently and don't trip the circuit. For this to happen, the OV/UV and OF/UF relay settings need to be relaxed or else they will trip the circuit during such conditions.

Voltage schemes

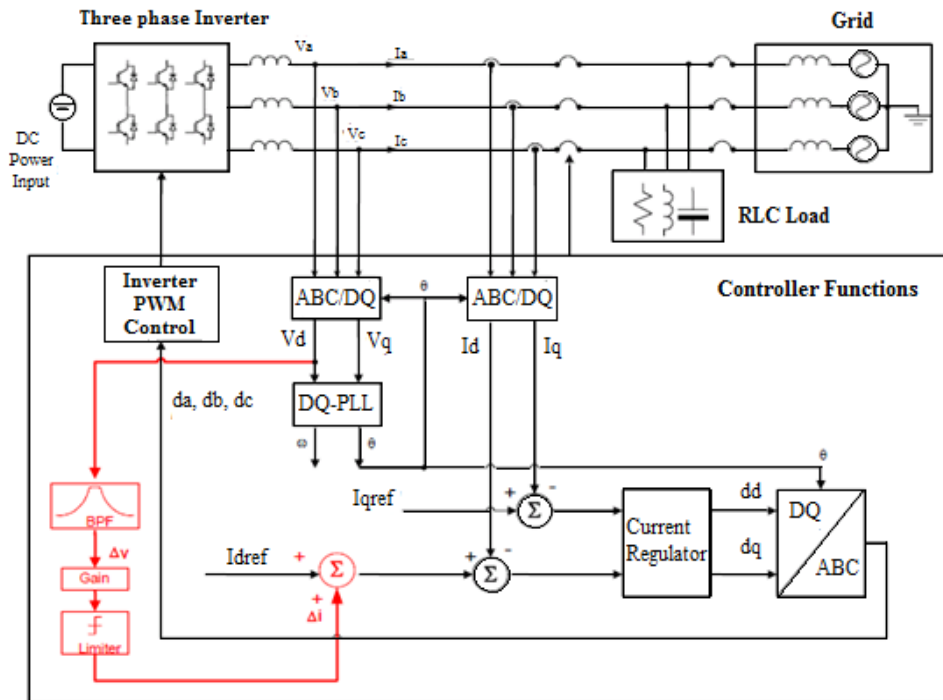


Fig. 3.5. Block diagram of the voltage based island detection scheme with V_d to I_{dref} positive feedback [12].

In this scheme, V_d is passed through a BPF, a gain and a limiter and produces a current variation Δi which is added to I_{dref} . This is shown in Fig. 3.5. This addition in d-axis current consequently increases the voltage and drives it out of limits during an islanding situation. The

OV/UV relays trip the circuit and switches off the inverter. Other voltage schemes involve V_d to I_{qref} , V_q to I_{dref} and V_q to I_{qref} .

Frequency schemes

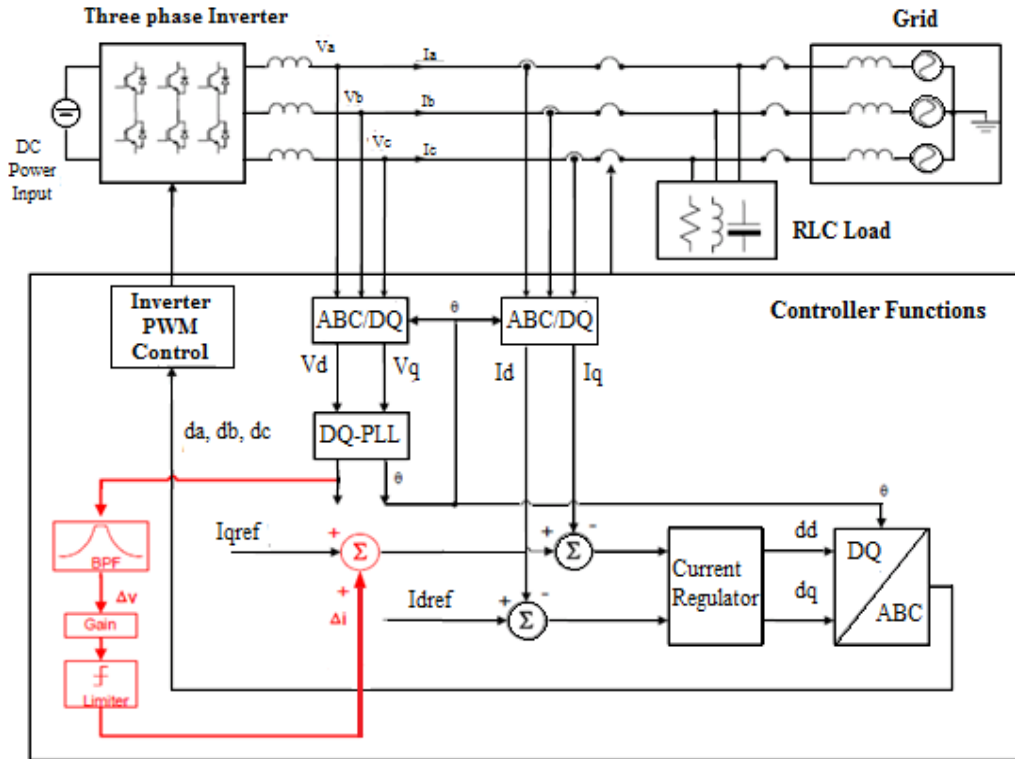


Fig. 3.6. Block diagram of the frequency based island detection scheme with ω to I_{qref} positive feedback [12].

Similar to the voltage scheme, the frequency scheme comprises of the frequency ω being passed through the BPF, gain and limiter to produce a current variation which is added to I_{qref} . Fig. 3.6 shows this scheme. A modification of this scheme is the addition of the current variation to I_{dref} .

There are two critical design criteria for the gain. A higher gain indicates that larger disturbance becomes added to real power output of the inverter for the same amount of voltage variation. In island condition, a higher gain will positively contribute to anti-islanding, whereas, in grid-tied condition, a lower gain will mitigate negative impacts on the grid. For the lower bound,

the BPF gain must be large enough to destabilize system voltage in island condition to be out of the specified thresholds. Here, the lower bound is defined as the lowest value at which the islanded system starts being destabilized. For the upper bound, the gain must be small enough to limit the real power variation due to a step change of feeder voltage in grid-connected condition within a pre-set value specified by a system designer or user. The reason for using a BPF is to avoid noise injection (low-pass needed) and DC offset (high-pass needed) caused by an anti-islanding loop. The noise will cause power-quality problems, and the DC offset will impact the steady-state reference tracking. Because of these two conflicting requirements, an appropriate band with both high-frequency noise and low-frequency offset performance must be traded off. Given the 2-second anti-islanding protection requirement, a 1–10Hz (0.1s–1s response time) BPF is chosen for the design. The limiter function is to specify the maximum allowable current injection. There are two factors that determine the limiter settings. One is the inverter over-current capability. The other is the maximum allowable power factor, if injecting the current to I_{qref} . In the design, 150% current and 0.8 power factors are assumed as limits.

3.3 Simulink Model of Anti-Islanding Techniques

The anti-islanding techniques described were implemented in the three phase grid-tied PV inverter model in Simulink. Two blocks were created which simulated the voltage and frequency feedback schemes. Fig. 3.7 through Fig. 3.9 shows the implementation of the gain, filter and limiter configuration.

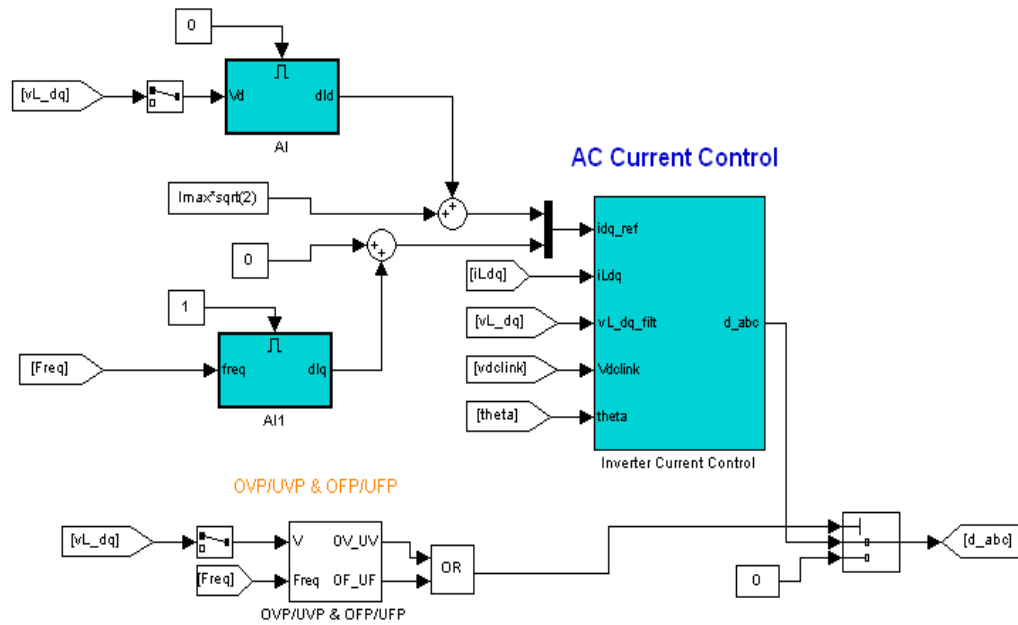


Fig. 3.7. Simulink model of feedback mechanism for V_d to I_{dref} and ω to I_{qref} with OV/UV and OF/UF protection.

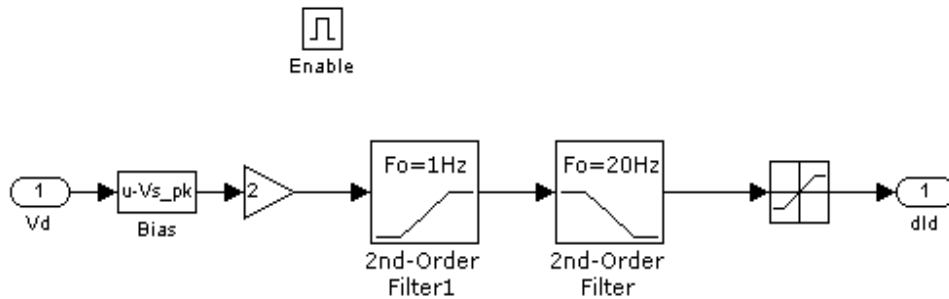


Fig. 3.8. Blocks representing the voltage feedback scheme.

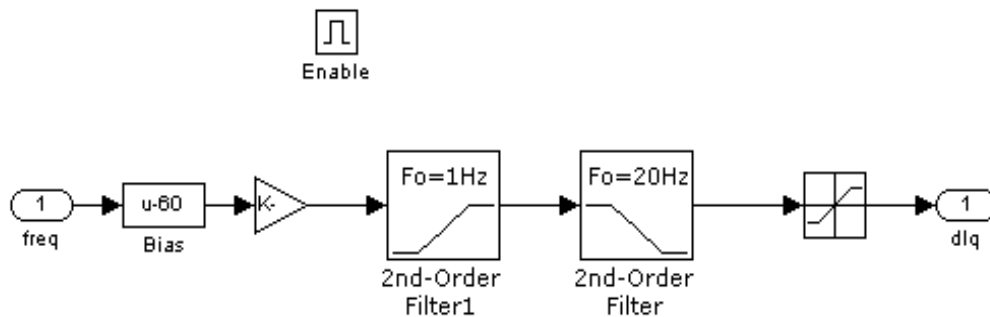


Fig. 3.9. Blocks representing the frequency feedback scheme.

In order to cut off the inverter from the grid, OV/UV relays and OF/UF relays were used. According to IEEE 929-2000, whenever the inverter starts operating beyond the threshold values mentioned in chapter 2, these relays switch on and trip the circuit. The Simulink model of this is shown in Fig. 3.10.

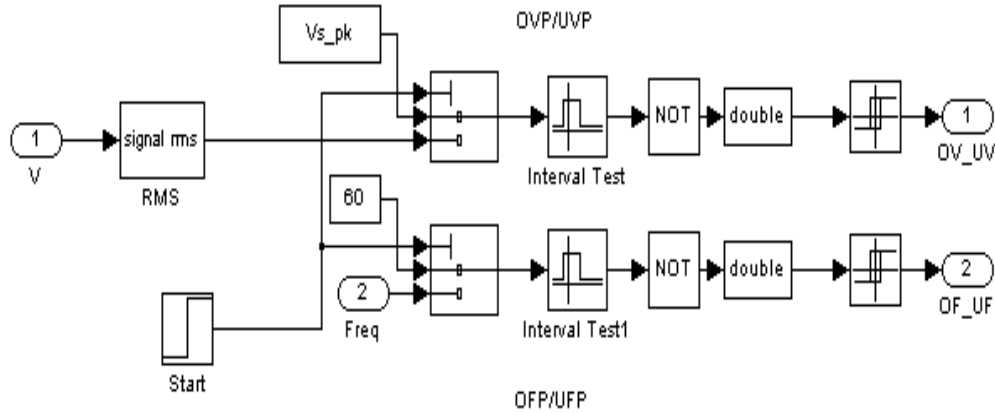


Fig. 3.10. Implementation of over voltage/under voltage and over frequency/under frequency protection in Simulink.

3.4 Anti-Islanding Results

In order to test the effectiveness of the anti-islanding techniques considering that the three phase inverter is connected to the grid as shown in Fig. 2.4, an islanding condition is simulated where the breaker is opened at time $t=1$. The gain of the AI system, which determines the speed at which the system responds to any undesirable transient behavior, was found using trial and error. The anti-islanding techniques implemented were the V_d to I_{dref} and V_d to I_{qref} voltage scheme, the ω to I_{qref} frequency scheme and a combined voltage and frequency scheme.

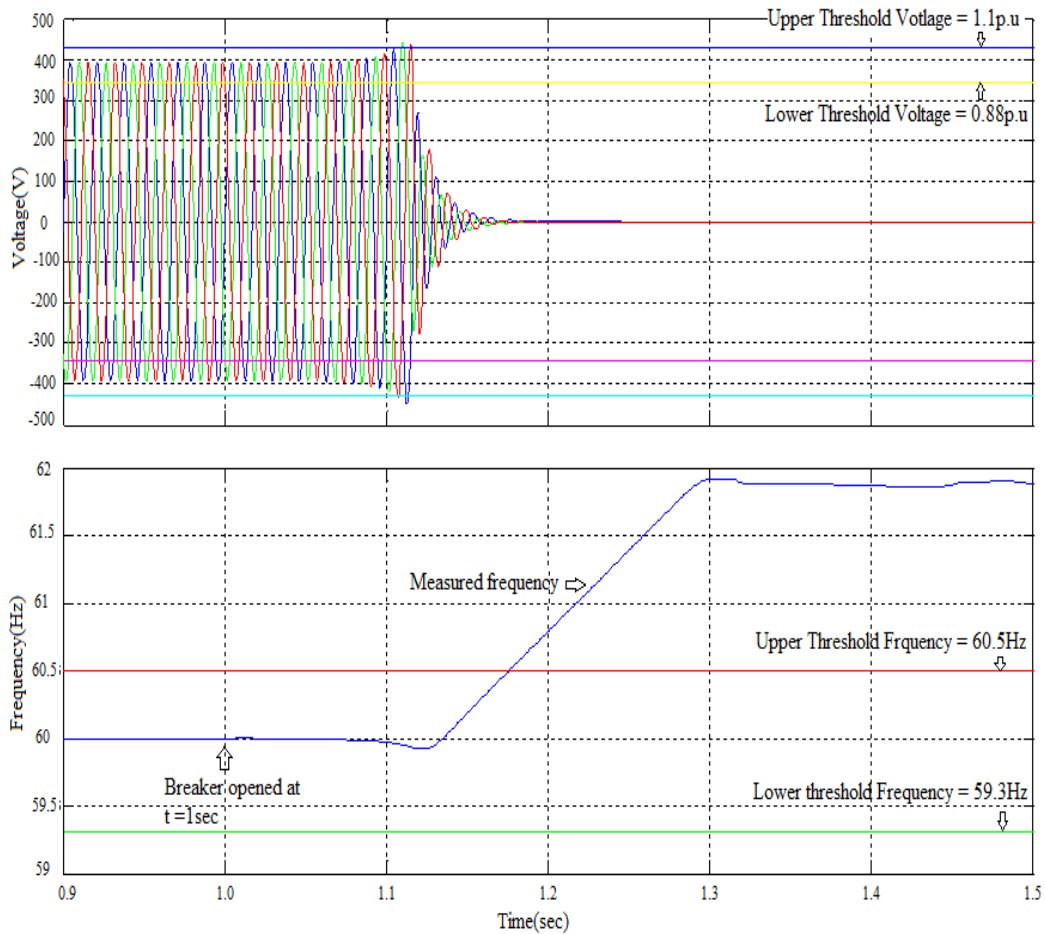


Fig. 3.11. Voltage and frequency waveforms corresponding to the voltage based island detection scheme with V_d to I_{dref} positive feedback

Fig. 3.11 shows the V_d to I_{dref} voltage scheme. It is seen that after about 0.133 second of the breaker opening, the voltage goes beyond the specified limits and the OV relay functions to island the inverter from the grid. The inverter switches off in less than 0.2 second of the fault occurrence which is well within the standard.

Fig. 3.12 shows the ω to I_{qref} voltage scheme. Once the breaker is opened, the frequency is seen to start deviating from 60Hz. At after 0.7 second of the breaker opening, the frequency is seen to go out of bounds by crossing the upper threshold value. When this happens, the OF relay trips the circuit and islands the system. The inverter is switched off. Fig. 3.13 depicts the V_d to

Iqref scheme. Similar to the other voltage scheme, once the positive feedback pushes the voltage beyond the limits after the breaker is opened, the system is islanded and the inverter is switched off. The functioning of the system when both the voltage and frequency schemes are on is shown in Fig. 3.14. The trip time is seen to be equal to 0.133 second which is same as the voltage scheme.

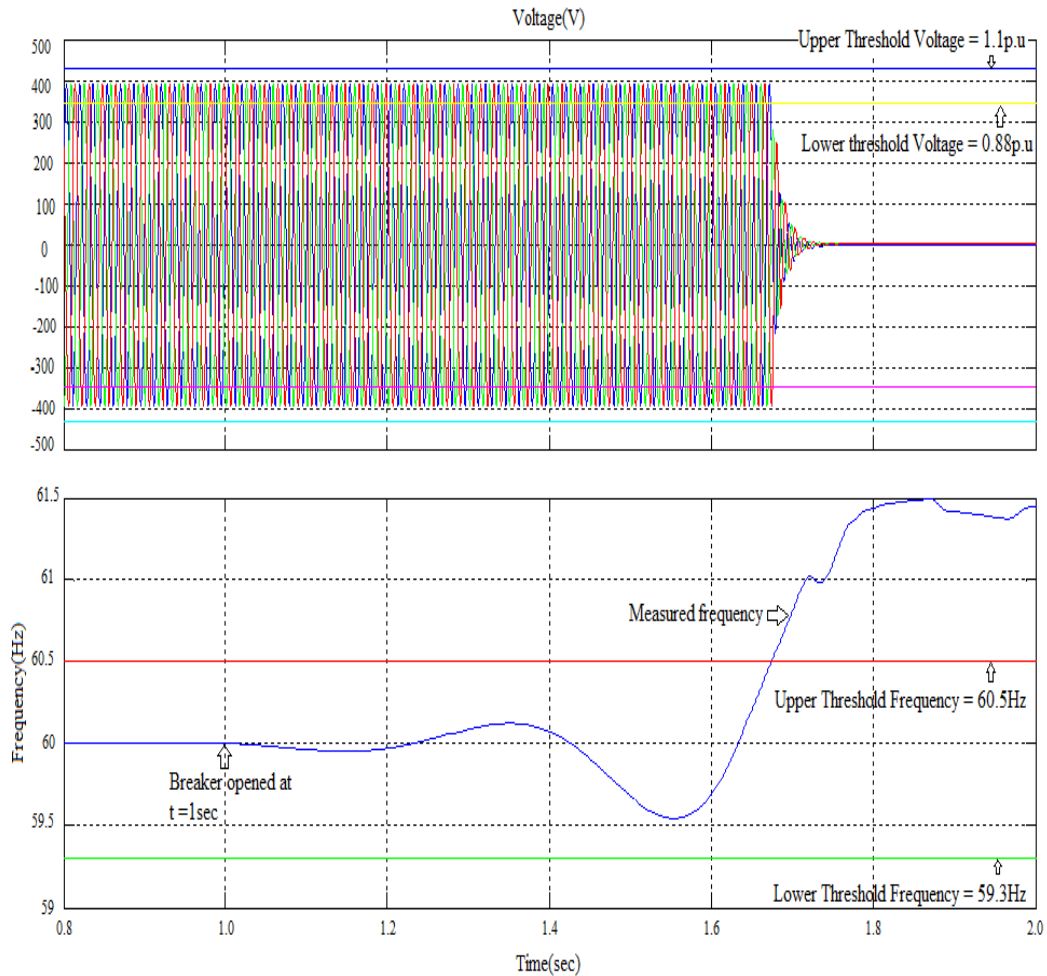


Fig. 3.12. Voltage and frequency waveforms corresponding to the frequency based island detection scheme with ω to Iqref positive feedback

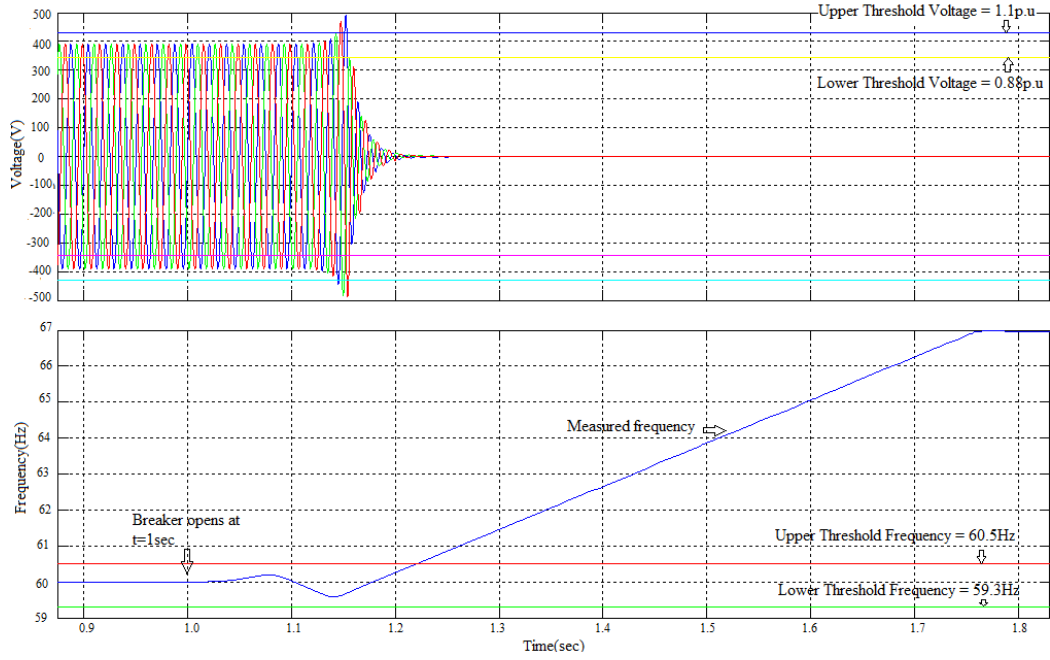


Fig. 3.13. Voltage and frequency waveforms corresponding to the voltage based island detection scheme with V_d to I_{qref} positive feedback

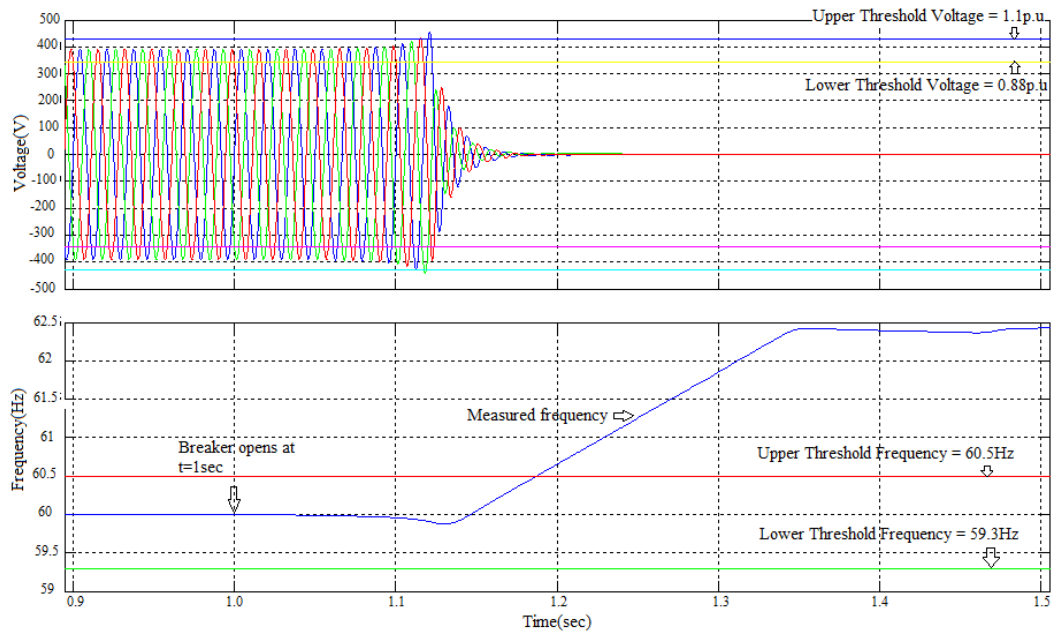


Fig. 3.14. Voltage and frequency waveforms corresponding to the combined island detection scheme with V_d to I_{dref} and ω to I_{qref} positive feedback

Fig. 3.15 depicts a LVRT event. The grid disturbance occurs at $t=0.4$ seconds and last till $t=0.7$ sec. An islanding event occurs at $t=1$ s where there is a grid failure. It is seen that the voltage feedback anti-islanding schemes are capable of differentiating between an LVRT event and an islanding event. When the low voltage event occurs, the frequency oscillates and then comes back to normal frequency. This is not the case when an island occurs. It is seen that the measured frequency deviates away from the nominal grid frequency. Once the low voltage event is over, normal grid voltage and frequency is restored. The OV/UV and OF/UF relays had been disabled to see the difference in response of the inverter for a grid disturbance and grid failure. The LVRT requirement indicates that simple application of under- and over-voltage tripping may not result in adequate discrimination between islanding and grid disturbances. This further implies that OV/UV is not appropriate for islanding protection. Dedicated anti-islanding protection, such as the schemes discussed is needed and these will not cause adverse impact on the low-voltage-ride-through.

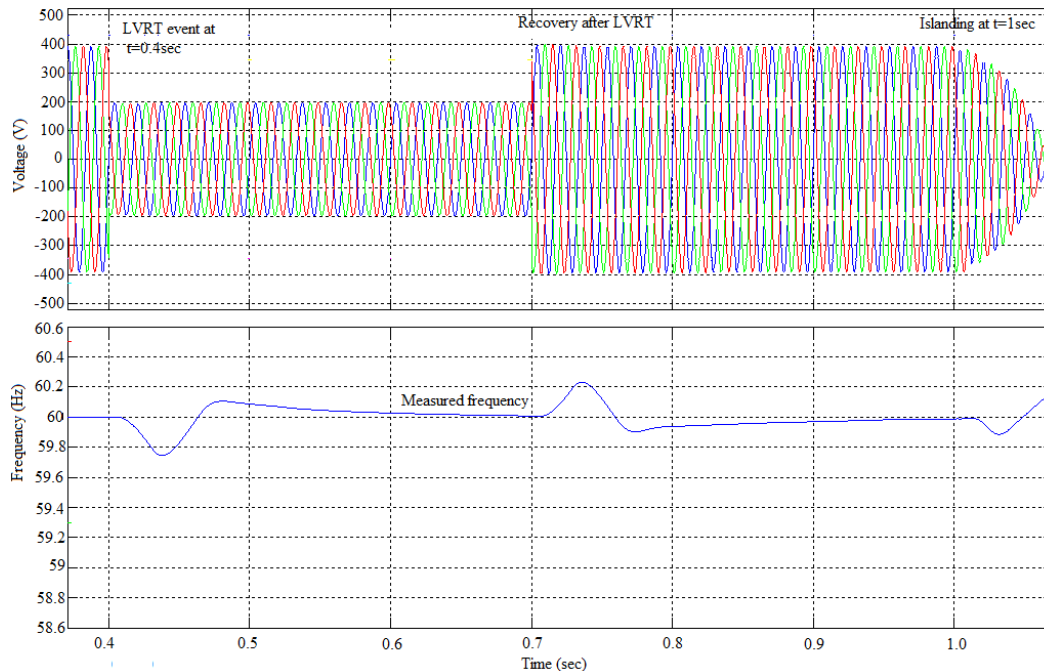


Fig. 3.15. Voltage and frequency waveforms corresponding to the voltage based island detection scheme with V_d to I_{dref} positive feedback for a LVRT event

3.5 Summary

It was seen that with the recommended anti-islanding parameter settings which include the worst case generation/load balance mentioned in IEEE 929-2000 and UL 1741 [35], the schemes work effectively and trip within 2 seconds. It was also seen that with the gain reduced to a certain level, the positive feedback was not effective. This indicates that even if a positive feedback control is employed, there is a critical gain below which the positive feedback control will fail to detect unintentional islanding and result in certain NDZ. Another finding was that when both voltage and frequency anti-islanding schemes are enabled, tripping time was not faster which possibly indicates some interaction between the schemes. Hence, for a more predictable performance, it is recommended that only one scheme be used. A complete review of anti-islanding schemes indicated that other solutions are too expensive (e.g., transfer trip), not secure (e.g., NDZ), or cause power quality degradation (waveform distortion). Overcoming these problems are the described family of anti-islanding controls which are low-cost, certain, robust to grid disturbances and has negligible power quality effect.

CHAPTER 4

POWER FLOW MODEL

4.1 Introduction

In power engineering, the power flow study is an important tool which involves numerical analysis applied to a power system. A power flow study usually uses simplified notation such as a one-line diagram and per-unit system. It analyzes the power systems in normal steady-state operation. There exist a number of software implementations of power flow studies. Some application in distribution automation and distribution management like VAR planning, switching, state estimation and especially optimization need repeated power flow solutions. In these applications it is imperative that power flow be calculated as efficiently as possible.

The objective of a power flow is to analyze the steady-state performance of the power system under various operating conditions. It is the basic analysis tool for the planning, design and operation of any electrical power systems. These could be distribution, industrial or transmission networks. The basic power flow question for a known power system is to find the voltage magnitude and phase angle at each bus and the power flow through each line and transformer given the load power consumption at all buses and the power production at each generator.

The solution to the power flow problem begins with identifying the known and unknown variables in the system. The known and unknown variables are dependent on the type of bus. A bus without any generators connected to it is called a load bus. With one exception, a bus with at least one generator connected to it is called a generator bus. The exception is one arbitrarily-selected bus that has a generator. This bus is referred to as the slack bus. In the power flow problem, it is assumed that the real power and reactive power are known at each load bus. For this reason, load buses are also known as PQ buses. For generator buses, it is assumed that the real power generated and the voltage magnitude is known. Hence these are known as PV buses. For the slack bus, it is assumed that the voltage magnitude and voltage phase are known. For each load bus,

both the voltage magnitude and angle are unknown and must be solved. The voltage angle must be found for each generator bus. There are no variables that need to be solved for the slack bus.

The method of symmetrical components is used to simplify analysis of unbalanced three phase power systems under both normal and abnormal conditions. Symmetrical components are balanced three-phase vectors derived from the unbalanced phase vectors in a three phase electric system. An unbalanced three phase system of voltages or currents can be regarded as due to two symmetrical three phase systems having opposite phase sequence and a system of zero phase sequence. If there is a path for flow of positive sequence current, then there is a path for negative sequence current, and this is because both are similar, but in case of zero sequence components to flow, then a fourth wire is necessary in the system. Hence, a set of unbalanced 3-phase line to line voltages may be represented by a positive and a negative sequence system of balanced voltages, which are known as symmetrical components.

4.2 Data Acquisition for the ASU Distribution System

It is important to use real distribution system data as test beds in order for the proposed research work to have good practical significance. The ASU Tempe campus distribution system is chosen as a representative distribution system for large institutions. The ASU system so far has the largest PV installation among all universities in the United States, with 2 MW existing installation. Further, ASU has aggressive plans for future PV installation, with 2.5 MW capacity in construction and 4.6 MW capacity planned for sites being reviewed for 2010/2011. Thus, the ASU distribution system is a good test bed for the study of impact of PV generation on distribution systems. This section gives some brief description of the data obtained for the ASU distribution system, including the system physical data, PV installation physical data and the historical load and PV generation data from the EIS.

ASU distribution system map and one-line diagram

The ASU distribution system physical data was received from ASU Central Plant and APSES in the form of a system map and a one-line diagram. The system map shows the physical locations of the plants/stations, transformers, and the 4-pole Kearney switches, and the routing of the feeder cables. Fig. 4.1 shows this map, with the locations of the existing PV installations labeled. The one-line diagram shows the electrical connections and cable type, parameters for the transformers (kVA rating, high side and low side voltages and connection type, and impedance in percent) and ratings for the circuit breaker. Fig. 4.2 shows a portion of this one-line diagram.

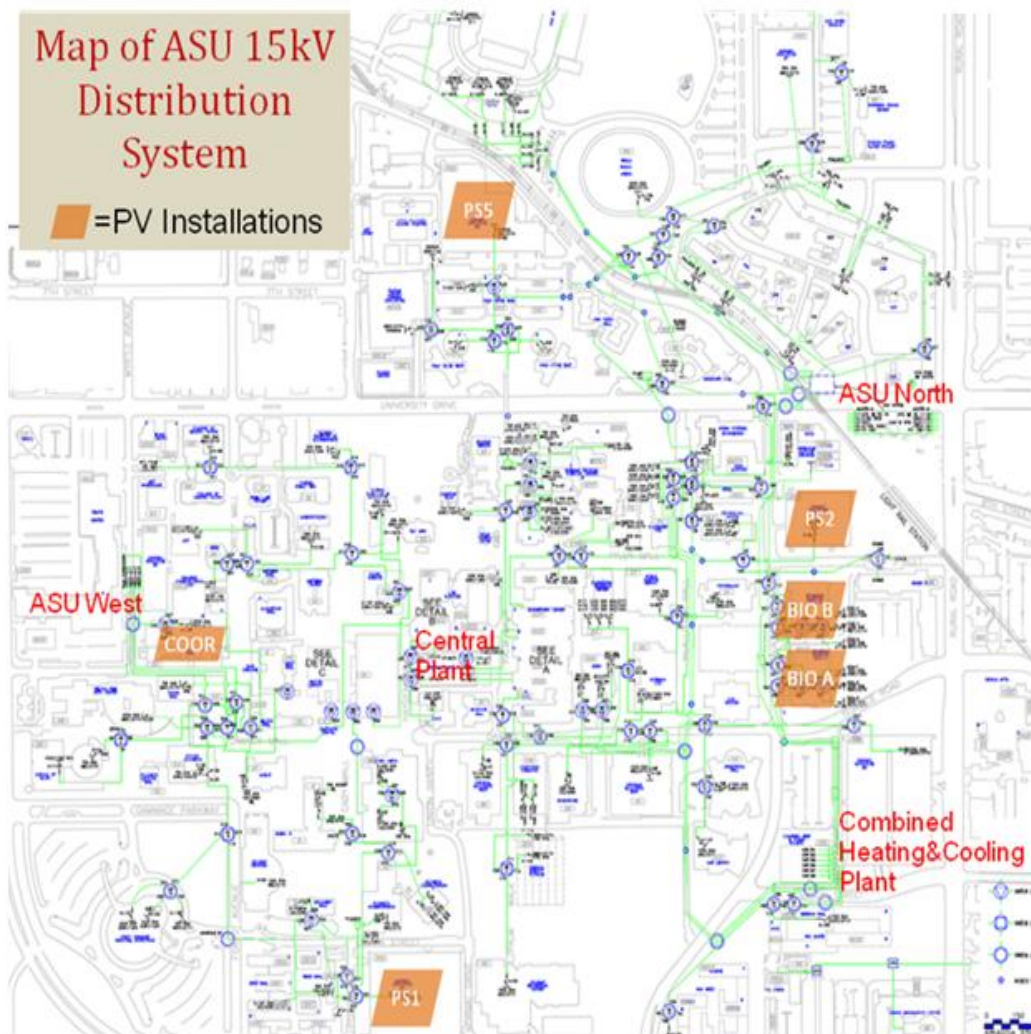


Fig. 4.1. Map of ASU 15 kV distribution system, with existing PV installations labeled.

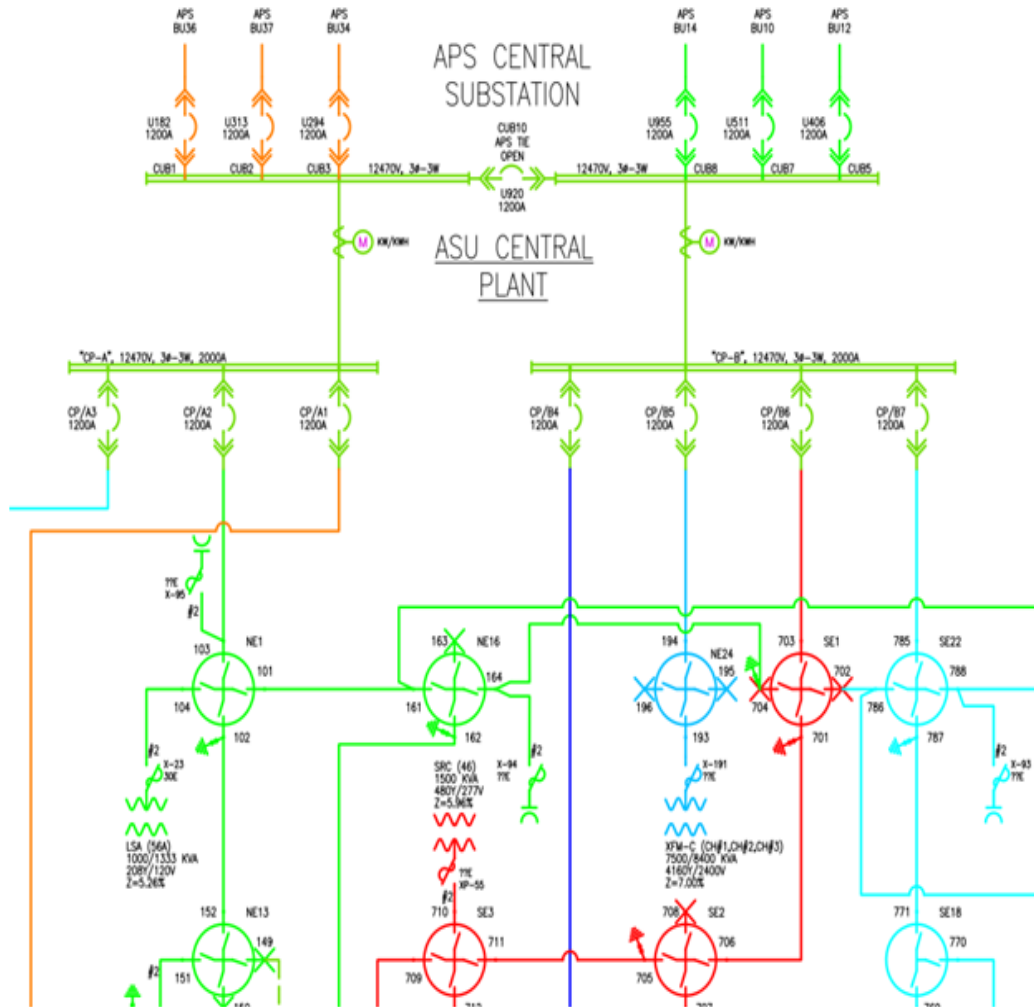


Fig. 4.2. A portion of the one-line diagram of the ASU 15 kV distribution system.

The power distribution system of ASU Tempe campus can be divided into four substations, namely, ASU West, ASU Central, ASU North, and ASU South or the ASU Combined Heating and Cooling Plant. They are supplied by different APS 15 kV feeders. At normal conditions, these four substations are not interconnected. However, lines exist that can be put into service at abnormal conditions to support excess load, e.g., to interconnect a part to its neighbor during an outage of its supplying feeder.

ASU PV physical data

Diagrams for the PV systems at parking structure 1 and parking structure 5 were received from ViaSol Energy Solutions. These diagrams contained information such as physical data of the devices (e.g. PV modules, inverters, switches, circuit breakers, transformers, cables) as well as the electrical connections. Fig. 4.3 shows a simplified diagram of the PV system at parking structure 1. The PV system has a concentrated PV array configuration. All the PV panels (modules) are first connected in series to make PV strings, with 15 modules in each string. Then the PV strings are connected in parallel to make PV arrays. Each array is then connected to an inverter. At parking structure 1, there are 288 strings, which have a total capacity of approximately 815 kW. Four 250 kVA GT-250 inverters are used; each converts the DC power from an array consisting of 72 strings. Appendix A shows the list of PV generation sites in the Tempe campus with their kW ratings and status of construction.

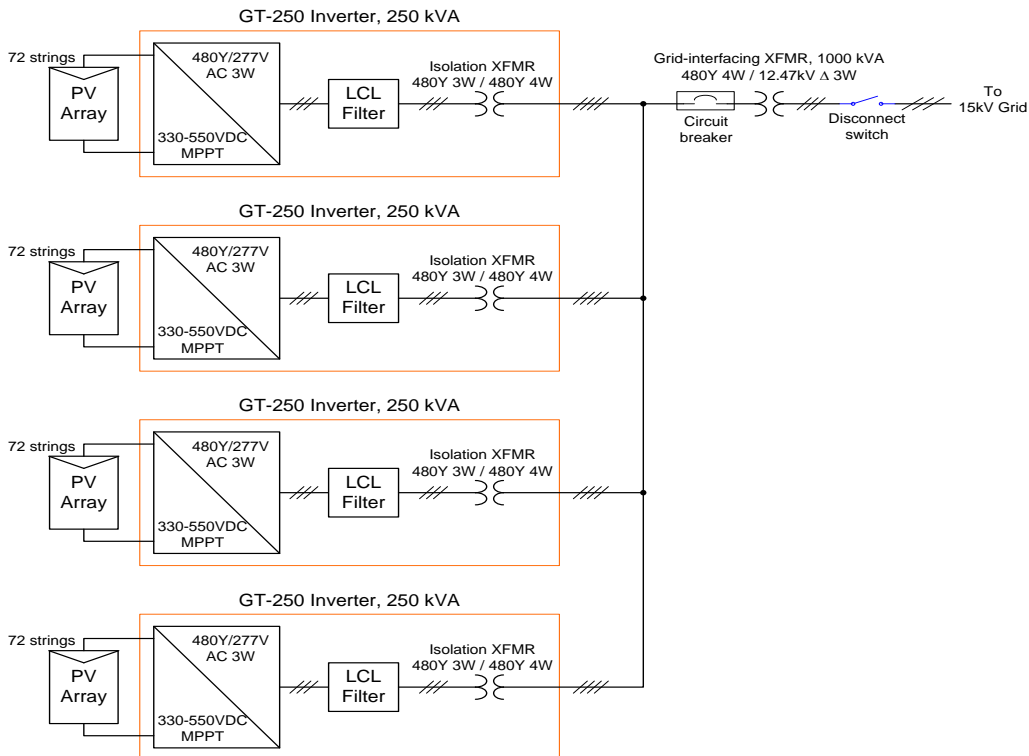


Fig. 4.3. A simplified diagram of the PV system at ASU parking structure 1.

The PV system at parking structure 5 has a configuration similar to that at parking structure 1, but it has only 234 strings and use three GT-250 inverters. Table 4.1 and Table 4.2 show the PV module specifications data and the PV string specifications data, respectively. These data will be used later for detailed PV generator modeling.

TABLE 4.1
SOLAR MODULE SPECIFICATION

Module manufacturer, Model	SunTech STP210-18/Ub-1
Max power, STC	210 W
Max power, PVUSA	188.5 W
Max power voltage, Vmp	26.4 VDC
Max power current, Imp	7.95 A
Open circuit voltage, Voc	33.6 VDC
Short circuit current, Isc	8.33 A
Max series fuse	20 A

TABLE 4.2
SOLAR STRING CIRCUIT SPECIFICATION

Modules per string	15
Max power, STC	3,150 W
Max power, PVUSA	2,827 W
Max power voltage, Vmp	396 VDC
Max power current, Imp	7.95 A
Open circuit voltage, Voc	504 VDC
Short circuit current, Isc	8.33 A

ASU load data and solar generation data from EIS website—EIS data

The ASU load data and the solar generation data were obtained through limited access to the Energy Information System (EIS) website controlled by ASU central plant. This website displays the real-time monitoring data, which are updated every minute. These one-minute-interval data are saved only for the previous one hour. Beyond that, 15-minute-interval historical data are available, and downloadable to Excel files. The PV generation data are only available starting from 3/9/2009.

Fig. 4.4 shows one-day EIS data for the load at ASU Engineering Research Center, and Fig. 4.5 shows one-day EIS data for solar generation at parking structure 1, both on 8/20/2009. How-

ever, not all the building loads in the Tempe campus are monitored. For those loads that are not monitored, simulated data was created and used in the power flow studies. The correspondence between the EIS data and the loads in the system model (as represented by the one-line diagram) is not straight forward. Engineering judgment was used when rendering the EIS data on the system.

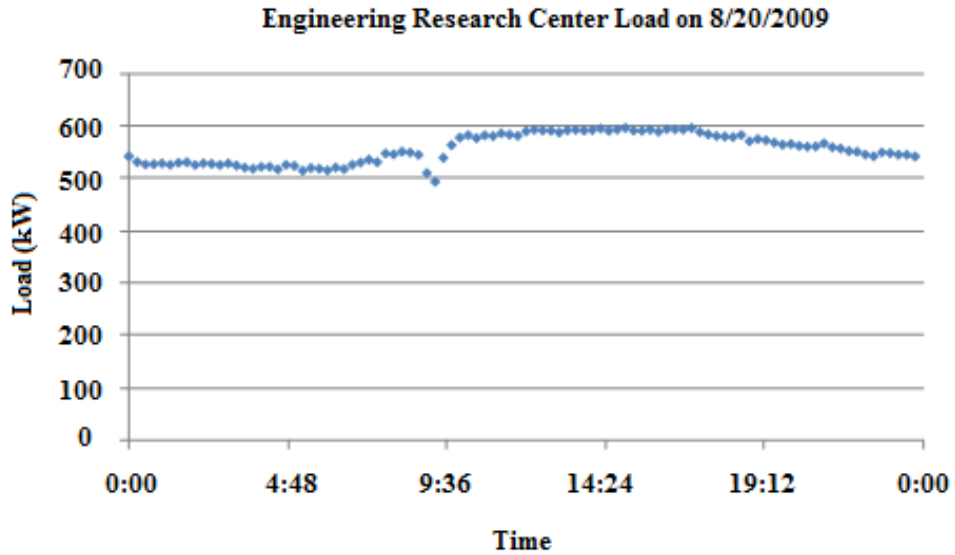


Fig. 4.4. EIS load data for ASU Engineering Research Center on 8/20/2009.

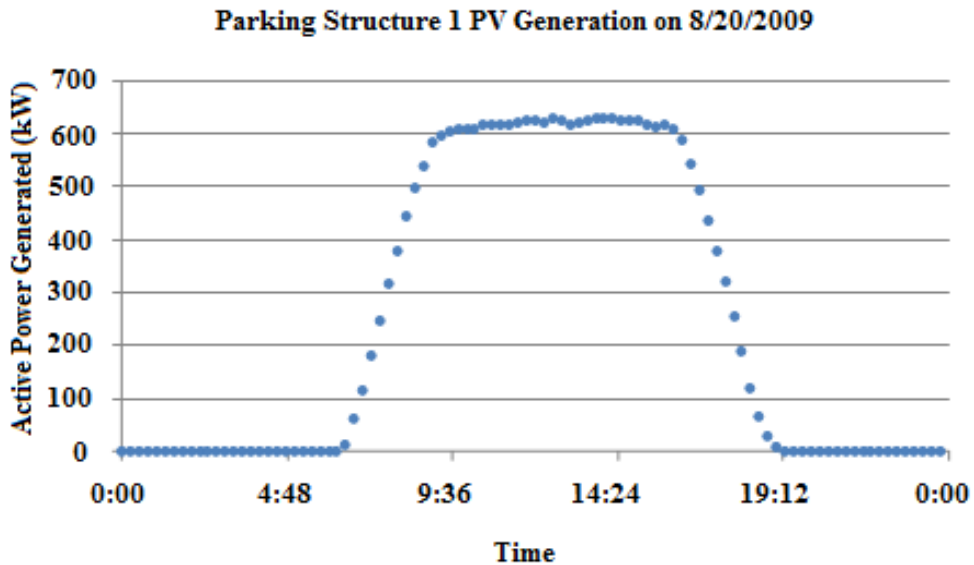


Fig. 4.5. EIS solar generation data for ASU parking structure 1 on 8/20/2009.

Impedances of the APS grid

For the study of the ASU distribution system, the APS grid is modeled as a Thevenin equivalent model, i.e., voltage source in series with equivalent impedance. Since the ASU distribution system has four separate parts, each supplied by a separate set of feeders, a Thevenin model is used for each set of feeders. The Thevenin equivalent impedances were calculated based on a document given by APS. This document has the impedances of the feeders and transformers that feed the ASU West, and fault duties on the buses that feed the other parts of the ASU system.

4.3 Development of a Model in PowerWorld for the Entire ASU Distribution System

PowerWorld Simulator® has been used for the ASU distribution system study. It has a good graphical user interface such as interactive one-line diagram drawing, animated power flow labeling, contour plots for voltage profile, market price and GIS support [36]. It supports imports from and exports to Excel, and has an auxiliary script language, which makes it easier to interface with other software tools.

Creation of the system model

To create a model for the ASU distribution system in PowerWorld, the impedances of all the lines and transformers are needed. The one-line diagram provides impedance percentages for each transformer, which was converted to the per unit value. However, for the lines, only the cable types are provided. All the lines on the map had to be traced to measure their lengths. This was done using PDF Xchange Viewer. The parameters of the cables were found from [37] (as listed in Table 4.3). The impedance of each line was calculated and entered in PowerWorld.

TABLE 4.3
CALCULATED IMPEDANCE VALUES FOR CABLE TYPES IN ASU DISTRIBUTION SYSTEM

Size(AWG)	Resistance at 90°C (Ω/ft)	Reactance (Ω/ft)	Capacitance (μF/ft)
#2	0.202	0.105	0.047
#1/0	0.127	0.099	0.055
#1/0AL	0.206	0.102	0.051
#2/0	0.102	0.097	0.059
#4/0	0.0635	0.092	0.07
#350	0.0385	0.085	0.085
#500	0.027	0.082	0.098
#750	0.018	0.077	0.116

The buses where PV generators are connected were modeled as PQ buses since PV generators do not regulate the bus voltage. In PowerWorld, this was done by modeling the PV generators as conventional generators, but with AVR disabled so that the injected real and reactive powers are constant and known. Fig. 4.6 shows the PowerWorld model of the entire ASU distribution system, which is built according to the one-line diagram. Fig. 4.7 through Fig. 4.10 shows the West, Central, North and South parts, respectively. There are two synchronous generators for the central, north and south substations. These have been marked as CP-A and CP-B for the central feeder, NORTH-A and NORTH-B for the generators located in the north substation and CHP-A and CHP-B for the south substation. The West substation has one 69 kV generator.

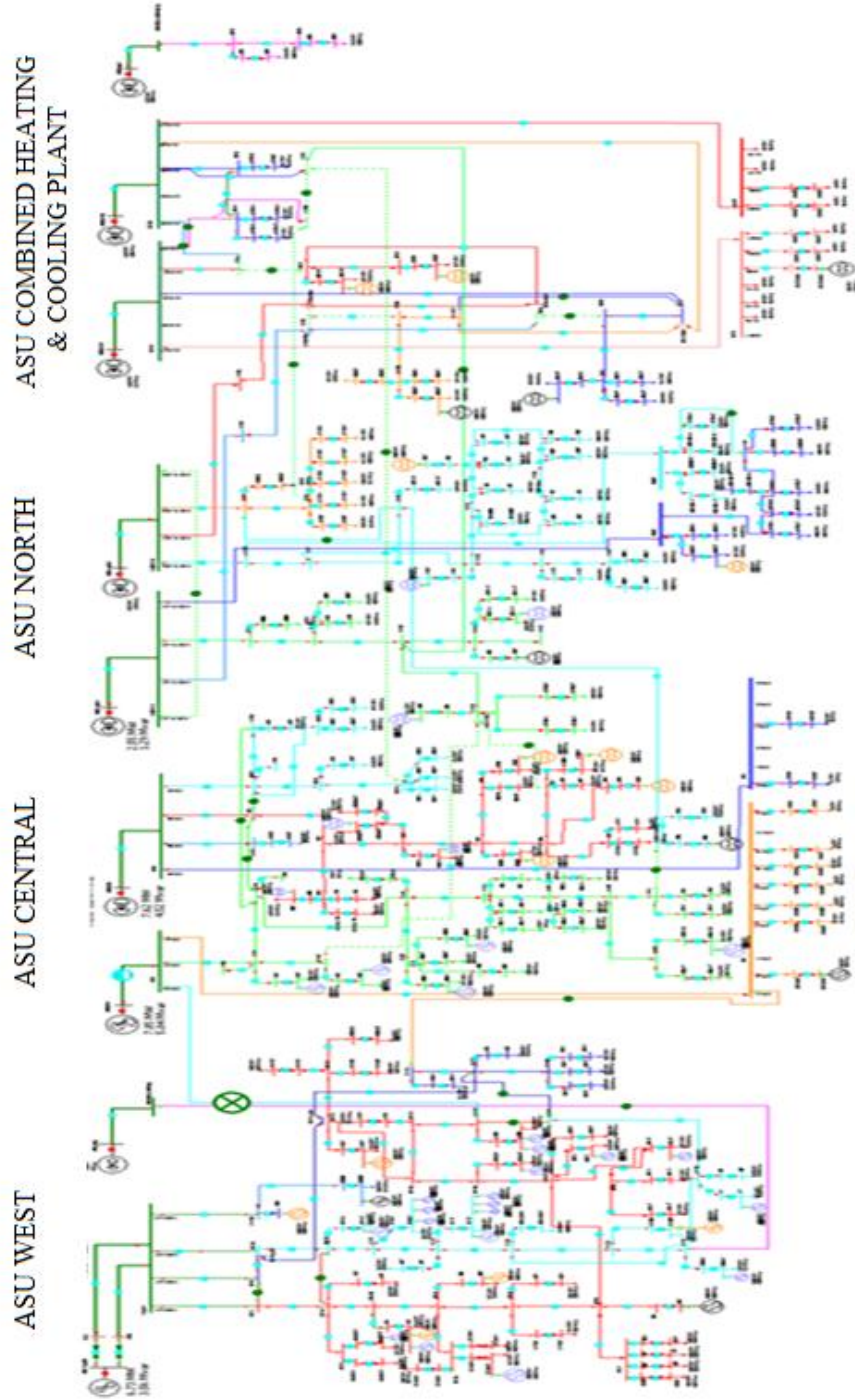


Fig. 4.6. PowerWorld model of the entire ASU distribution system.

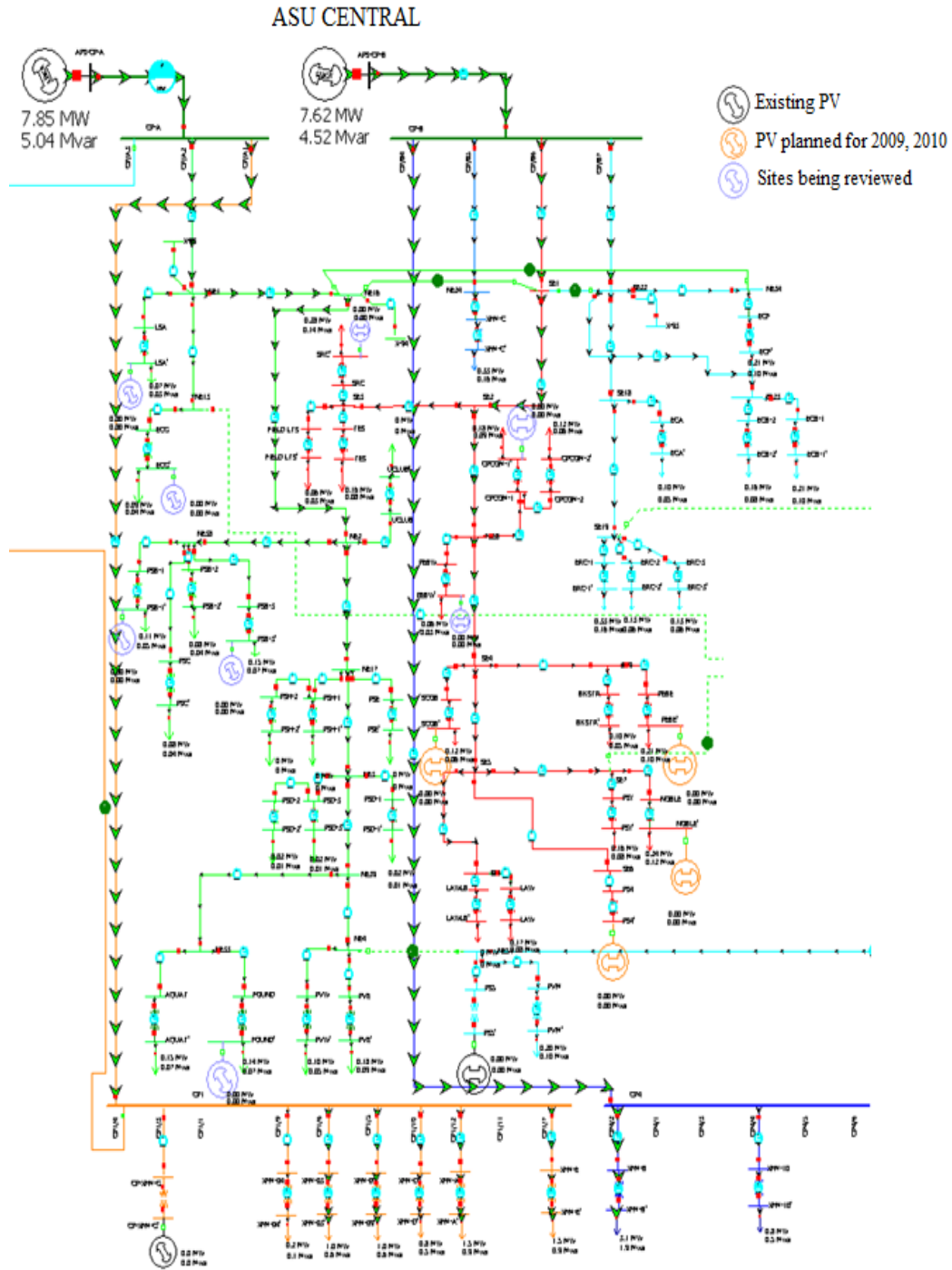


Fig. 4.8. PowerWorld model of the ASU Central distribution system.

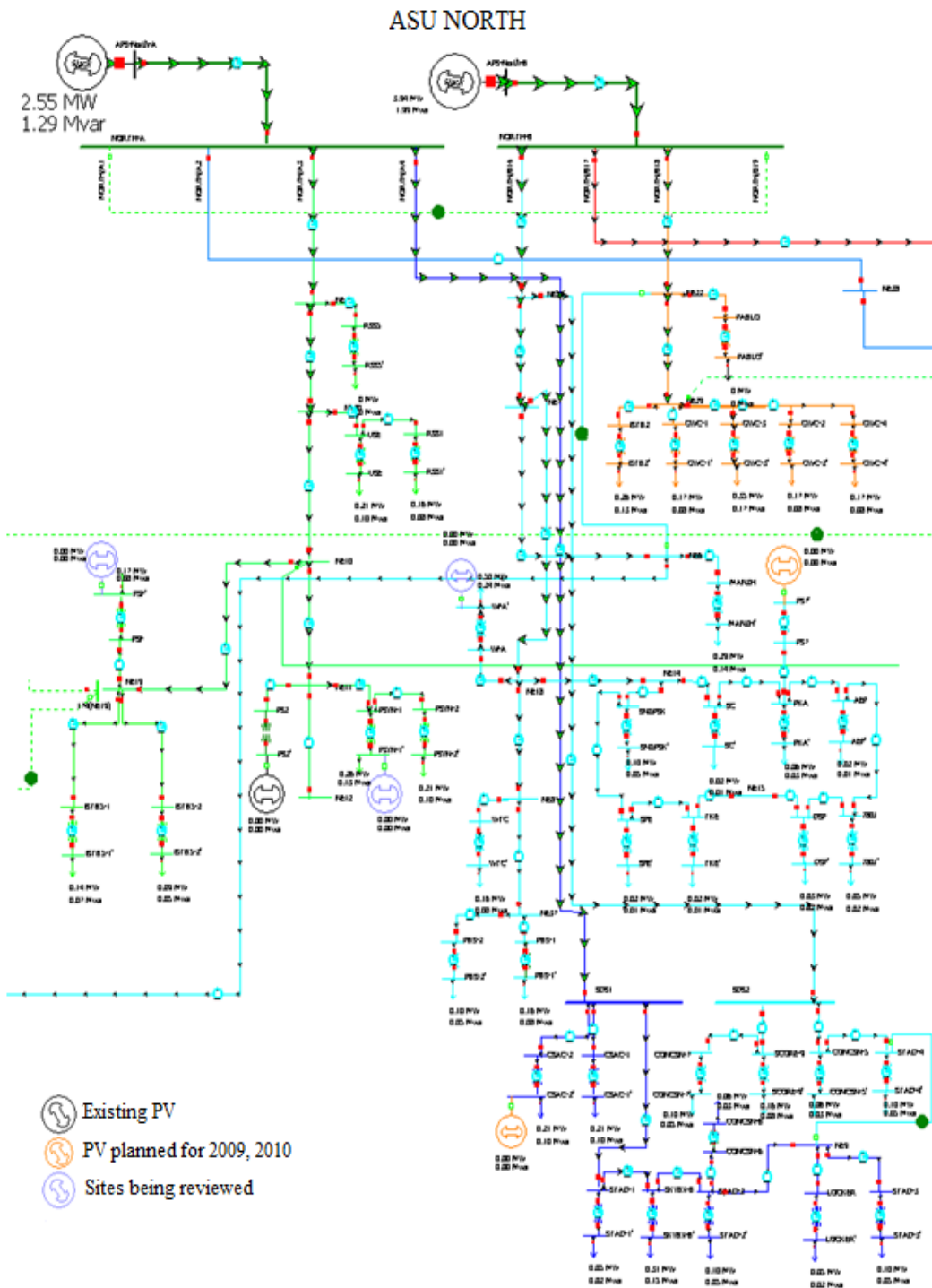


Fig. 4.9. PowerWorld model of the ASU North distribution system.

ASU COMBINED HEATING & COOLING PLANT

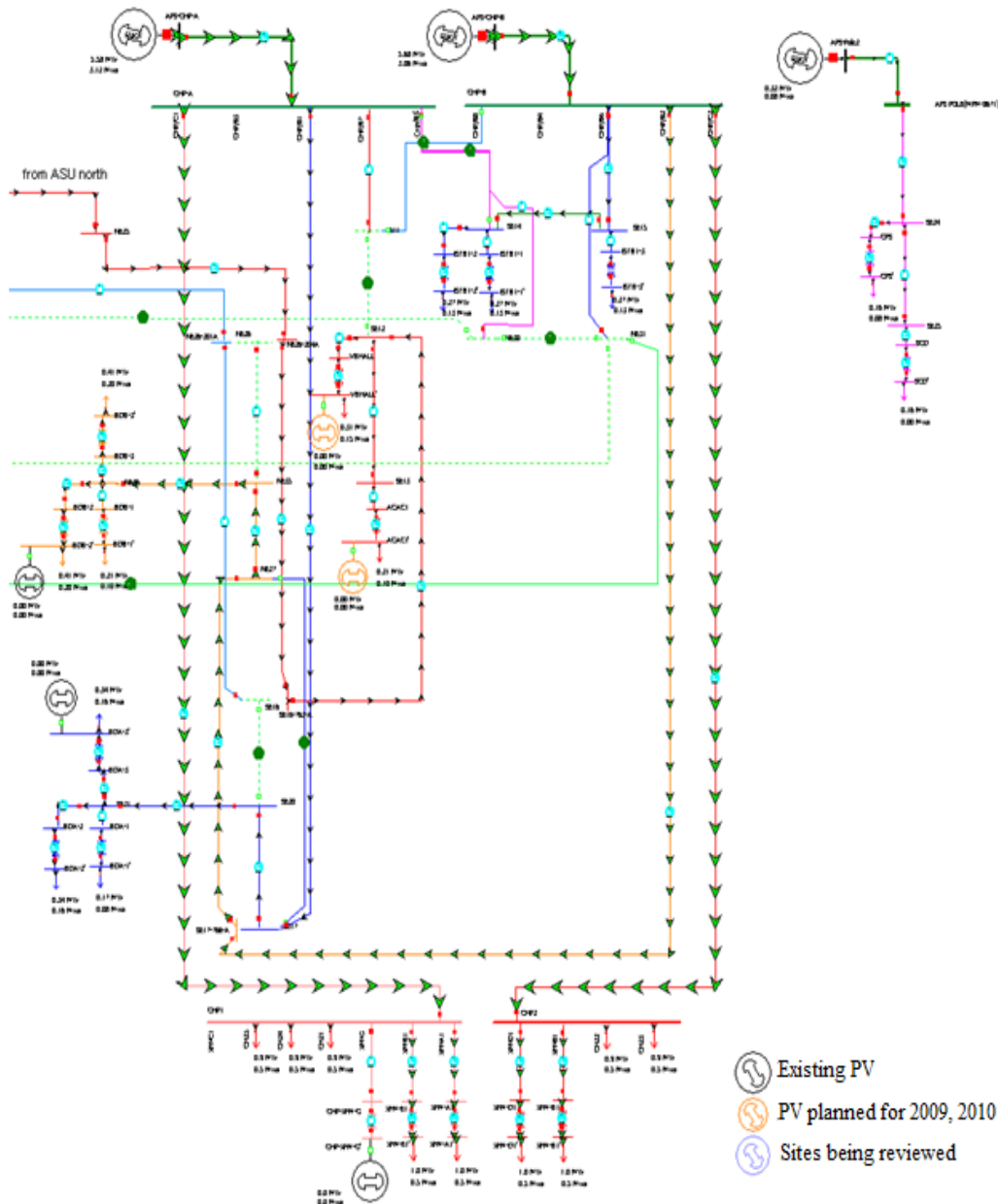


Fig. 4.10. PowerWorld model of the ASU South distribution system and APS pole (top right).

Note that the PV generators modeled include the 2 MW existing installation, the 2.5 MW planned capacity for fiscal year 2009-2010 and the 4.6 MW capacity for sites being reviewed for future phases.

Rendering the EIS load data and solar data suitable for power flow studies

Rendering the EIS data on the system was not straight-forward. For example, the name correspondence between the EIS meters and the transformer loads in the one-line diagram was not obvious, and thus name mapping was done through personal judgment. The correspondences between the meters and the transformer load are usually not one-to-one. In most cases, the EIS data had only one meter for a building, while most buildings had more than one transformer. In this work, the load has been divided according to the transformer ratings. MATLAB programs and PowerWorld scripts were extensively used for the data processing. Excel files were used for storing data and doing simple calculation; MATLAB codes read Excel files, rendered the EIS data on the system, and created PowerWorld scripts; PowerWorld then loaded the scripts to update the system with a new data set. The main purpose of this process was to save manual work while updating the system with new device statuses and new sets of loads and PV generations needed for different case studies. These subroutines have been included in Appendix B

4.4 Model development in CYMDIST

CYMDIST distribution analysis program is designed for planning studies and simulating the behavior of electrical distribution networks under different operating conditions and scenarios. It includes several built-in functions that are required for distribution network planning, operation and analysis. The functions such as power-flow analysis and short-circuit analysis are performed on balanced or unbalanced distribution network that are built with any combination of phases and configurations. In CYMDIST, the DG models are divided in three categories depending on how they are coupled with the electrical network:

- Synchronous generators that can be operated in three different modes: voltage control, fixed generation or swing.
- Induction generators that provide constant power.

- Inverter-based generators used with wind turbines (synchronous or induction), gas turbine (high speed), energy storage, photovoltaic source and fuel cells.

These enhanced DG models are used in power flow, short-circuit, and transient stability studies. The inability of PowerWorld to model DG in such detail makes the modeling and analysis of the system in CYMDIST appealing. For the purpose of this work, the power flow analysis, short circuit analysis and fault flow analysis features of CYMDIST have been used. The inverter-based generators, otherwise known as electronically coupled generators, have been used to model the PV generation system. The electronically coupled generators have been modeled as PQ buses. The real and reactive power which they inject remains constant. In the presence of another module called CYMSTAB, which is predominantly used for transient stability analysis, these generators could be used to represent inverter-based generation with user-defined specifications. The ability to predict the dynamic behavior of distributed generation unit under island mode of operation is possible with this module. Active and passive anti-islanding schemes could be implemented in the presence of this module.

The entire ASU distribution system similar to the model created in PowerWorld was created in CYMDIST. Data was entered for the cable and transformer impedances and the loading condition chosen was the same information as the one used for PowerWorld. In the case for PV systems, the electronically coupled generators were not directly connected to the system. They were connected via inverter-based units. The inverter control mode is set such that, during short circuits, the source will continue to contribute 100% of its rated current. Fig. 4.11 shows the CYMDIST model of the entire ASU distribution system. Fig. 4.12 through Fig. 4.15 shows the zoomed version of the West, Central, North and South parts, respectively.

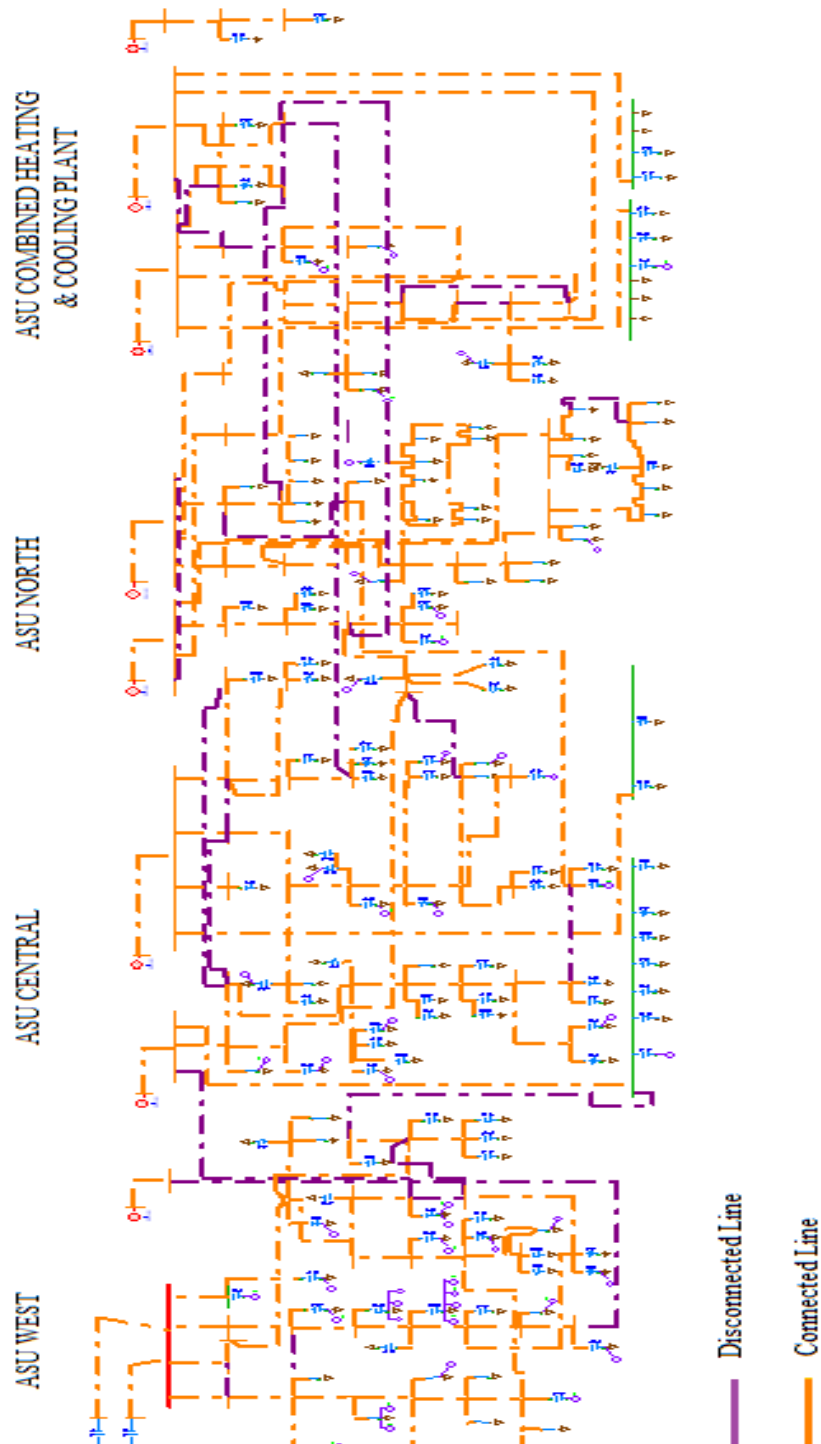
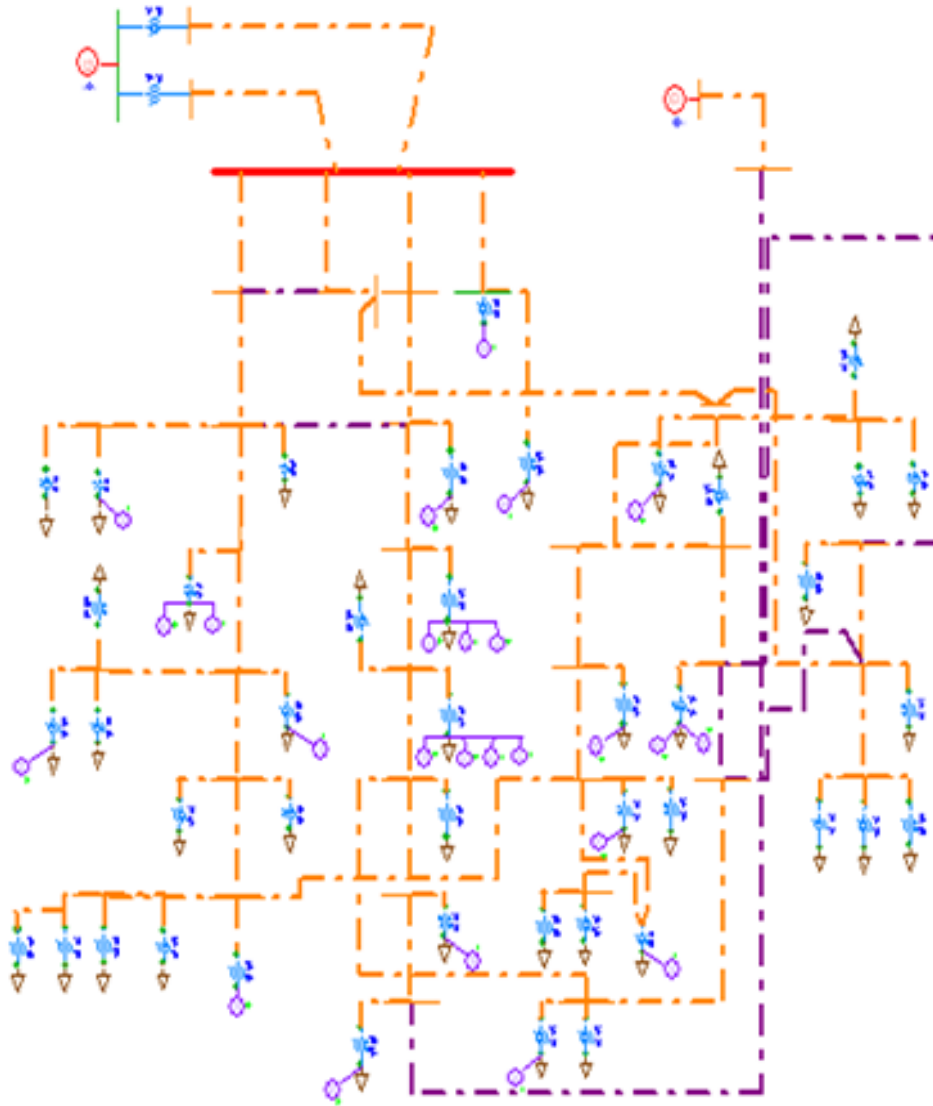


Fig. 4.11. CYMDIST model of the entire ASU distribution system.

ASU WEST



Legend

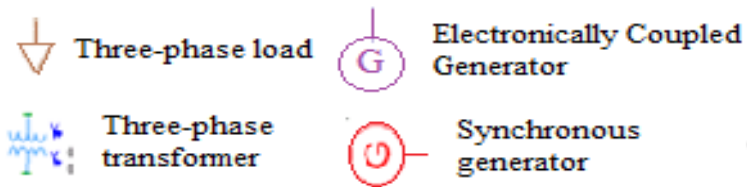
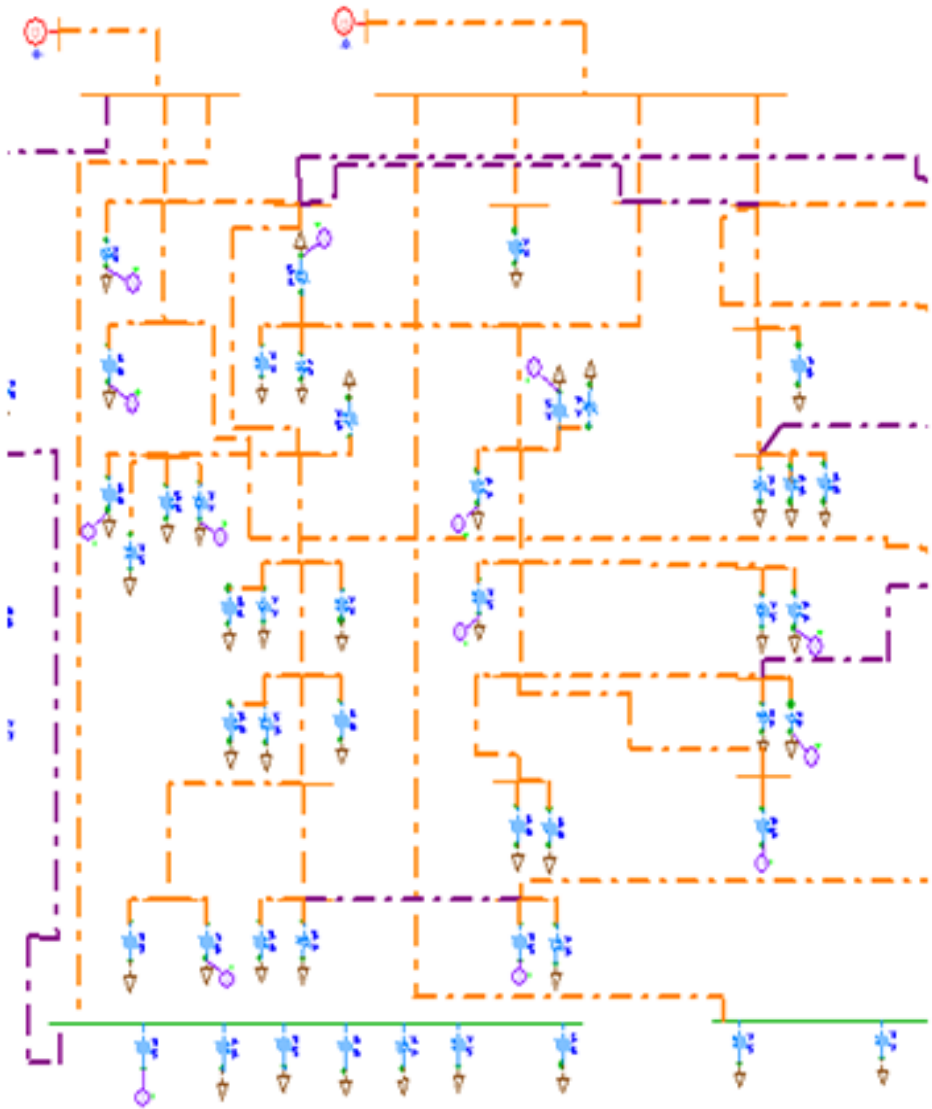


Fig. 4.12. CYMDIST model of the ASU West distribution system.

ASU CENTRAL



Legend





- | | | | |
|---|-------------------------|---|----------------------------------|
|  | Three-phase load |  | Electronically Coupled Generator |
|  | Three-phase transformer |  | Synchronous generator |

Fig. 4.13. CYMDIST model of the ASU Central distribution system.

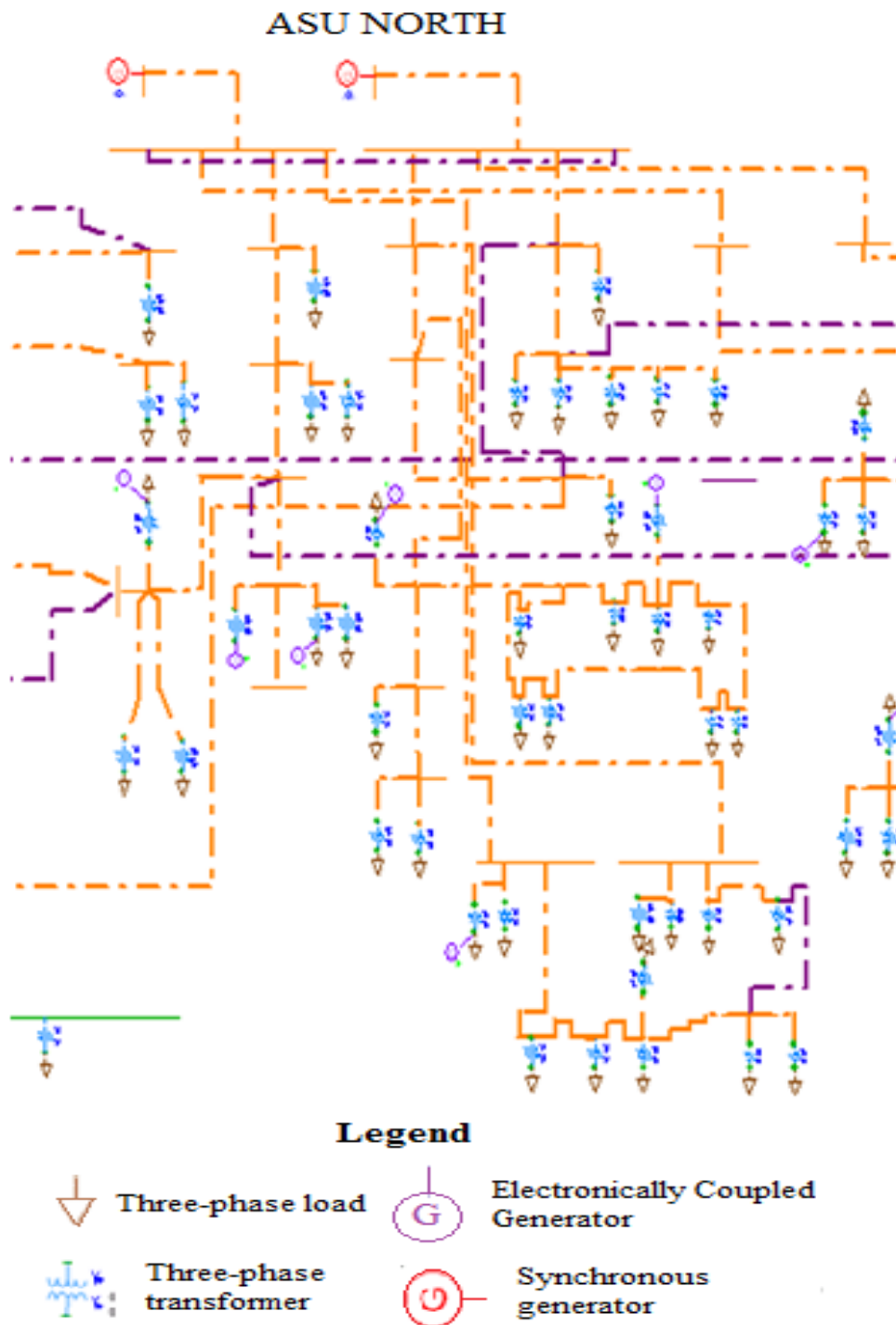


Fig. 4.14. CYMDIST model of the ASU North distribution system.

ASU COMBINED HEATING & COOLING PLANT

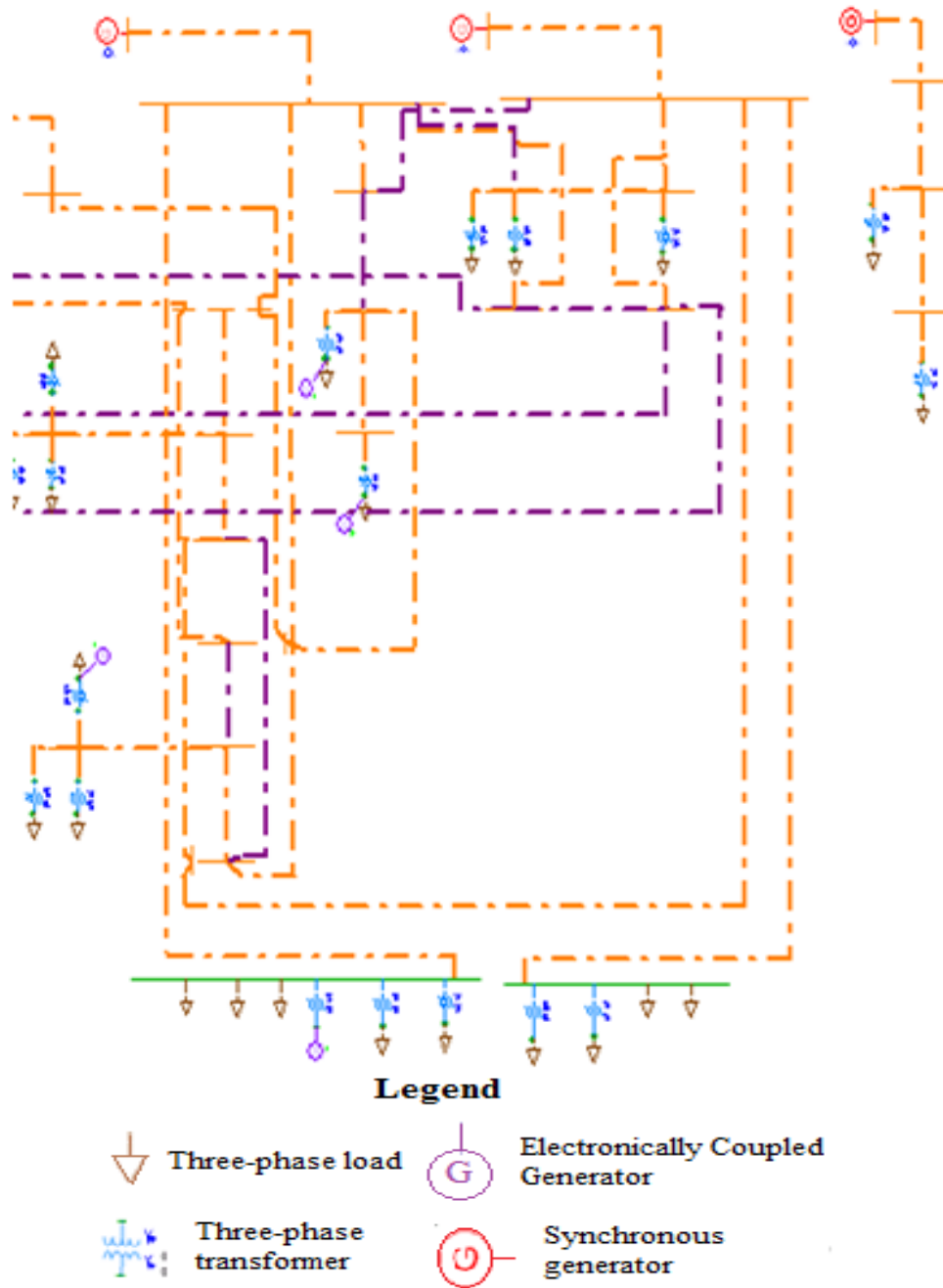


Fig. 4.15. CYMDIST model of the ASU South distribution system.

CHAPTER 5

POWER FLOW RESULTS AND FAULT ANALYSIS

5.1 Introduction

This chapter discusses the power flow results corresponding to the distribution system of ASU Tempe campus with various levels of PV and obtained from PowerWorld and CYMDIST. Cases are considered where one of the feeders has an outage, which causes a blackout to a part of the system. Then a backup line is energized to supply those loads and the effect of PV generation on the voltage profile of the system is studied. The positive impact of reactive power injection from PV systems is also studied in this case. Time step simulation is done in PowerWorld which gives results for hourly load data. Fault current analysis is conducted in CYMDIST to find out the effect of DG on fault current.

5.2 Case Study Results using the PowerWorld ASU Distribution Model

Table 5.1 shows the power flow results without PV generation for 8/20/2009 at 3PM. This date was one of the hottest days of 2009 in Tempe and there was highest load at 3PM. PV insolation data from EIS was seen to be the highest at this time. Table 5.2 gives a summary of the power flow results on the same load data with only existing PV installations as of 8/20/2009 included.

TABLE 5.1
POWER FLOW STUDY WITHOUT PV GENERATION

	MW	MVAR
Total Load	39.9	21
Total Generation	40.28	22.65
Total Gen. from Feeders	40.28	22.65
Total PV Generation	0	0
Losses	0.38	1.65

TABLE 5.2
POWER FLOW STUDY WITH EXISTING PV INSTALLATION

	MW	MVAR
Total Load	39.9	21
Total Generation	40.26	22.62
Total Gen. from Feeders	38.42	22.62
Total PV Generation	1.879	0
Losses	0.36	1.62

TABLE 5.3
POWER FLOW STUDY WITH PLANNED PV INSTALLATION

	MW	MVAR
Total Load	39.9	21
Total Generation	40.197	22.48
Total Gen. from Feeders	31.54	22.48
Total PV Generation	8.657	0
Losses	0.297	1.48

Table 5.3 gives a summary of the power flow results based on the same load but in addition to the existing PV generation, those PVs planned and under review are also included. A comparison of Table 5.2 and Table 5.3 reveals a reduction in losses of about 25% by increasing the PV penetration from 4.7% to 22%. This clearly indicates the effect of PV penetration on the overall efficiency of the system.

An example is used to show a case in which PV generation significantly reduces the system congestion and improve the voltage profile. Four cases have been considered and the voltage profile in each of these cases was observed. The cases are:

- Case 0: Base Case. No outages and no PV generation
- Case 1: One of the feeders that supply ASU central is off. The backup line between ASU west and ASU central is put in service. No PV generation.
- Case 2: Same as case 1, but with PV generation (All PVs including existing, planned and sites under review).
- Case 3: Same as case 2, but assuming all PVs also generate a reactive power in an amount equal to their active power.

The results in Fig. 5.1 through Fig. 5.4 clearly show the difference between situations when there is PV generation and when there is no PV generation. These results also demonstrate the capability of PowerWorld of providing an excellent graphical presentation of power flow results, such as animated power flows and voltage contour. It must be mentioned here that the rating of the backup line between ASU West and ASU Central was reduced slightly from the nominal value to help create an overload scenario when the central feeder A was removed from service.

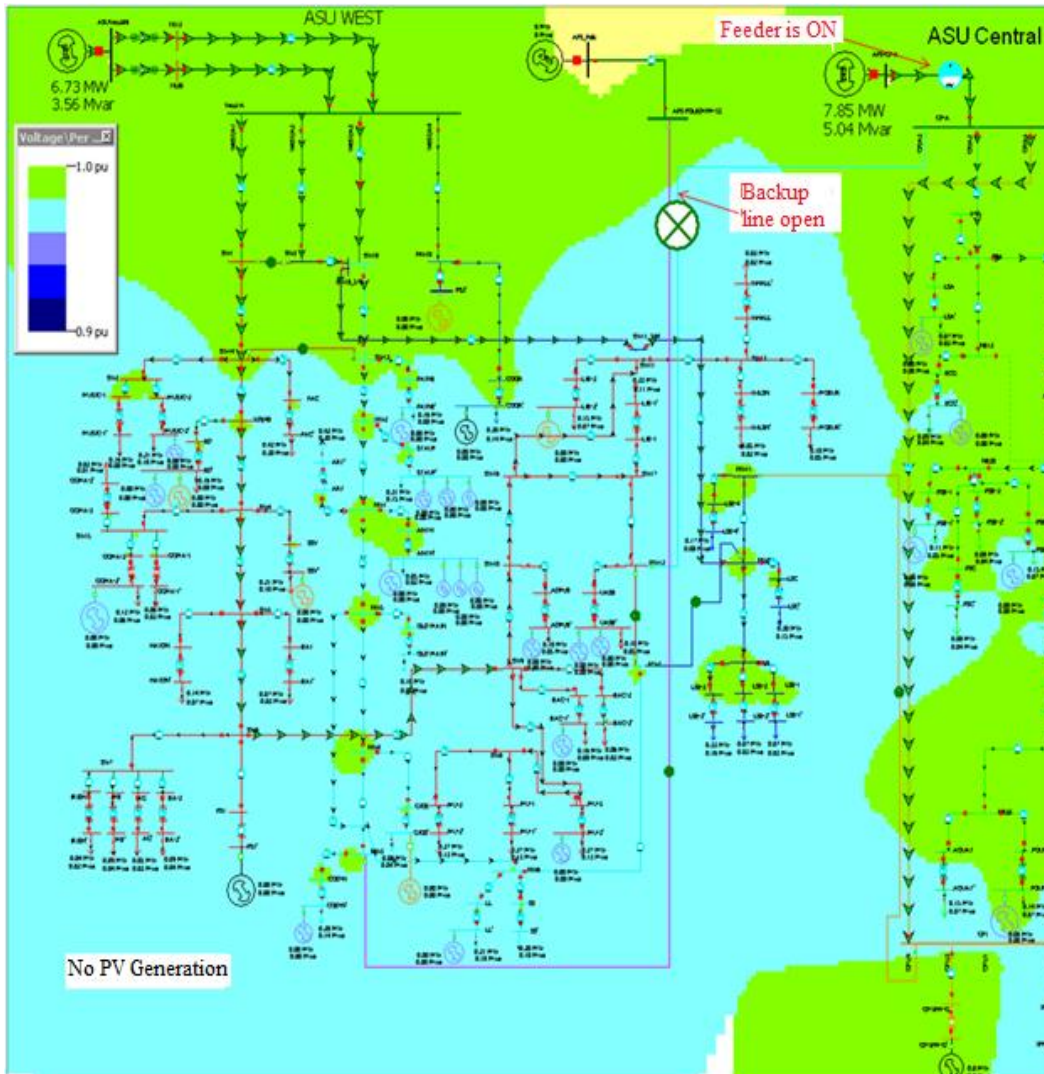


Fig. 5.1. Voltage profile for Case 0: All lines are well below their thermal loading limits. The system voltage profile is also normal.

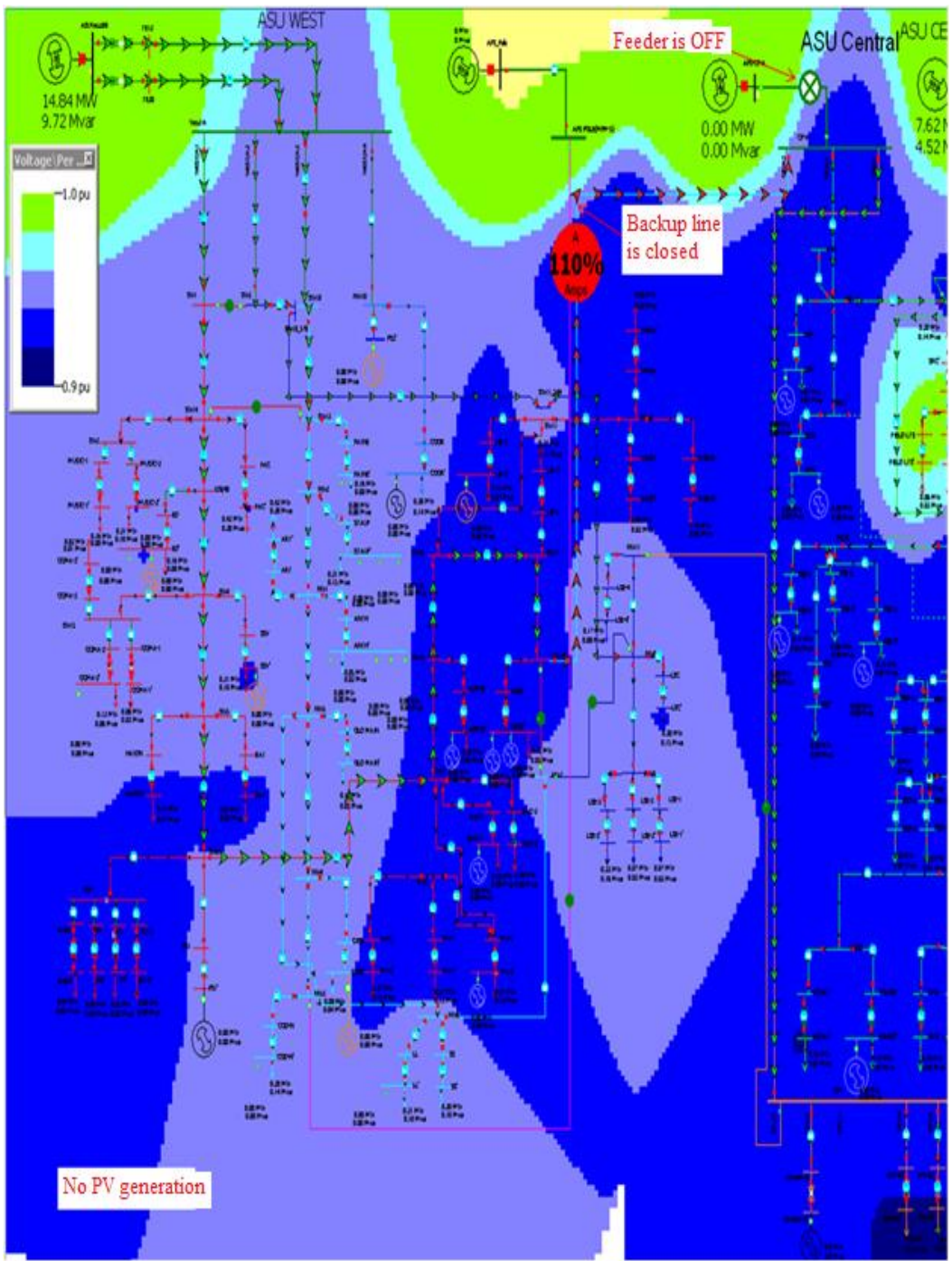


Fig. 5.2. Voltage profile for Case 1: The backup line is overloaded and the voltage profile is poor.

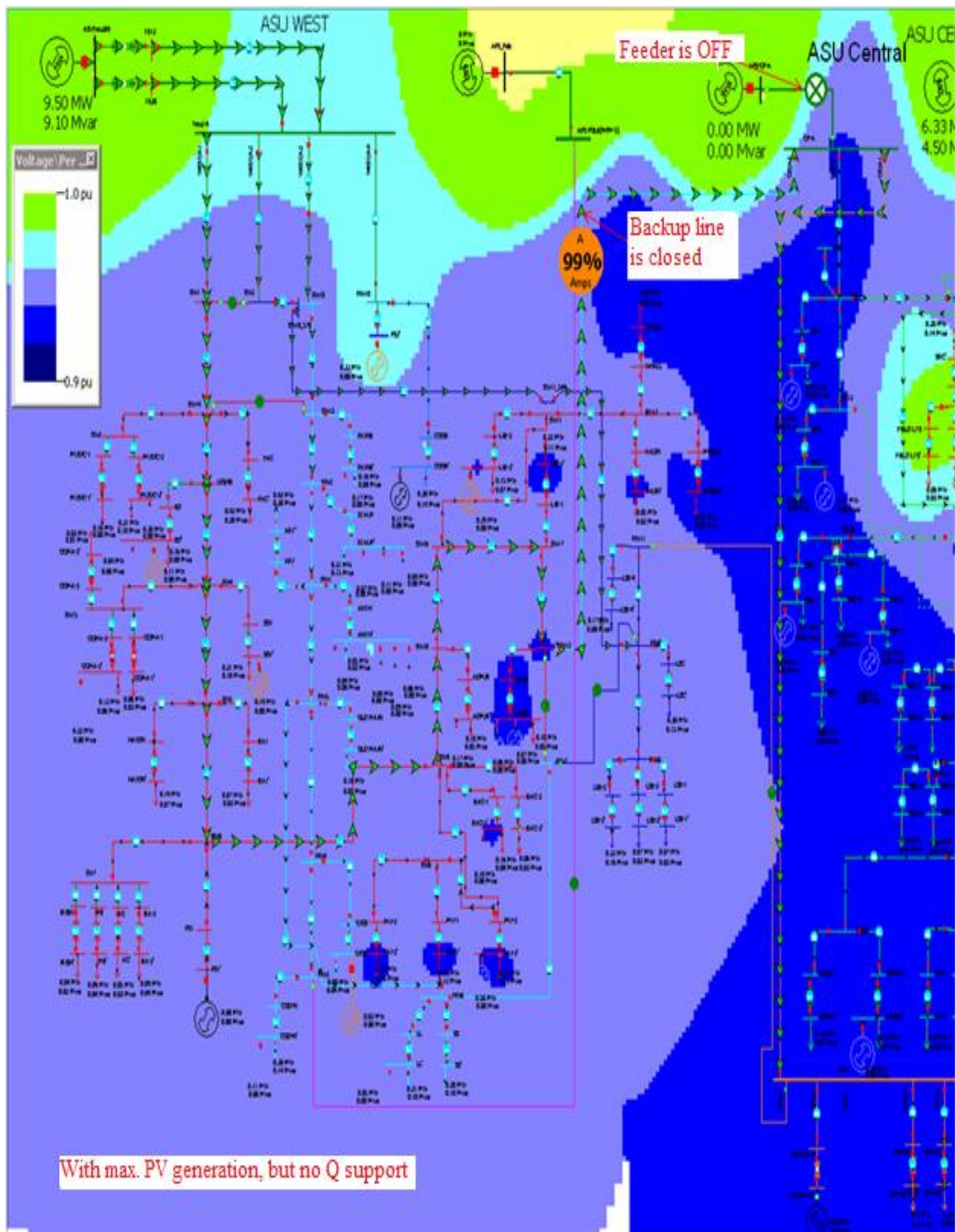


Fig. 5.3. Voltage profile for Case 2: The backup line is not overloaded, though it is still in a warning condition. The voltage profile has improved.

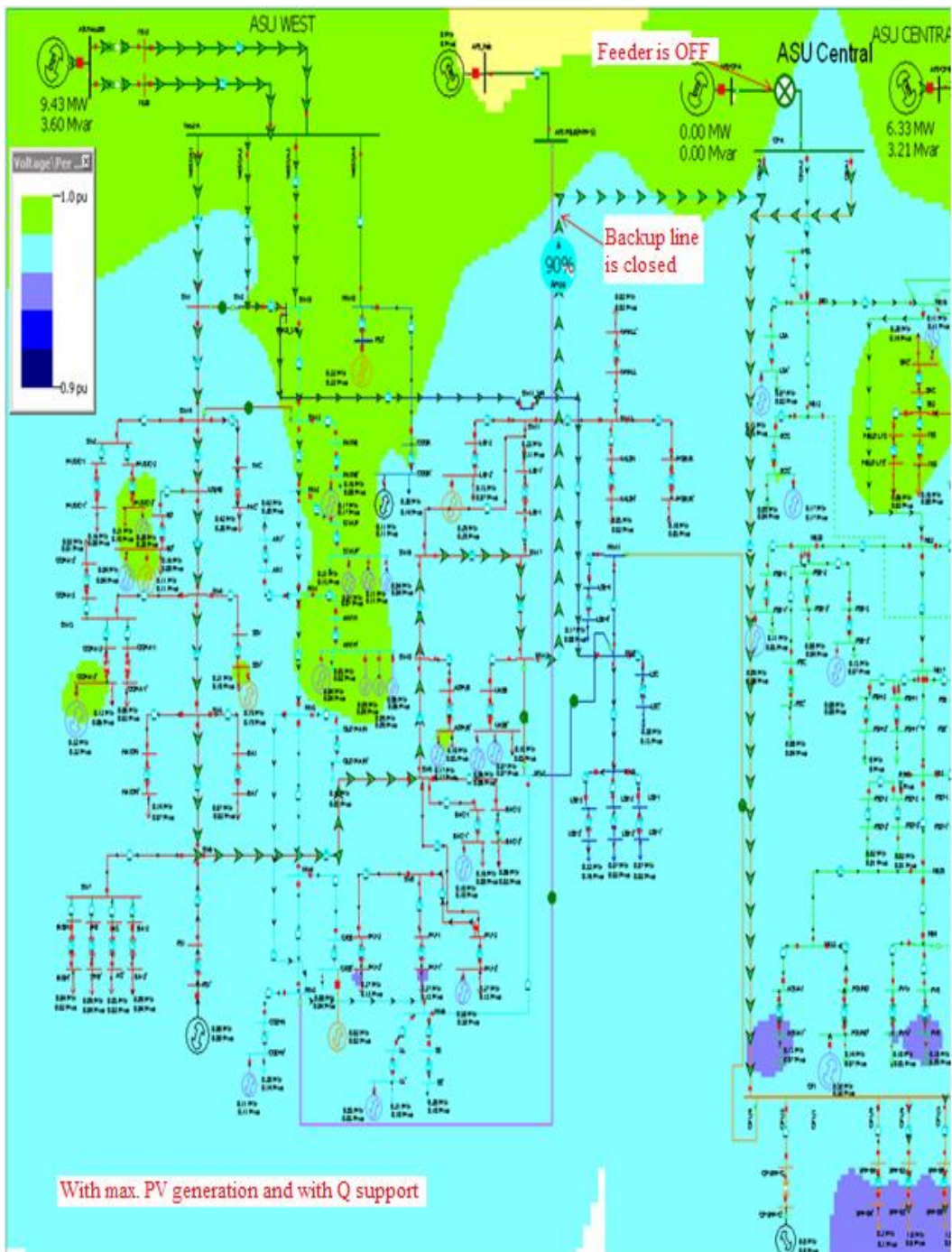


Fig. 5.4. Voltage profile for Case 3: The backup line is now in a normal condition. The voltage profile becomes much better.

5.3 Case Study Results using the CYMDIST ASU Distribution Model

Similar test cases were run for the CYMDIST model. This is shown in Fig. 5.6 through Fig. 5.9.

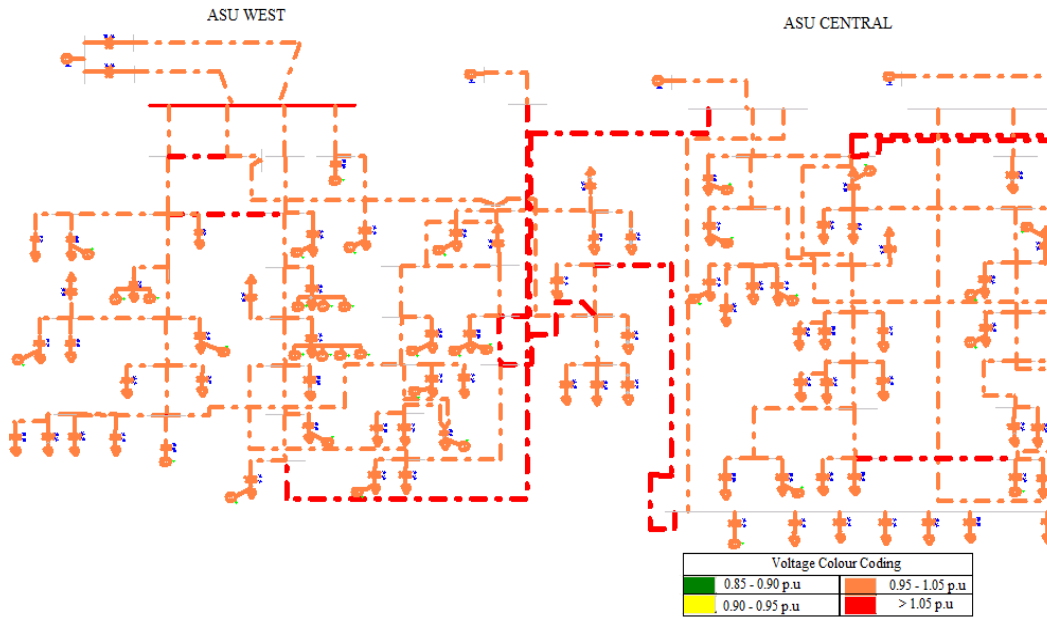


Fig. 5.5. Voltage profile in CYMDIST for Case 0.

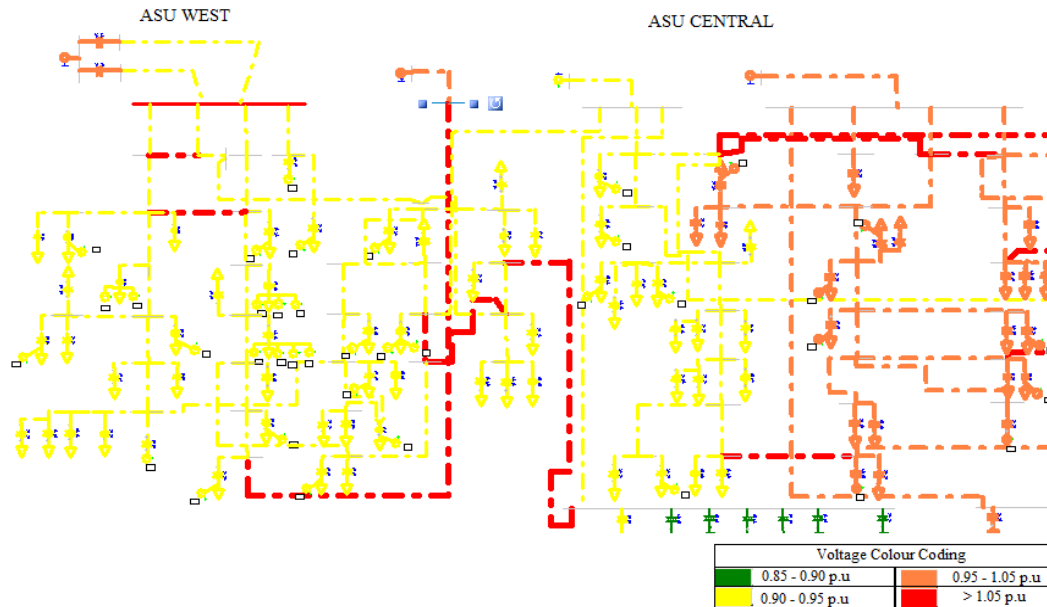


Fig. 5.6. Voltage profile in CYMDIST for Case 1: there is a significant drop in the voltage level.

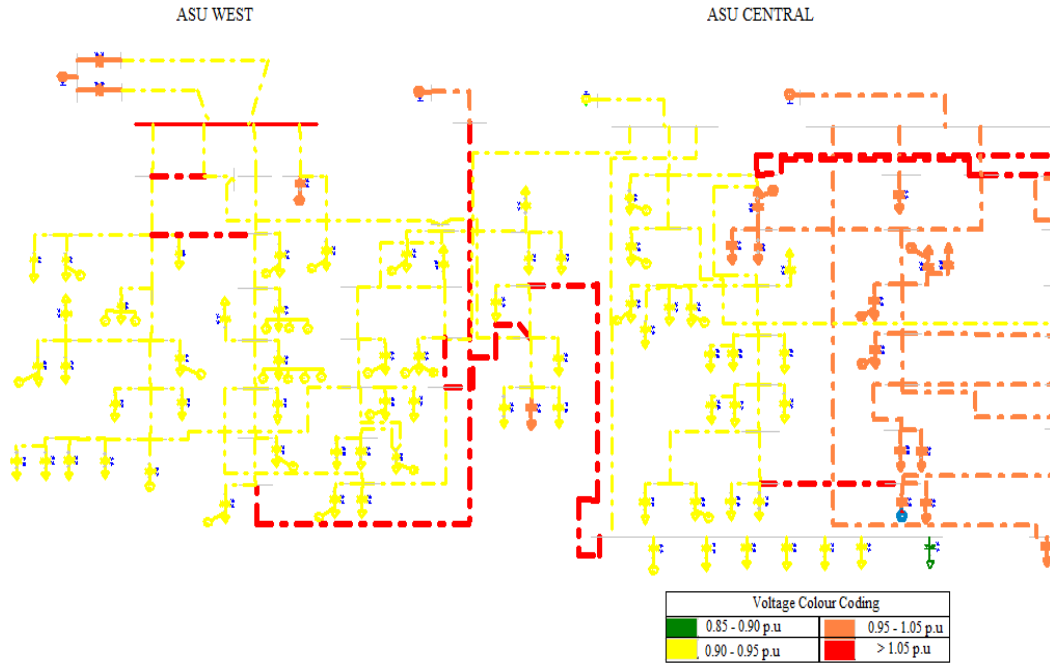


Fig. 5.7. Voltage profile in CYMDIST for Case 2: there is improvement in the voltage profile at a few places.

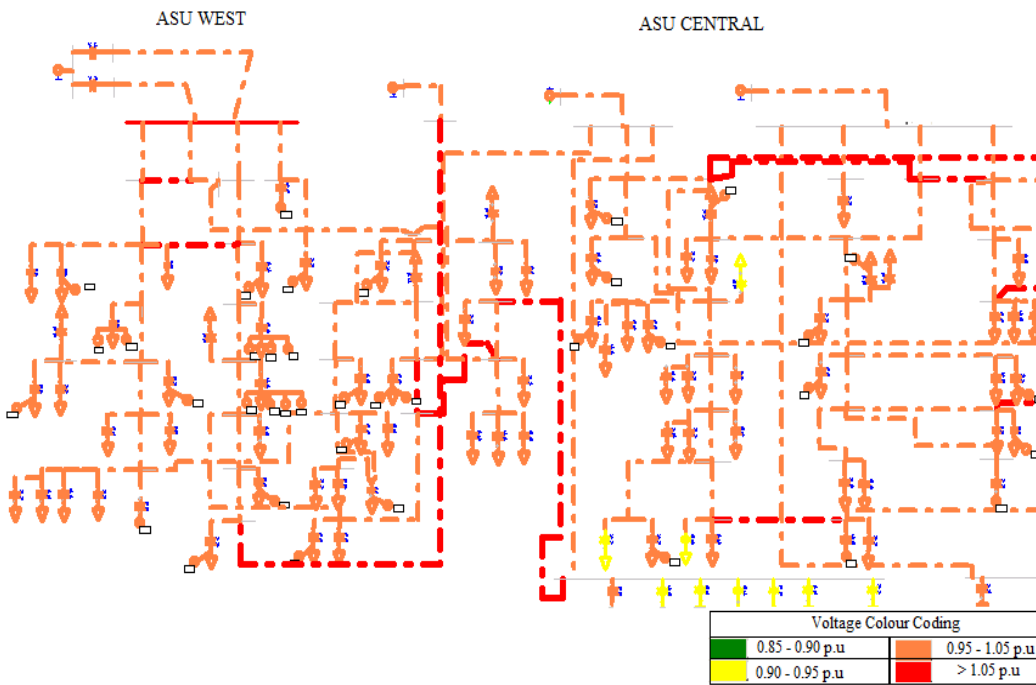


Fig. 5.8. Voltage profile in CYMDIST for Case 3: the voltage profile becomes much better.

The PowerWorld and CYMDIST cases indicate the effect of including distributed generation on the overall voltage profile of the system. It is seen that the PV systems, when included in the network, significantly reduce the voltage stress on distribution lines caused due to an outage of a feeder. Table 5.3 through Table 5.6 compares values of power generated by the various feeders in the ASU distribution system in PowerWorld and CYMDIST. It is seen that there is good match in the values of power in both cases and a balance in power generation. The values have been mentioned for all the four cases discussed. This further validates the fact that with increase in PV penetration in the system, the voltage profile of the network greatly improves.

TABLE 5.4
FEEDER GENERATION FOR CASE 0

Feeder	MW	MVAR	MW	MVAR
	CYMDIST		PowerWorld	
APS-CHP-A	5.57	3.015	5.58	3.12
APS-CHP-B	5.677	2.969	5.68	3.06
APS-CP-A	7.832	4.898	7.85	5.04
APS-CP-B	7.60	4.382	7.62	4.52
APS-NORTH-A	2.545	1.206	2.55	1.29
APS-NORTH-B	3.935	1.863	3.94	1.99
APS-POLE	0	-0.04	0.01	-0.01
APS-POLE2	0.317	0.059	0.32	0.08
ASU-WEST-69	6.725	3.497	6.73	3.56

TABLE 5.5
FEEDER GENERATION FOR CASE 1

Feeder	MW	MVAR	MW	MVAR
	CYMDIST		PowerWorld	
APS-CHP-A	5.57	3.015	5.58	3.12
APS-CHP-B	5.677	2.969	5.68	3.06
APS-CP-A	0	0	0	0
APS-CP-B	7.6	4.382	7.62	4.52
APS-NORTH-A	2.545	1.206	2.55	1.29
APS-NORTH-B	3.935	1.863	3.94	1.99
APS-POLE	0	-0.04	0.01	-0.01
APS-POLE2	0.317	0.059	0.32	0.08
ASU-WEST-69	14.804	10.112	14.84	9.72

TABLE 5.6
FEEDER GENERATION FOR CASE 2

Feeder	MW	MVAR	MW	MVAR
	CYMDIST		PowerWorld	
APS-CHP-A	5.489	3.012	5.51	3.12
APS-CHP-B	5.596	2.966	5.61	3.06
APS-CP-A	0	0	0	0
APS-CP-B	6.317	4.375	6.34	4.5
APS-NORTH-A	2.163	1.199	2.17	1.28
APS-NORTH-B	2.258	1.926	2.25	2.01
APS-POLE	0	-0.04	0.01	-0.01
APS-POLE2	0.317	0.059	0.32	0.08
ASU-WEST-69	9.488	9.232	9.53	9.1

TABLE 5.7
FEEDER GENERATION FOR CASE 3

Feeder	MW	MVAR	MW	MVAR
	CYMDIST		PowerWorld	
APS-CHP-A	5.489	2.931	5.51	3.04
APS-CHP-B	5.596	2.885	5.61	2.98
APS-CP-A	0	0	0	0
APS-CP-B	6.317	3.101	6.34	3.22
APS-NORTH-A	2.163	0.816	2.17	0.9
APS-NORTH-B	2.269	0.286	2.36	0.34
APS-POLE	0	-0.04	0.01	-0.01
APS-POLE2	0.317	0.059	0.32	0.08
ASU-WEST-69	9.425	3.594	9.45	3.63

5.4 Time Step Simulation

Time step simulation in PowerWorld was used to obtain the power flow of ASU's distribution system for an entire day. The time step simulation tool allows one to specify operating conditions and obtain power flow solutions for a set of points in time. It provides the tools needed to analyze the operation of a power system hour by hour. The tool can obtain the optimized generation dispatch for each hour of the analysis horizon.

In order to use time step simulation, hourly load data had to be created from the 15 minute data available through the EIS website. As mentioned earlier, all the buildings are not metered and hence engineering judgment was used to get data for those buildings. Solar insolation data was

available only for parking structure 1 and 5. For all the other buildings, data was obtained by scaling the generation data of parking structure 1 with respect to the location's PV generation rating. For each building, data was obtained and mapped on to the corresponding transformer name in PowerWorld. PV generators were assigned with generation data. Both these were done using MATLAB code mentioned in the Appendix B. The day that was considered for this was 8/20/2009. Fig. 5.5 shows the load profile and PV generation data for the entire day.

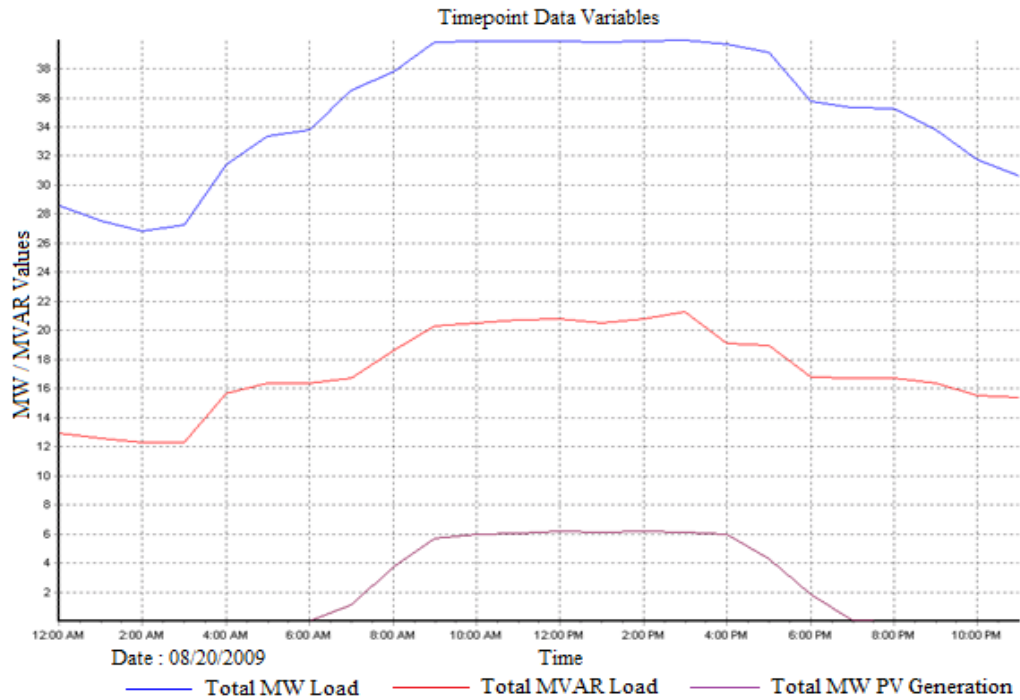


Fig. 5.9. Load and generation profile for 8/20/2009.

The voltage profile at three different places; one close to the feeder, one in between and another at a PV generation site was studied. The central feeder A was considered to be out of service and the voltage profiles at these three location were found for the entire day and plotted with respect to time. It is seen that when PV generation begins and reactive power equal to real power is supplied by them, the voltage profile at these buses become better. A comparison of the voltage profiles with PV generation (and reactive power support) and without PV generation is shown in Fig. 5.10 and Fig. 5.11.

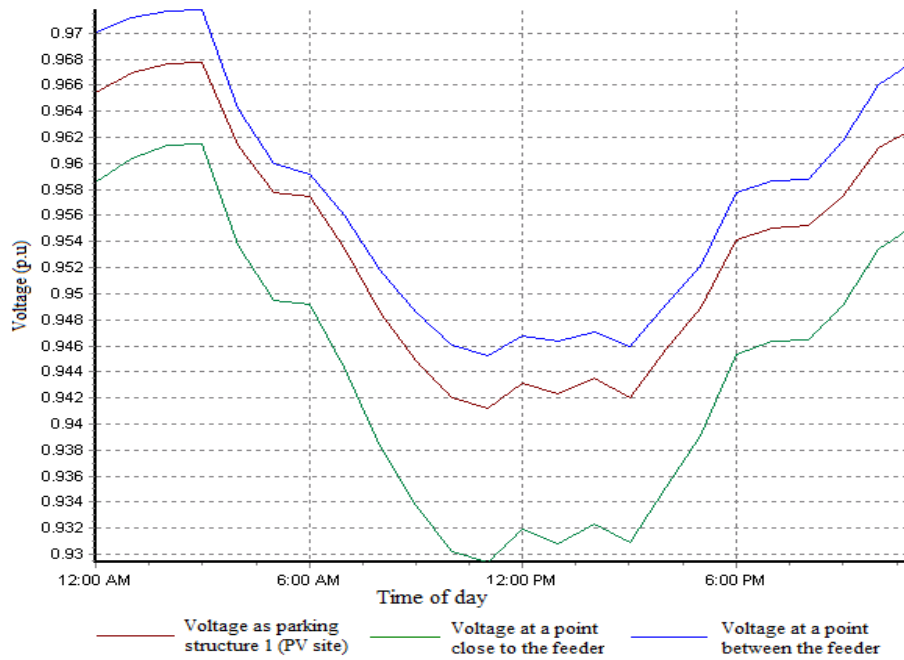


Fig. 5.10. Hourly voltage profile at three locations when central feeder A is out of service without PV generation.

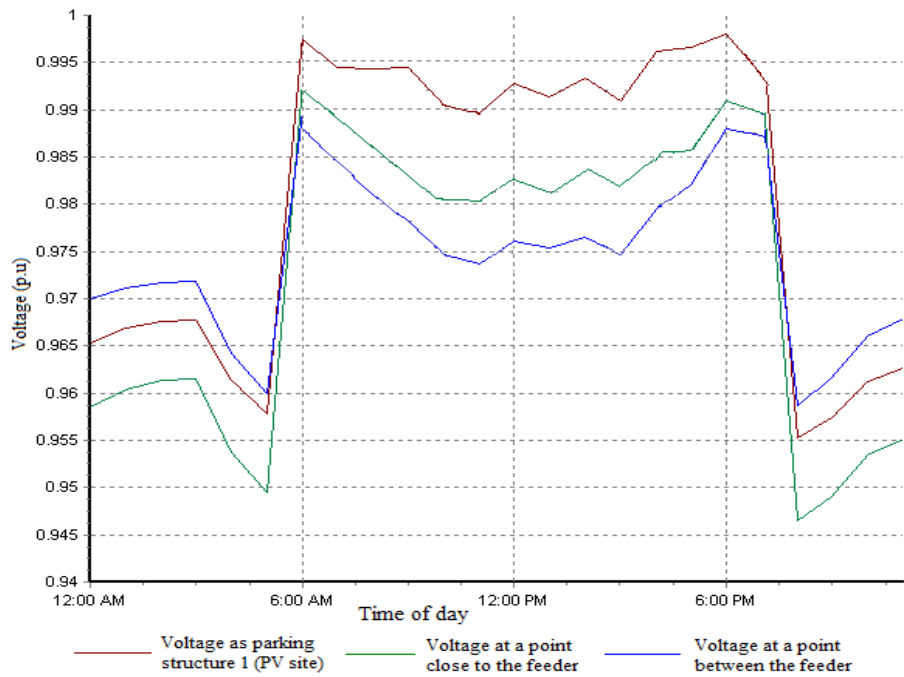


Fig. 5.11. Hourly voltage profile at three locations when central feeder A is out of service with PV generation and reactive power injection.

5.5 Fault Current Analysis

Analysis of the prospective short-circuit current is required for selection of protective devices such as fuses and circuit breakers. If a circuit is to be properly protected, the fault current must be high enough to operate the protective device within as short a time as possible; also the protective device must be able to withstand the fault current and extinguish any resulting arcs without itself being destroyed or sustaining the arc for any significant length of time. This makes fault level and fault level calculations indispensable for distribution system design. A symmetric, symmetrical or balanced fault is one which affects each of the three-phases equally. This is in contrast to an asymmetric fault, where the three phases are not affected equally. In practice, most faults in power systems are unbalanced. With this in mind, symmetric faults can be viewed as somewhat of an abstraction; however, as asymmetric faults are difficult to analyze, analysis of asymmetric faults is built up from a thorough understanding of symmetric faults. Common types of asymmetric faults, and their causes:

- LL fault - a short circuit between lines, caused by ionization of air, or when lines come into physical contact, for example due to a broken insulator.
- LG fault - a short circuit between one line and ground, very often caused by physical contact, for example due to lightning or other storm damage
- LLG fault - two lines come into contact with the ground (and each other), also common due to storm damage.

The short circuit analysis feature in CYMDIST is used for this study. The analysis can calculate fault currents for every type of fault at every section, and can also compute the fault contributions in the network due to a single fault. Conventional short circuit analysis was done for the ASU West system. The assumptions for the conventional short circuit analysis were:

- Positive- and negative-sequence impedances were identical.

- Lines were perfectly symmetrical; there is no mutual coupling between sequences.
- The pre-fault voltage was defined by the user among the choices of using the base voltage, the operating voltage, or the voltage obtained from a power flow solution.

For each section, the equivalent positive-sequence and zero-sequence impedances as seen from the fault location were computed. On conducting short circuit analysis of the ASU West distribution system, it was seen that there was an increase in the fault current level due to the introduction of PV generators. The fault current at the high voltage side was measured. This was done for three cases: without PV generation, with PV generation only and with PV generation and reactive power support. Fig. 5.12 shows the fault current values plotted with respect to distance for a LLL fault. Fig. 5.13 through Fig. 5.15 shows the same for LLG, LL and LG faults. It is seen that with the injection of reactive power, the fault current is greatly minimized and almost similar to the value of current when there is no PV generation.

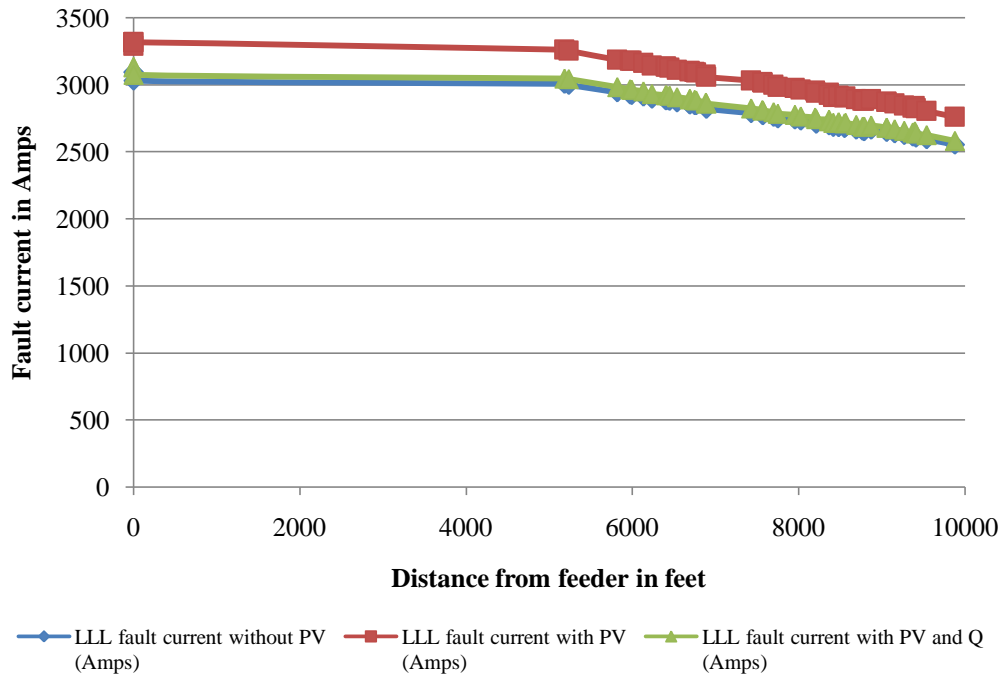


Fig. 5.12. LLL fault current versus distance from feeder.

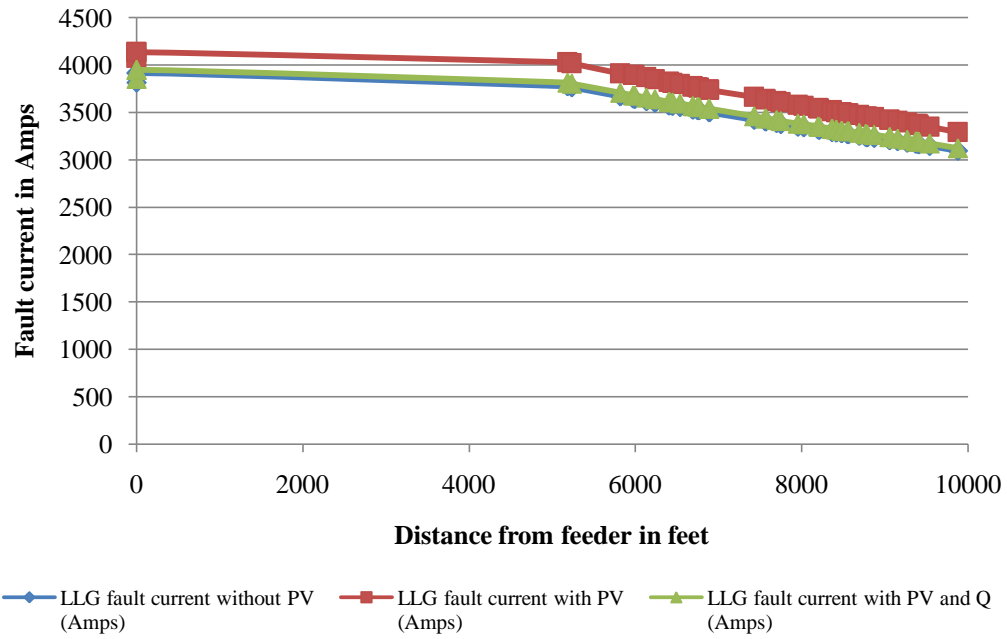


Fig. 5.13. LLG fault current versus distance from feeder.

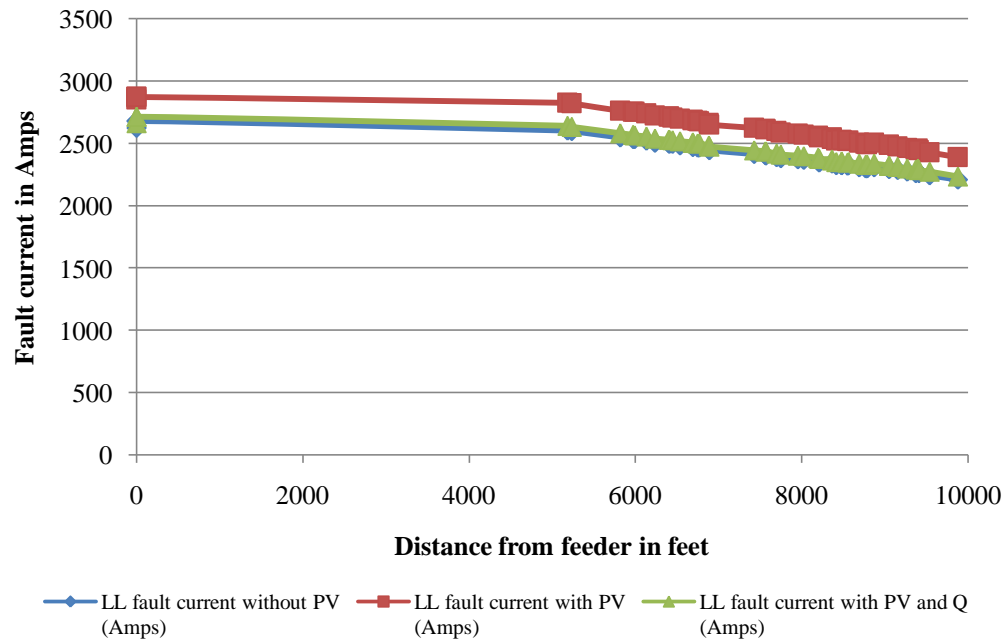


Fig. 5.14. LL fault current versus distance from feeder.

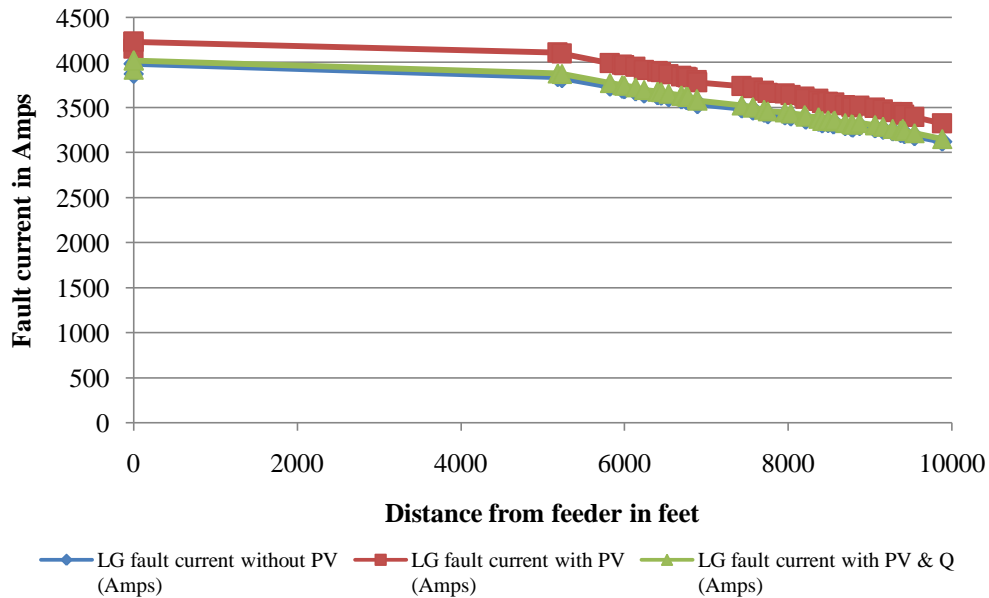


Fig. 5.15. LG fault current versus distance from feeder.

Table 5.7 shows the percentage increase in fault current due the impact of DG. It is seen that there is a 6-7% increase in fault current when PV generation is included into the system. When reactive power, equal to the real power, is injected into the system from the PV generators, fault current is greatly reduced compared to the case when only real power is injected. When PV generators with unity power factors are added to the system, the current injected by them is in phase with the grid. Hence, during faults, the overall fault current is the vector sum of all the currents in the network. When reactive power equal to the real power is injected, the current leads by 45° and this reduces the overall fault current. Fig. 5.16 shows the phasor diagram indicating this.

TABLE 5.8
PERCENTAGE INCREASE IN FAULT CURRENT DUE TO PV REPRESENTING 22% PENETRATION

Type of fault	% increase with PV	% increase with PV and Q
LG fault	6.48	1.05
LL fault	7.77	1.27
LLG fault	6.28	0.98
LLL fault	7.8	1.27



Fig. 5.16. Phasor diagram indicating decrease in fault current due to reactive power injection.

Generally, the 3-phase fault current typically provides the highest available fault current. However, there are situations where this is not the case. For instance, if a single line-to-ground fault occurs and there is an effective ground path for current to flow (zero-sequence network), then several current sources could contribute to this fault and exceed the 3-phase fault current. This will depend on how the fault current source or sources are connected to the system (i.e. transformer connection delta or wye). In this case the zero sequence impedance of the generator was lower than the positive sequence impedance and hence, the ground fault current was larger than three phase fault current.

Fault flow analysis

In order to find the effect of PV generation on fault current at a single bus, fault flow analysis was done in CYMDIST which calculates the power flow of the network system when a fault is applied to a specific location. The calculation assumptions were:

- The Pre-fault voltage was taken into account during the calculation.
- Motors were considered as current injecting sources in series with the internal sub-transient impedance of the specific motor
- Generators, during the fault, were represented by their sub-transient impedance.
- Positive and zero sequence impedances were considered

For the purpose of analysis, the parking structure 1 node was considered and various types of faults were applied at this location. An increase in fault current was observed in all cases. It was seen that when the PV generators were added into the system, the fault current increased. The fault current reduced to a value slightly greater than the normal fault current when reactive power was injected from the PV generators in addition to the real power. The reason for this has been discussed. The segments in red are under-voltage segments and the segments in yellow are overloaded. Fig. 5.17 through Fig. 5.20 show the various fault conditions at that PV generation node.

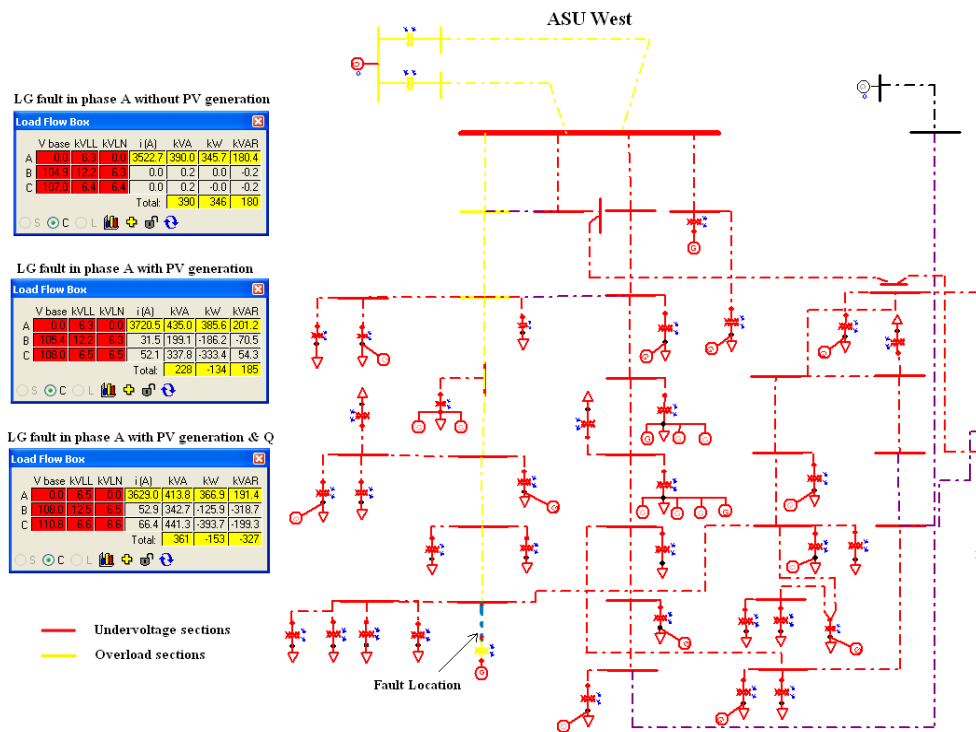


Fig. 5.17. Under-voltage and overload lines in ASU West for a LG fault in phase A at a PV generator location

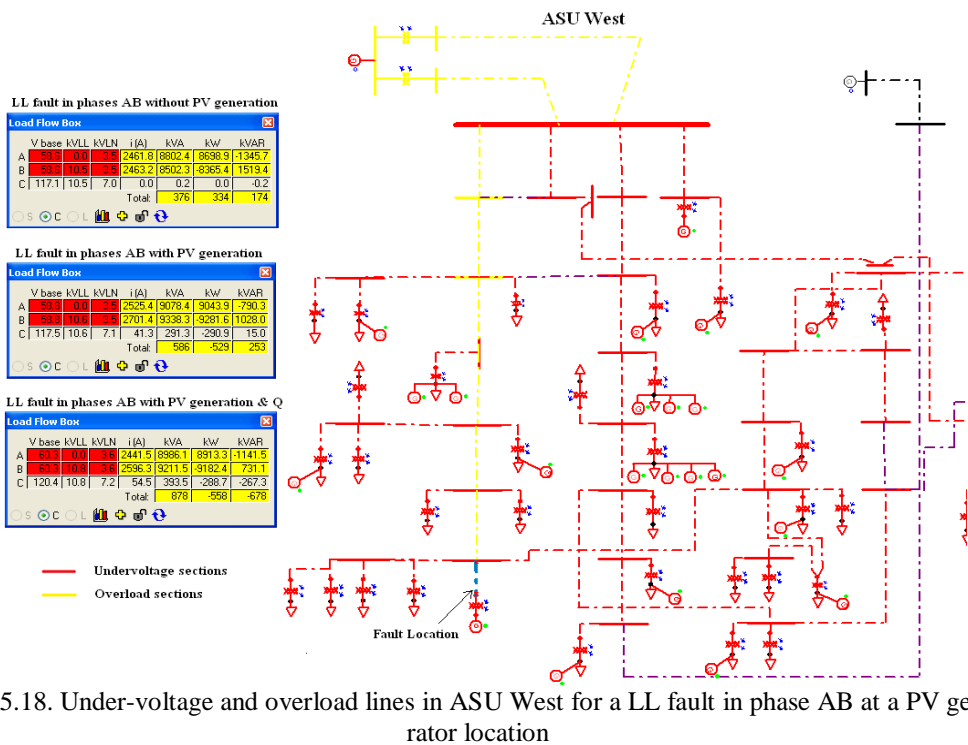


Fig. 5.18. Under-voltage and overload lines in ASU West for a LL fault in phase AB at a PV generator location

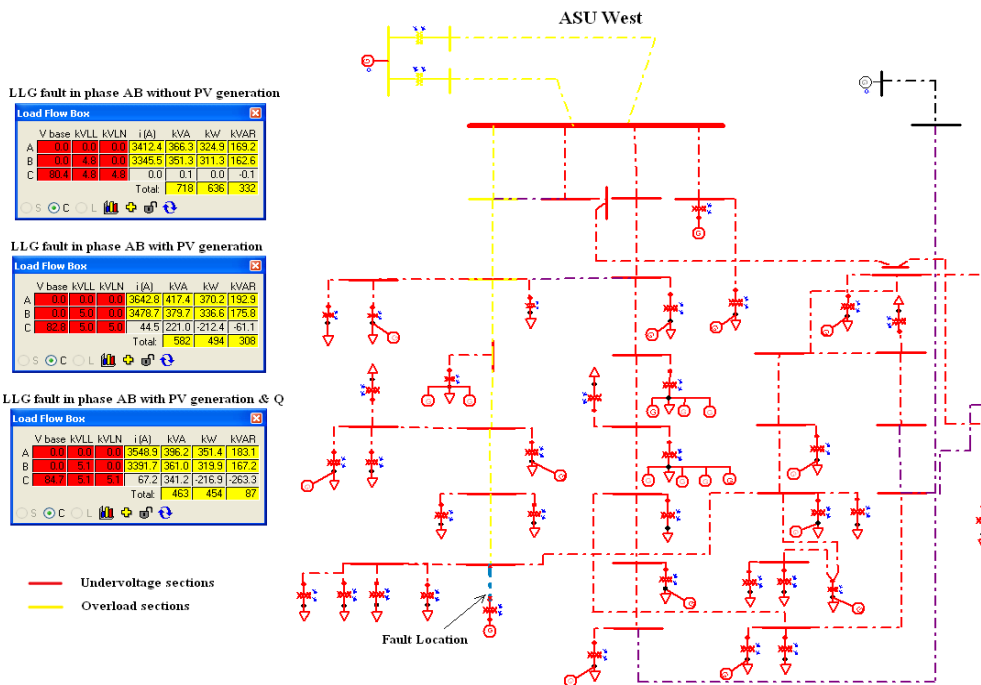


Fig. 5.19. Under-voltage and overload lines in ASU West for a LLG fault in phase AB at a PV generator location

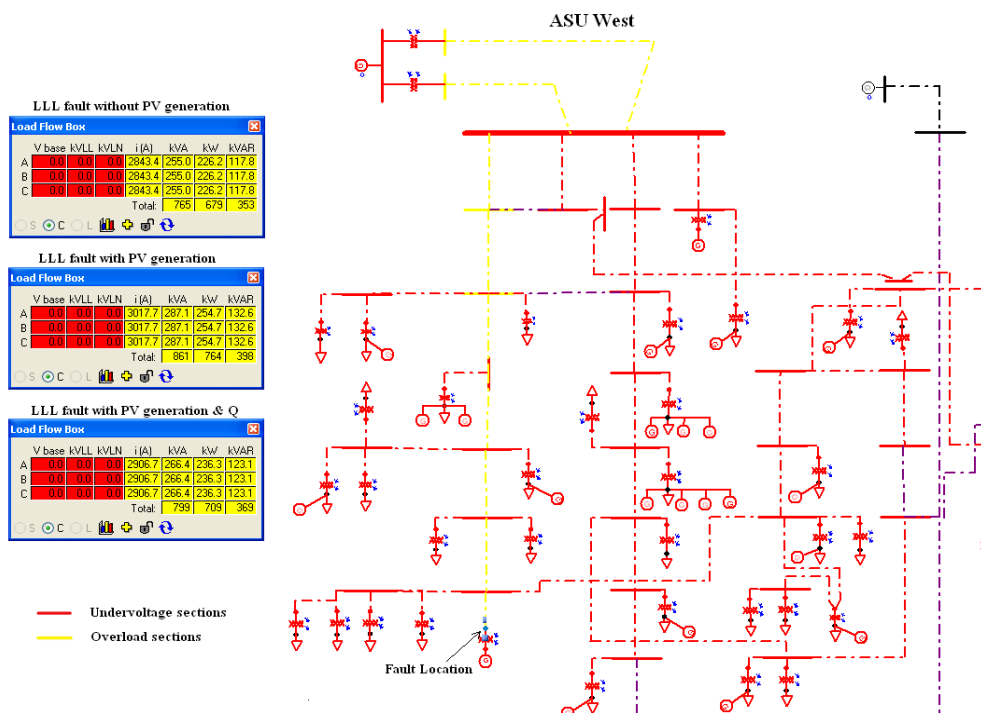


Fig. 5.20. Under-voltage and overload lines in ASU West for a LLL fault at a PV generator location

CHAPTER 6

CONCLUSIONS AND FUTURE WORK

6.1 Conclusions

This thesis focused on analyzing the impact of PV installations representing high levels of penetration in relatively large load centers such as university campuses or industrial/commercial complexes. The power distribution system of ASU Tempe campus was selected as a representative system for this study and the impact of PV penetration on the system performance was analyzed. The connection point between the distributed generation and distribution system, the three-phase PV inverter, was modeled in MATLAB. The protection features which are embedded in today's inverters, namely the anti-islanding techniques were implemented. One line diagram of ASU's distribution system was created in PowerWorld. The EIS data was used to obtain the load information of all the buildings at ASU. The voltage profile of the system was tested for various cases. The entire distribution system modeling was carried out in CYMDIST as well to make use of the DG capabilities and other analyses such as short circuit analysis and fault flow analysis. The conclusions of the work are:

- The anti-islanding techniques made use of positive feedback for voltage and frequency schemes and this was seen to work efficiently and satisfied constraints imposed by standards very well.
- Though the voltage and frequency schemes did not produce faster tripping times when enabled together, individually they were seen to have tripping times which satisfied industry standards very well. This showed effectiveness of the techniques and a relatively small NDZ.
- Power flow analysis was done for the base case which had no PV generation and was repeated for cases where a central feeder was disconnected and distributed generation was turned on. It was seen that the voltage profile improved on the addition of PV systems.

- There was a reduction in the losses of the system when PV generation was included. With an increase in the penetration level of 4.7% to 22%, there was a 25% reduction in loss.
- The benefits of leveraging the reactive power capabilities of the PV inverters (electronically coupled generators) were apparent in all of the simulations, providing improved voltage profiles throughout the feeder circuit in both softwares. The simulation proves that DG can influence the voltage profile and should be well planned to ensure that the static voltage of each node is within the permitted range.
- The inclusion of distributed generation increased the fault current limits. Hence, it is necessary to assess the protection system of the distribution network and make sure ratings of equipments can handle the excess fault current.
- When reactive power equal to real power was supplied by the PV systems, it was seen that the fault current which was initially injected by the PV's real power decreased. The percentage increase in fault dropped from 6-7% with PV alone to 1% when reactive power was injected.

The key conclusion drawn from this work is that coordinated control of utility equipment and DG assets can be used to enhance the performance of distribution systems. As demonstrated by the simulations portrayed in this work, the distributed fleet of PV systems can be controlled to provide reactive power support and improve the voltage profile at different operating conditions. At sufficiently high penetration levels, PV inverters may even be able to regulate the feeder voltage, reducing the need for capacitors. As the penetration levels of PV rise in distribution systems around the world, it would be a good idea to get ahead of the problem of uncoordinated DG, and to proactively seek to transform DG interconnection requirements to allow utilities to extract the performance from these assets that is inherently built into them already. It is also necessary to have a thorough understanding of the fault current contribution of DG under different levels of reactive power support in order to design suitable protection system.

6.2 Future Work

This work presents the voltage impact due to the penetration of PV in the distribution system. In continuation, the impact of DG on electric distribution system reliability could be done. This could include verification of the impact on distribution reliability indices such as SAIDI, CAIDI, ENS and SAIFI and on system losses. A model using optimization methods such as genetic algorithm for problem solving in large scale distribution systems could be used. A few more areas of work could be:

- Inclusion of the three phase grid tied inverters into the distribution system and the application and effectiveness of anti-islanding techniques to real system disturbances in the distribution network.
- Development of intentional islanding techniques for distributed generation.
- A more complete understanding on the implications of DG islanding on the power system dynamic performance.
- There is a need for fault current modeling of inverter based DG to have a better understanding of how over current protection of inverters affect fault current values.

REFERENCES

- [1] T.A. Short, Electric Power Distribution Handbook, CRC Press, 2004
- [2] Z. Ye, R. Walling, N. Miller, P. Du, K. Nelson, "Facility Microgrids," NREL Report No. NREL/SR-560-38019, 2005.
- [3] In-Su Bae and Jin-O Kim, "Reliability evaluation of distributed generation based on operation mode," *IEEE Trans. on Power Systems*, vol. 22, no. 2, pp.785-790, May 2007.
- [4] Y. Mao and K.N. Miu, "Switch placement to improve system reliability for radial distribution systems with distributed generation," *IEEE Trans. on Power Systems*, vol. 18, pp.1346-1352, Nov. 2003.
- [5] M. Dai, M. Nanda, and Jin-Woo Jung, "Power flow control of a single distributed generation unit," *IEEE Trans. on Power Electronics*, vol. 23, no. 1, pp.343 -352, Jan. 2008.
- [6] Y. Zhu and K. Tomsovic, "Adaptive power flow method for distribution systems with dispersed generation," *IEEE Trans. on Power Delivery*, vol. 17, no. 3, pp. 822-827, 2002.
- [7] Y.Y. Thong, I. Driesen, and R. Belmans, "The influence of the connection technology of dispersed energy sources on grid stability," *Second International Conference on Power Electronics, Machines and Drives*, vol. 2, pp.742 -745, April 2004.
- [8] T.G. Hazel, N. Hiscock, and I. Hiscock, "Voltage regulation at sites with distributed generation," *IEEE Trans. on Industry Applications*, vol. 44, no. 2, pp.445 -454, April 2008.
- [9] Y. Calderaro, I.Y. Milanovic, M. Kayikci, and A. Piccolo, "The impact of distributed synchronous generators on quality of electricity supply and transient stability of real distribution network," *Electric Power Systems Research*, vol. 79, no. 1, pp.134-143, May 2008.
- [10] W. El-Khattam, and T.S. Sidhu, "Restoration of directional over-current relay coordination in distributed generation systems utilizing fault current limiter," *IEEE Trans. on Power Delivery*, vol. 3, no. 2, pp.576-585, April 2008.
- [11] F. Katiraei, R. Iravani, N. Hatziargyriou, A. Dimeas, "Microgrids management," *IEEE Power and Energy Magazine*, vol. 6, no. 3, pp.54-65, May-June 2008
- [12] Z. Ye, R. Walling, L. Garces, R. Zhou, L. Li, T. Wang, "Study and development of Anti-Islanding Control for Grid-Connected Inverters," NREL/SR-560-36243. Golden, CO: National Renewable Energy Laboratory. May 2004.
- [13] R.A. Walling, N.W. Miller, "Distributed Generation Islanding - Implications on Power System Dynamic Performance," Power Engineering Society Summer Meeting, 2002 IEEE, vol. 1, Page(S): 92 -96, 2002
- [14] J. Driesen and R. Belmans, "Distributed Generation: Challenges and Possible Solutions" *IEEE Power Engineering Society General Meeting*, 18-22 June 2006.
- [15] IEEE, "IEEE Recommended Practices and Requirements for Harmonic Control in Electrical Power Systems," IEEE Std. 519-1992, 1993

- [16] P. Mahat, Zhe Chen, B. Bak-Jensen, "Review of islanding detection methods for distributed generation," *Third International Conference on Electric Utility Deregulation and Restructuring and Power Technologies, 2008. DRPT 2008.*, pp. 2743-2748, 6-9 April 2008
- [17] J. Stevens, R. Bonn, J. Ginn, S. Gonzalez, and G. Kern, "Development and testing of an approach to anti-islanding in utility interconnected photovoltaic systems," Sandia Report SAND 2000- 1939, August, 2000.
- [18] M. E. Ropp, M. Begovic, A. Rohatgi, "Analysis and performance assessment of the active frequency drift method of islanding prevention," *IEEE Trans. on Energy Conversion*, vol. 14, no. 3, September 1999.
- [19] S.J. Huang and F.S. Pai, "Design and operation of grid-connected photovoltaic system with power factor control and active islanding detection," *IEEE Proceeding in Generation Transmission and Distribution*, vol. 148, no. 2. March 2001.
- [20] H. Kobayashi and K. Takigawa, "Statistical evaluation of optimum islanding preventing method for utility interactive small scale dispersed PV systems," *IEEE First World Conference on Photovoltaic Energy Conversion*, December 5-9, 1994.
- [21] A. Woyte, R. Belmans and J. Nijs, "Islanding of grid-connected AC module inverters," *Conference record of the 28th IEEE Photovoltaic Specialists Conference*. pp. 1683-1686, Anchorage (Alaska), September 2000.
- [22] T. Ishida, R. Hagihara, M. Yugo, Y. Makino, M. Maekawa, A. Takeokq R. Suruki, and S. Nakana, "Anti-islanding protection using a twin-peak band-pass filter in interconnected PV systems, and substantiating evaluations," *IEEE First World Conference on Photovoltaic Energy Conversion*, December 5-9, 1994.
- [23] Jun Yin, Liuchen Chang, and C. Diduch, "Recent developments in islanding detection for distributed power generation," Large Engineering systems Conference of Power Engineering, pp. 124-128, July 2004.
- [24] R. A. Walling, and N. W. Miller, "Distributed generation islanding implications on power system dynamic performance," *IEEE Power Engineering Society Summer Meeting*, vol. 1, pp. 92-96, 2002.
- [25] T. Ackermann, G. Andersson, and L. Soder, "Distributed generation: a definition," *Electric Power System Research*, vol. 57, pp. 195-204, 2001.
- [26] S. Boljevic, M.F. Conlon, "Fault current level issues for urban distribution network with high penetration of distributed generation," *Energy Market, 2009. EEM 2009. 6th International Conference on the European*, vol., no., pp.1-6, 27-29 May 2009.
- [27] I.H. Hwang, K.S. Ahn, H.C. Lim, S.S. Kim, "Design, development and performance of a 50 kW grid connected PV system with three phase current-controlled inverter," *Photovoltaic Specialists Conference, 2000. Conference Record of the Twenty-Eighth IEEE*, vol., no., pp.1664-1667, 2000.

- [28] T. Kerekes, R. Teodorescu, C. Klumpner, M. Sumner, D. Floricau, R. Rodriguez, "Evaluation of three phase transformer less photovoltaic inverter topologies," *European Conference on Power Electronics and Applications*, 2nd-5th Sep. 2007, pp. 1-10.
- [29] K. Alafodimos, P. Fetfatzis, P. Kofinas, M. Kallousis, X. Kikidakis, "Design Simulation for a 3-Phase grid connected PV Inverter in Simulink," eRA-3 proceedings, 2009.
- [30] M. Ciobotaru, T. Kerekes, R. Teodorescu, A. Bouscayrol, "PV inverter simulation using MATLAB/Simulink graphical environment and PLECS blockset," *IEEE* 1-4244-0136-4, pp.5313-5318, June 2006.
- [31] S.K. Kim, J.H. Jeon, C.H. Cho, E.S. Kim, J.B. Ahn, "Modeling and simulation of a grid-connected PV generation system for electromagnetic transient analysis," *Solar Energy*, vol. 83, issue 5, Pages 664-678, May 2009.
- [32] IEEE, "IEEE Standard for Interconnecting Distributed Resources with Electric Power," New IEEE Std. 1547-2003, August 2003.
- [33] IEEE, "IEEE Recommended Practice for Utility Interface of Photovoltaic (PV) Systems," IEEE Std. 929-2000. January 2000.
- [34] N. Mohan, T.M. Undeland, W.P. Robbins, Power Electronics – Converters, Application and Design, John Wiley andSons, New York, 1995
- [35] UL 1741, "Inverter, converter, and controllers for use in independent power systems," June 2002.
- [36] PowerWorld Simulator. (<http://www.powerworld.com/products/simulator.asp>)
- [37] Underground Cable Engineering Handbook, Essex International, Inc.

APPENDIX A

PV GENERATION SITES IN TEMPE CAMPUS

TABLE A.1
PV SITES IN ASU TEMPE CAMPUS

Location	kW Rating	Status of Construction
Parking Structure 2	30	Existing PV
Parking Structure 5	711	Existing PV
Parking Structure 1	880	Existing PV
Lattice COOR Hall	108	Existing PV
Bio Design A	75	Existing PV
Bio Design B	75	Existing PV
Parking Structure 4	296	Existing PV
Parking Structure 7	290	Existing PV
Parking Structure 3	215	Existing PV
Global Institute of Sustainability	24	Existing PV
Hassayampa Academic Village	138	Existing PV
Hayden Library	290	Existing PV
Barrett College	154	Existing PV
Student Services Building	185	Under Construction
Farmer	111	Under Construction
Noble Science	108	Under Construction
Carson Student Athletic Center	70	Under Construction
Physical Education East	218	Under Construction
Schwada	87	Under Construction
Education Lecture Hall	45	Under Construction
Fulton Parking Structure	500	Under Review
Business Administrative Center	95	Under Review
Payne Hall	165	Under Review
Center for Family Studies	36	Under Review
Cowden Family Resources	86	Under Review
Durham Language and Literature	48	Under Review
Anthropology	86	Under Review
Matthews Hall	60	Under Review
Bateman Physical Sciences Center F	147	Under Review
Psychology North	126	Under Review
Engineering Center G	168	Under Review
Life Science Center A	150	Under Review
Physical Sciences Center A	93	Under Review
Physical Sciences Center B Wing	78	Under Review
College of Design South	107	Under Review

Stauffer Communication Arts A	67	Under Review
Stauffer Communication Arts B	112	Under Review
Neeb Hall	41	Under Review
Murdock Lecture Hall	56	Under Review
Physical Education Building West	246	Under Review
Undergraduate Academic Services	73	Under Review
Wells Fargo Arena	400	Under Review
Music	300	Under Review
Computing Commons	200	Under Review
Gammage Auditorium	320	Under Review
Interdisciplinary B	173	Under Review
Memorial Union	500	Under Review
Student Recreation Center	114	Under Review

APPENDIX B

SUBROUTINES TO READ EIS DATA, CREATE LOAD PROFILE AND LOAD IT IN POWERWORLD

ReadDataFromEIS.m

```
% Read load data downloaded from EIS
function BldgLoadList = ReadDataFromEIS

xls_files = dir(...\Data\EIS\Aug\*.xls');
xls_newest = max([xls_files.datenum]);

% check if their's any update
matfilename = 'BldgLoadList.mat';
if exist(matfilename,'file')
fMAT = dir(matfilename);
    if fMAT.datenum>xls_newest
        s = load(matfilename);
        BldgLoadList = s.BldgLoadList;
        return;
    end
end

len = length(xls_files);
BldgLoadList.Name = cell(len,1);
BldgLoadList.kW = cell(len,1);
for i=1:len,
    [kW,txt] = xlsread(...\Data\EIS\Aug\' xls_files(i).name);
    t = txt{2,1};

    % check data validity
    assert(length(kW)==2976, 'Wrong data in %s\n', xls_files(i).name);
    assert(ischar(t) &&strcmp(t,'8/1/2009'));
    % if ~(ischar(t) &&strcmp(t,'8/1/2009')),
    %     fprintf('i=%d name=%s\n',i,xls_files(i).name);
    % end

    % create hourly data
    kW = (kW(1:4:end)+kW(2:4:end)+kW(3:4:end)+kW(4:4:end))/4;

    % save hourly data together with building name
    [ignore,bldgname]=fileparts(xls_files(i).name);
    BldgLoadList.Name{i} = bldgname;
    BldgLoadList.kW{i} = kW;
end
BldgLoadList.Date = datenum(2009,8,1,(0:length(BldgLoadList.kW{1})-1),0,0);

save(matfilename, 'BldgLoadList');
```

LoadProfileData.m

```
% Load system data
[BusRec, BranchRec, GenRec, LoadRec] = ...
ReadPWXLSSystemData('SystemDataFromPW.xls');

% Load building load data
BldgLoadList = ReadDataFromEIS;

%% From bldg load to transformer loading
% Read mapping data
[Xfrmr.MVARating,txt] = xlsread('TF_Bldg_Mappingfull_X.xls','mapping');
Xfrmr.Name = txt(2:end,1);
Xfrmr.MeteredBy = txt(2:end,4);
Xfrmr.ConstructedFrom = txt(2:end,5);
Xfrmr.HasEISData = txt(2:end,6);

%% Calculate MVA Ratings for the Bldg Loads
MeterList.Name = cell(1000,1);
MeterList.MVARating = zeros(1000,1);
len = 0;
for i=1:length(BldgLoadList.Name),
ind = strmatch(BldgLoadList.Name{i}, Xfrmr.MeteredBy, 'exact');
    if ~isempty(ind),
len = len+1;
MeterList.Name(len) = BldgLoadList.Name(i);
MeterList.MVARating(len) = sum(Xfrmr.MVARating(ind));
    end
end
MeterList.Name = MeterList.Name(1:len);
MeterList.MVARating = MeterList.MVARating(1:len);

%% Calculate transformer load
LoadData.Bus = LoadRec.Bus;
LoadData.ID = LoadRec.ID;
LoadData.kW = cell(size(LoadData.Bus));
LoadEx = zeros(size(LoadData.Bus)); %exclude these loads

for i=1:length(LoadData.kW),
    % find corresponding transformer name
xfrmrname = BusRec.Name{LoadData.Bus(i)};
    if xfrmrname(end) == '',
xfrmrname = xfrmrname(1:end-1);
    end
    %fprintf('%s\n',xfrmrname);

% ex = strmatch(xfrmrname, ExcludingBus, 'exact');
```

```

% if length(ex)>=1,
%   LoadEx(i) = 1;
%   continue;
% end

% find transformer record in the TF-BLDG mapping XLS file
iXfmr = strmatch(xfrmname, Xfmr.Name, 'exact');
assert(length(iXfmr)==1);

% meter name
metername = Xfmr.MeteredBy{iXfmr};
if ~isempty(metername), % if metered
idx = strfind(metername, ',');
if ~isempty(idx), % if this load is the sum of several meters
idx = [idx length(metername)+1]; %#ok<AGROW>
sp = 1;
data = zeros(size(BldgLoadList.kW{ 1 }));
for ep = idx-1,
namei = metername(sp:ep);
sp = ep+2;
ind = strmatch(namei, BldgLoadList.Name, 'exact');
assert(length(ind)==1);
data = data+BldgLoadList.kW{ ind };
end
LoadData.kW{i} = data;
else % only metered by one meter
ind = strmatch(metername, MeterList.Name, 'exact');
assert(length(ind)==1);
factor = Xfmr.MVARating(iXfmr)/MeterList.MVARating(ind);
ind = strmatch(metername, BldgLoadList.Name, 'exact');
LoadData.kW{i} = factor*BldgLoadList.kW{ ind };
end
else % data must be constructed from other meters
constrfrom = Xfmr.ConstructedFrom{iXfmr};
assert(~isempty(constrfrom));
ind = strmatch(constrfrom, MeterList.Name, 'exact');
assert(length(ind)==1);
factor = Xfmr.MVARating(iXfmr)/MeterList.MVARating(ind);
ind = strmatch(constrfrom, BldgLoadList.Name, 'exact');
LoadData.kW{i} = factor*BldgLoadList.kW{ ind };
end
end

LoadData.Bus(LoadEx==1) = [];
LoadData.ID(LoadEx==1) = [];
LoadData.kW(LoadEx==1) = [];

save LoadProfileDataLoadData

```

PWLoadProfilefull.m

```
[BusRec, BranchRec, GenRec, LoadRec] = ...
ReadPWXLSSystemData('SystemDatafromPWfull.xls');

% load load profile data
load LoadProfileData;

%% write a single load case to an AUX file
% on 8/20/09 at 3PM
idx = find(BldgLoadList.Date==datenum(2009,8,20,15,0,0));
DF = 0.9; % Displacement factor

fid = fopen('updateLoad.aux','wt');

fprintf(fid,'DATA (LOAD, [BusNum,LoadID,LoadMW,LoadMVR])\n{\n');
for i=1:length(LoadData.kW),
fprintf(fid,' %d "%s" %f %f\n', BusRec.Num(LoadRec.Bus(i)), ...
        LoadRec.ID{i}, LoadData.kW{i}(idx)/1000,LoadData.kW{i}(idx)*sqrt(1-DF^2)/DF/1000);
end
fprintf(fid,')\n{\n');

fclose(fid);

%% write a one-day load schedule data to CSV file
% select only one day data
SelDate = datenum(2009,8,20);
sp = find(BldgLoadList.Date==SelDate);
NofLoad = length(LoadData.kW);

fid = fopen('LoadMWTSS.csv','wt');
fprintf(fid,'Timepoint Load MW');
for i=1:NofLoad+2-1,
fprintf(fid,');
end
fprintf(fid,'\nDate,Hour');
for i=1:NofLoad,
fprintf(fid,',Bus %d #%s MW',BusRec.Num(LoadRec.Bus(i)),LoadRec.ID{i});
end
for i=sp:sp+23,
    fprintf(fid,'\n%s,%s',datestr(BldgLoadList.Date(i),'mm/dd/yyyy'), ...
            datestr(BldgLoadList.Date(i),'HH:MM:SS PM'));
    for j=1:NofLoad,
        fprintf(fid,'%f',LoadData.kW{j}(i)/1000);
    end
end
fprintf(fid,'\n');
```

```

fclose(fid);

%%
fid = fopen('LoadMvarTSS.csv','wt');
fprintf(fid,'Timepoint Load Mvar');
for i=1:NofLoad+2-1,
fprintf(fid,');
end
fprintf(fid,'\nDate,Hour');
for i=1:NofLoad,
fprintf(fid,','Bus %d #%s Mvar',BusRec.Num(LoadRec.Bus(i)),LoadRec.ID{i});
end
for i=sp:sp+23,
    fprintf(fid,'\n%s,%s',datestr(BldgLoadList.Date(i),'mm/dd/yyyy'), ...
datestr(BldgLoadList.Date(i),'HH:MM:SS PM'));
    for j=1:NofLoad,
fprintf(fid,','%f,LoadData.kW{j}(i)*sqrt(1-DF^2)/DF/1000);
    end
end
fprintf(fid,'\n');
fclose(fid);

```